UNIVERSITY OF CALIFORNIA SAN DIEGO

Functional Diversity of Corticothalamic Pathways Underlying Visual Processing

A dissertation submitted in partial satisfaction of the requirements for the degree

Doctor of Philosophy

in

Neurosciences

by

Megan Anne Kirchgessner

Committee in Charge:

Professor Edward Callaway, Chair
Professor Jeffry Isaacson, Co-Chair
Professor Timothy Gentner
Professor Christina Gremel
Professor Pamela Reinagel
Professor Kay Tye

2021

The dissertation of Megan Anne Kirchgessner is approved, and it is acceptable in quality and form for publication on microfilm and electronically.

University of California San Diego

2021

DEDICATION

This dissertation is dedicated to:

My mom – my lifelong role model, whose intelligence, charisma, resilience, and compassion are everything I aspire to.

My dad – my #1 cheerleader, whose sincere and unwavering support has meant the world to me, and whose genes are undoubtedly to blame for this dissertation.

And Brian – my best friend, who inspires me every day with his tenacity and heart.

EPIGRAPH

I have serious reservations about whether the functions of a circuit,
and especially its dysfunction in disease,
can be determined simply by adding up the pluses and minuses
to arrive at an overall excitatory or inhibitory effect.
The thalamus just does not work that way.

Edward G. “Ted” Jones
“Cortical development and thalamic pathology in schizophrenia”
Schizophrenia Bulletin 3, 483-501 (1997)

TABLE OF CONTENTS

LIST OF ABBREVIATIONS

CC	Corticocortical
CT	Corticothalamic
dLGN	Dorsolateral geniculate nucleus [of the thalamus]
ET	Extratelencephalic
FO	First-order [thalamus]
HO	Higher-order [thalamus, cortex, etc.]
L5, L6, etc.	Layers 5, 6, etc. of the cerebral cortex
lPulv	Lateral pulvinar
RF	Receptive field
rmPulv	Rostromedial pulvinar
RGC	Retinal ganglion cell
SC	Superior colliculus
TC	Thalamocortical
TRN	Thalamic reticular nucleus [of the thalamus]
V1	Primary visual cortex

LIST OF FIGURES

ACKNOWLEDGEMENTS

I am forever grateful to Professor Ed Callaway for his support as my mentor and committee chair. I have grown exponentially as a scientist under his mentorship, and the independence he has allowed me and trust he has put in me have made me a more competent and confident scientist as well.

I also wish to thank the other members of the Callaway Lab, past and present, for their technical, intellectual and emotional support for this work over the years. In particular, Alexis Franklin, who worked with me as a technician for 2.5 years, was an invaluable co-author of this work.

I am also grateful to my thesis committee for their encouragement of and constructive feedback on this work over the last number of years.

And finally, I wish to thank my friends and family who have provided me with an incomparable support network, without which none of this would have been possible.

Chapter 1, in full, is a reprint of the material as it appears in: Kirchgessner, MA, Franklin, AD, & Callaway, EM (2020). Context-dependent and dynamic functional influence of corticothalamic pathways to first- and higher-order visual thalamus. *Proceedings of the National Academy of Sciences*, *117*(23), 13066. The dissertation author was the primary investigator and author of this paper.

Chapter 2, in full, is currently being prepared for submission for publication and will include Alexis D. Franklin as a co-author and Professor Edward Callaway as the senior author. The dissertation author was the primary investigator and author of this material.

VITA

2014 Bachelor of Arts, Cognitive Sciences and Psychology with a Minor in Neuroscience
Rice University, Houston, TX, USA

2021 Doctor of Philosophy, Neurosciences
University of California San Diego, La Jolla, CA, USA

PUBLICATIONS

Kirchgessner, MA, Franklin, AD, & Callaway, EM (2020). Context-dependent and dynamic functional influence of corticothalamic pathways to first- and higher-order visual thalamus. *Proceedings of the National Academy of Sciences*, *117*(23), 13066.

Zhang, Z, Zhou, J, Tan, P, Pang, Y, Rivkin, A, **Kirchgessner, MA**, Williams, E, Lee, C-T, Liu, H, Franklin, AD, … Ecker, JR, & Callaway, EM (2020). Epigenomic Diversity of Cortical Projection Neurons in the Mouse Brain. Accepted, *Nature*.

Kirchgessner, MA, Chuang, AZ, Patel, SS, & Sereno, AB (2015). Intact reflexive but deficient voluntary social orienting in autism spectrum disorder. *Frontiers in Neuroscience*, *9 (453),* doi:10.3389/fnins.2015.00453. PubMed PMID: 26648841.

Geng, J, **Kirchgessner, M,** & Schnur, TT (2013). The mechanism underlying lexical selection: Evidence from the picture-picture interference paradigm. *Quarterly Journal of Experimental Psychology, 66*(2), 261-276, doi:10.1080/17470218.2012.705861. PubMed PMID: 22943494.

ABSTRACT OF DISSERTATION

Functional Diversity of Corticothalamic Pathways Underlying Visual Processing

by

Megan Anne Kirchgessner

Doctor of Philosophy in Neurosciences

University of California San Diego, 2021

Professor Edward Callaway, Chair
Professor Jeffry Isaacson, Co-Chair

The cerebral cortex and the thalamus are in constant communication with one another, and their interactions are thought to underlie fundamental brain functions such as perception, attention, sleep, cognitive flexibility, and even consciousness. Still, a multitude of questions remains as to *how* corticothalamic interactions subserve these functions. This dissertation explores one major aspect of these interactions - how the cortex communicates with the thalamus, using the mouse visual system as model. This is an area in which considerable groundwork has been laid by decades of research into the underlying anatomy and physiology of these connections, which have led to influential hypotheses about

how those attributes may relate to function. Yet, many of these hypotheses have been left untested, due to challenges and technical limitations in selectively perturbing different corticothalamic pathways and assessing their *in vivo* functions in an awake animal. In this dissertation, modern advances in mouse transgenics, extracellular electrophysiology, and circuit manipulation are harnessed to directly assess how distinct populations of corticothalamic neurons contribute to visual thalamic processing *in vivo*. Chapter 1 explores the role that a unique population of corticothalamic neurons in layer 6 of the mouse primary visual cortex play in the dorsolateral geniculate nucleus and the pulvinar, which represent two distinct classes of visual thalamic nuclei. By using optogenetics to selectively stimulate these neurons, we find that they act similarly upon both classes of thalamic nuclei, yet their influence in both is highly dynamic and dependent upon the context of their activation. In Chapter 2, the endogenous function of these layer 6 corticothalamic neurons is further examined with optogenetic *in*activation and contrasted with that of an additional corticothalamic population in cortical layer 5 that exclusively projects to the pulvinar. We find novel evidence in support of longstanding hypotheses that layer 5 corticothalamic projections "drive" visual responses in the pulvinar, whereas the layer 6 projections play a fundamentally "modulatory" role. Altogether, this dissertation reveals how functionally distinct corticothalamic pathways influence the visual thalamus and suggests fundamental principles in how corticothalamic communication is organized for sensory processing in the awake, behaving animal.

Introduction

In his 1906 Nobel Prize Lecture on "The Structure and Connexions of Neurons", the famed neuroanatomist Santiago Ramón y Cajal speculated upon the role of "centrifugal fibers", such as those he observed in the sensory thalamus that likely emanated from the sensorimotor cortex[1]:

> Are they […] conductors destined to produce in the sensory pathway articulations a very intimate contact which would be indispensable for the satisfactory propagation of the nervous impulse? Or rather do they transport some form of energy from the brain, the rapid accumulation of which in the sensory stations is necessary for the passage of ascending nerve currents? Unfortunately, at this stage of science, it is impossible to give satisfactory and categorical answers to these questions.

Cajal was incredibly prescient in his predictions of neural circuit organization and function – such as in his deduction of the presence of corticothalamic loops[1] – based entirely on his anatomical observations and drawings. Yet at the same time, he acknowledges the limitations of what one can infer based on that kind of data, highlighting at least two possible functions that a connection from one brain area to another might have in terms of propagating neural signals. Is that connection itself necessary for signal transmission, or is it instead permissive, somehow allowing other signals to be able to be transmitted but not itself the source of those signals?

The question of what purpose connections from one brain area to another serve for the transmission of neural signals is absolutely central to the field of neuroscience. Many neurodevelopmental and neuropsychiatric disorders are characterized by atypical or compromised connectivity[2,3], and so understanding how typical and atypical connectivity patterns are formed and what aspects are critical for healthy neural function is an overarching goal of the field. To this end, mapping brain connections has been, and continues to be, a major and fruitful endeavor[4]. In the pursuit of basic science research as well, an enhanced understanding of neural connectivity often sparks further hypotheses about brain function. Cajal's detailed anatomical studies and countless ensuing functional hypotheses were an early exemplar of this. In recent decades, full connectomic reconstructions of invertebrate nervous systems – such as those of *C. elegans* and the crustacean stomatogastric ganglion – have also sparked questions and ideas

that arguably led to significant advances in relating connectivity to neuronal activity patterns, and even to whole-animal behavior[5].

Yet, the more we have learned about the diversity of neural connections, the clearer it has become that reconstructing the "wiring diagram" of a circuit is insufficient for understanding circuit function[5]. The distinction between excitatory and inhibitory synapses provides a basic example of this, as these types of connections have very different consequences for "the satisfactory propagation of the nervous impulse". Moreover, we now know that there is considerable diversity even among excitatory connections, although our understanding of the functional implications of this diversity remains limited. Nevertheless, it was remarkably prescient of Cajal to have already anticipated some of this diversity, and it is particularly fitting that he did so in the context of speculating upon the functions of "centrifugal fibers" linking the cortex and the thalamus.

Diversity of excitatory connections in thalamocortical and corticothalamic circuitry

Corticothalamic circuitry is a fascinating system for exploring questions of long-range functional connectivity, as Cajal clearly appreciated. Because the thalamus lacks intrinsic excitatory synapses, most of its excitatory connections are with the cortex[6]. Thus, the cortex and the thalamus are engaged in constant, bidirectional communication with one another - so much so that certain parts of the thalamus (discussed below) have even been referred to as a "seventh layer" of the cortex[7]. Corticothalamic (CT) interactions appear to be important for a wide array of brain functions, ranging from perception and attention to cognitive flexibility and working memory, and even sleep and consciousness[8,9]. Yet understanding these various functions, especially for the purposes of developing targeted, effective interventions for when they are impaired, requires a mechanistic understanding of the underlying circuitry that supports those interactions.

As far as basic anatomical connectivity is concerned, much is already known about the connections between different types of thalamic nuclei and their cortical partners. In rodents, first-order (FO) thalamic nuclei, such as the dorsolateral geniculate nucleus (dLGN) in the visual system, send

excitatory projections to cortical layers 4 and 5B, and to some extent to upper cortical layers as well, of primary sensory cortex (e.g., the primary visual cortex, V1)[10]. The cortex, in turn, sends feedback projections to FO thalamus through a dedicated population of excitatory corticothalamic neurons in cortical layer 6 (L6CTs)[11]. Meanwhile, higher-order (HO) thalamic nuclei, such as the visual pulvinar, also receive cortical input from some of these same L6CTs, as well as from a subset of subcortically-projecting (extratelencephalic) L5 excitatory neurons (L5ETs)[12,13]. HO nuclei then excite layers 1 and 5A of primary cortex, as well as layers 4/5B of higher-order cortical areas (resembling FO thalamic projections to primary cortex)[10,14,15]. These connectivity motifs are strikingly conserved across different sensory systems, and to a large extent even across species[16,17].

One example of different excitatory projections that putatively serve different functions can be found in the distinct patterns of thalamocortical (TC) axons. Specifically, so-called "core" projections to L4/5B are thought to arise from TC relay cells that form a feedforward pathway, whereas "matrix" cells project more diffusely to L1/5A and might provide a means by which the thalamus can synchronize activity across cortical areas[10,18]. While these TC connections are known to originate from different classes of thalamic neurons in primates[18], their distinction may be more complicated in other species[15]. Overall, there is still a considerable amount of complexity in this circuitry that needs to be disentangled[9], and functions directly assessed in vivo.

Meanwhile, projections in the opposite direction – from the cortex to the thalamus - also exhibit a number of distinguishing features that have led many to speculate upon their roles in thalamic processing. First, L6CT inputs from V1 to both dLGN (FO) and the pulvinar (HO), as well as in other sensory and non-sensory systems[16], are characterized by their small synaptic profiles, activation of both ionotropic and metabotropic glutamate receptors, considerable convergence, and relatively weak synapses exhibiting short-term facilitation as a consequence of their low probability of glutamate release; these are called "type 1" synapses[19]. In contrast, L5 inputs to the pulvinar are described as "type 2" inputs. They are large terminals that activate exclusively ionotropic glutamate receptors, result in "all or none" postsynaptic responses, and are sparser than L6CT inputs but have strong synapses with high release probabilities that

lead to short-term depression[17,19]. Although these L5 neurons do not project to the dLGN, it is notable that retinal ganglion cell inputs to the dLGN (like other sensory peripheral inputs to other FO nuclei) exhibit these same "type 2" synaptic features; consequently, FO and HO nuclei are distinguished by the origins of their type 2 inputs[19,20]. On the other hand, these different classes of thalamic nuclei have in common that they both receive L6CT inputs with "type 1" features. One could therefore imagine that these L6CT projections might play similar roles in both FO and HO thalamus.

L6 CT pathways to FO and HO thalamus

L6CT projections to FO nuclei like the dLGN have been the focus of considerable interest in the field. Any number of these projections' unique features may account for this interest, such as their "feedback" nature, their strength in numbers (accounting for the largest proportion of synapses in the dLGN) and their unique engagement of the thalamic reticular nucleus (TRN)[11,21]. This latter feature is especially noteworthy because the TRN in turn sends GABAergic projections to other thalamic nuclei – including both the dLGN and the pulvinar[6,22]. Thus, L6CTs are capable not only of monosynaptically exciting, but also disynaptically inhibiting, their thalamic targets. This raises questions as to how these excitatory and inhibitory influences are balanced and whether that balance might shift under different circumstances.

There has been considerable debate over what kind of influence L6CT feedback has in FO thalamus. On one hand, a handful of studies that used optogenetics to stimulate V1 L6CTs in anesthetized mice observed pronounced suppression of activity in the dLGN[23,24]. These observations suggested a net inhibitory influence of L6CT feedback in the dLGN, likely mediated by engagement of the TRN. On the other hand, other studies in more recent years have highlighted the complicated nature of L6CT feedback that cannot easily be distilled down to "excitatory" or "inhibitory". For instance, in awake mice, whether L6CT stimulation excites or suppresses activity in FO thalamus has been shown to depend on the topographic alignment between cortical L6CT and thalamic cells. Specifically, L6CTs directly excite topographically matched neurons in the FO thalamus and indirectly inhibit unmatched neurons,

apparently through their broad excitation of the TRN[25]. Moreover, experiments conducted in the somatosensory slice preparation demonstrated that the TRN also plays a key role in a frequency-dependent shift between a net-inhibitory or net-excitatory L6CT influence over FO thalamus[26]. Other studies in awake mice have identified other temporal factors that determine the direction of L6CT modulation as well[27]. Overall, there is much that still needs to be understood about how L6CTs influence FO thalamic activity under various conditions and the mechanisms that underlie their apparent flexibility.

Moreover, the contribution of L6CTs to HO thalamic nuclei like the pulvinar has not previously been explored in an awake animal, leaving open the question of what role type 1 CT inputs play in HO compared to FO thalamus. Although their shared morphological and physiological properties could belie similar functions, they also differ in their cortical distribution (whether they come from primary and/or higher-order cortical areas)[14,28–30] and their relative prevalence compared to type 2 inputs[31,32]. Furthermore, recent work has revealed how largely separate sectors of the TRN are reciprocally connected with FO versus HO nuclei[33,34], raising the possibility of major differences in how the TRN is disynaptically engaged by L6CTs to influence each class of nuclei. Thus, whether shared synaptic and morphological features of diverging L6CT projections to FO and HO thalamic nuclei are indicative of common functional influence is not presently known.

"Driver" versus "modulator" corticothalamic pathways

In contrast to HO thalamic nuclei, type 1 and type 2 inputs to FO nuclei are known to come from different sources and to play fundamentally different roles. Specifically, the dLGN inherits its visual response properties from retinal ganglion cells (RGCs) with type 2 synaptic features, rather than from their type 1, L6CT inputs[35]. For this reason, type 2 inputs have been termed "drivers", since RGCs "drive" receptive fields in the dLGN[36–38]. On the other hand, type 1 inputs are deemed "modulators" because they are not strictly necessary for the dLGN's visual response properties but instead exert more subtle influences[35,38]. It is noteworthy that these distinct "driving" versus "modulatory" functions of RGC versus

L6CT inputs to the dLGN bear some resemblance to the two possible roles of centrifugal connections proposed by Cajal in 1906[1].

What, then, can be said of the distinct type 1 and type 2 CT inputs to the pulvinar and other HO nuclei? Because of their similarities to the different synapse types that are found in the dLGN, L5CT and L6CT projections to HO nuclei are routinely referred to as "drivers" and "modulators", respectively[17,39]. However, their functions have never been directly assessed, likely because of the technical difficulties associated with selectively manipulating one or the other CT population. This is fundamentally different from the dLGN, whose "driver" and "modulatory" inputs are physically segregated between the retina and the cortex. Consequently, studies have specifically manipulated cortical activity – through ablation, cooling, electrical stimulation or optogenetics – and conclusively shown that the dLGN does not depend on its cortical inputs – which only come from L6CTs - for its visual response properties[23,40–43]. In contrast, the relatively few studies that have assessed the effects of cortical manipulation on pulvinar activity have found that many pulvinar neurons depend on their cortical inputs for visual drive[44–47], and this is at least true of the HO somatosensory nucleus, POm, as well[48,49]. However, when considering HO nuclei, these broad approaches for cortical manipulation cannot distinguish between the contributions of L6CTs versus L5CTs. Thus, whether these different CT pathways truly serve separable "driving" versus "modulatory" functions has never been directly tested.

This dissertation seeks to address these various questions pertaining to the roles that CT projections play in both FO and HO nuclei. As our model system, we focus on the CT projections from the mouse primary visual cortex to the dLGN (FO) and the pulvinar (HO), as the visual system has proved to be a fruitful area for studying and generating hypotheses about CT circuitry and excitatory connectivity more broadly[35,38]. Chapter 1 focuses on the L6CT pathways to different classes of thalamic nuclei, describing how optogenetic L6CT stimulation has similar effects in both the dLGN and pulvinar but also highlighting the complex, dynamic nature of L6CT influence in both nuclei. In Chapter 2, we turn to the question of the proposed "driving" versus "modulatory" functions of L5CT versus L6CT

pathways to the HO thalamus. By selectively, optogenetically inactivating these distinct pathways, we find evidence that they do, indeed, differ considerably in the extent to which they convey visual information to the pulvinar. We thus provide compelling evidence in support of longstanding hypotheses about their distinct functions based on their distinct anatomical and physiological properties. Altogether, this dissertation aims to reveal organizing principles of corticothalamic functional connectivity and to inspire new hypotheses about how these circuit features are important for sensory processing in the awake, behaving animal.

References

1. Cajal, S. R. y. The Structure and Connexions of Neurons - Nobel Lecture. (1906).

2. Menon, V. Developmental pathways to functional brain networks: emerging principles. *Trends Cogn Sci* **17**, 627–640 (2013).

3. Parnaudeau, S., Bolkan, S. S. & Kellendonk, C. The Mediodorsal Thalamus: An Essential Partner of the Prefrontal Cortex for Cognition. *Biological Psychiatry* **83**, 648–656 (2017).

4. Abbott, L. F., Bock, D. D., Callaway, E. M., Denk, W., Dulac, C., Fairhall, A. L., Fiete, I., Harris, K. M., Helmstaedter, M., Jain, V., Kasthuri, N., LeCun, Y., Lichtman, J. W., Littlewood, P. B., Luo, L., Maunsell, J. H. R., Reid, R. C., Rosen, B. R., Rubin, G. M., Sejnowski, T. J., Seung, H. S., Svoboda, K., Tank, D. W., Tsao, D. & Essen, D. C. V. The Mind of a Mouse. *Cell* **182**, 1372–1376 (2020).

5. Bargmann, C. I. & Marder, E. From the connectome to brain function. *Nat Methods* **10**, 483–490 (2013).

6. Jones, E. G. *The Thalamus*. (Plenum Press, 1985). doi:10.1007/978-1-4615-1749-8_15.

7. Shipp, S. The functional logic of corticopulvinar connections. *Philosophical Transactions of the Royal Society of London. Series B: Biological Sciences* **358**, 1605–24 (2003).

8. Halassa, M. M. & Kastner, S. Thalamic functions in distributed cognitive control. *Nature neuroscience* **20**, 1669–1679 (2017).

9. Halassa, M. M. & Sherman, S. M. Thalamocortical Circuit Motifs: A General Framework. *Neuron* **103**, 762–770 (2019).

10. Harris, K. D. & Shepherd, G. M. The neocortical circuit: themes and variations. *Nature neuroscience* **18**, 170–81 (2015).

11. Briggs, F. & Usrey, W. M. Emerging views of corticothalamic function. *Current opinion in neurobiology* **18**, 403–7 (2008).

12. Bourassa, J., Pinault, D. & Deschênes, M. Corticothalamic Projections from the Cortical Barrel Field to the Somatosensory Thalamus in Rats: A Single-fibre Study Using Biocytin as an Anterograde Tracer. *Eur J Neurosci* **7**, 19–30 (1995).

13. Bourassa, J. & Deschênes, M. Corticothalamic projections from the primary visual cortex in rats: a single fiber study using biocytin as an anterograde tracer. *Neuroscience* **66**, 253–63 (1995).

14. Roth, M. M., Dahmen, J. C., Muir, D. R., Imhof, F., Martini, F. J. & Hofer, S. B. Thalamic nuclei convey diverse contextual information to layer 1 of visual cortex. *Nature neuroscience* **19**, 299–307 (2016).

15. Nakamura, H., Hioki, H., Furuta, T. & Kaneko, T. Different cortical projections from three subdivisions of the rat lateral posterior thalamic nucleus: a single-neuron tracing study with viral vectors. *The European journal of neuroscience* **41**, 1294–310 (2015).

16. Rouiller, E. M. & Welker, E. A comparative analysis of the morphology of corticothalamic projections in mammals. *Brain Research Bulletin* **53**, 727–41 (2000).

17. Sherman, S. M. Thalamus plays a central role in ongoing cortical functioning. *Nature Neuroscience* **16**, (2016).

18. Jones, E. G. Viewpoint: the core and matrix of thalamic organization. *Neuroscience* **85**, 331–345 (1998).

19. Bickford, M. E. Thalamic Circuit Diversity: Modulation of the Driver/Modulator Framework. *Frontiers in neural circuits* **9**, 86 (2015).

20. Reichova, I. & Sherman, S. M. Somatosensory corticothalamic projections: distinguishing drivers from modulators. *Journal of neurophysiology* **92**, 2185–97 (2004).

21. Briggs, F. Role of Feedback Connections in Central Visual Processing. *Annu Rev Vis Sc* **6**, 1–22 (2020).

22. Conley, M. & Diamond, I. T. Organization of the Visual Sector of the Thalamic Reticular Nucleus in Galago. *The European journal of neuroscience* **2**, 211–226 (1990).

23. Olsen, S. R., Bortone, D. S., Adesnik, H. & Scanziani, M. Gain control by layer six in cortical circuits of vision. *Nature* **483**, 47–52 (2012).

24. Denman, D. J. & Contreras, D. Complex Effects on In Vivo Visual Responses by Specific Projections from Mouse Cortical Layer 6 to Dorsal Lateral Geniculate Nucleus. *The Journal of neuroscience : the official journal of the Society for Neuroscience* **35**, 9265–80 (2015).

25. Born, G., Erisken, S., Schneider, F. A., Klein, A., Mobarhan, M. H., Lao, C. L., Spacek, M. A., Einevoll, G. T. & Busse, L. Corticothalamic feedback sculpts visual spatial integration in mouse thalamus. *Biorxiv* 2020.05.19.104000 (2020) doi:10.1101/2020.05.19.104000.

26. Crandall, S. R., Cruikshank, S. J. & Connors, B. W. A corticothalamic switch: controlling the thalamus with dynamic synapses. *Neuron* **86**, 768–82 (2015).

27. Guo, W., Clause, A. R., Barth-Maron, A. & Polley, D. B. A Corticothalamic Circuit for Dynamic Switching between Feature Detection and Discrimination. *Neuron* **95**, 180-194.e5 (2017).

28. Blot, A., Roth, M. M., Gasler, I. T., Javadzadeh, M., Imhof, F. & Hofer, S. B. Visual intracortical and transthalamic pathways carry distinct information to cortical areas. *Biorxiv* 2020.07.06.189902 (2020) doi:10.1101/2020.07.06.189902.

29. Souza, B. O. F. de, Frigon, É., Tremblay-Laliberté, R., Casanova, C. & Boire, D. Laminar distribution of cortical projection neurons to the pulvinar: A comparative study in cats and mice. *J Comp Neurol* (2020) doi:10.1002/cne.25072.

30. Scholl, L. R., Foik, A. T. & Lyon, D. C. Projections between visual cortex and pulvinar in the rat. *J Comp Neurol* (2020) doi:10.1002/cne.24937.

31. Wang, S., Eisenback, M. A. & Bickford, M. E. Relative distribution of synapses in the pulvinar nucleus of the cat: implications regarding the "driver/modulator" theory of thalamic function. *The Journal of comparative neurology* **454**, 482–94 (2002).

32. Horn, S. C. V. & Sherman, S. M. Fewer driver synapses in higher order than in first order thalamic relays. *Neuroscience* **146**, 463–70 (2007).

33. Li, Y., Lopez-Huerta, V. G., Adiconis, X., Levandowski, K., Choi, S., Simmons, S. K., Arias-Garcia, M. A., Guo, B., Yao, A. Y., Blosser, T. R., Wimmer, R. D., Aida, T., Atamian, A., Naik, T., Sun, X., Bi, D., Malhotra, D., Hession, C. C., Shema, R., Gomes, M., Li, T., Hwang, E., Krol, A., Kowalczyk, M., Peça, J., Pan, G., Halassa, M. M., Levin, J. Z., Fu, Z. & Feng, G. Distinct subnetworks of the thalamic reticular nucleus. *Nature* **583**, 819–824 (2020).

34. Martinez-Garcia, R. I., Voelcker, B., Zaltsman, J. B., Patrick, S. L., Stevens, T. R., Connors, B. W. & Cruikshank, S. J. Two dynamically distinct circuits drive inhibition in the sensory thalamus. *Nature* **583**, 813–818 (2020).

35. Sherman, S. M. & Guillery, R. W. Functional organization of thalamocortical relays. *Journal of neurophysiology* **76**, 1367–95 (1996).

36. Cleland, B. G., Dubin, M. W. & Levick, W. R. Sustained and transient neurones in the cat's retina and lateral geniculate nucleus. *The Journal of physiology* **217**, 473–96 (1971).

37. Usrey, W. M., Reppas, J. B. & Reid, R. C. Specificity and strength of retinogeniculate connections. *Journal of neurophysiology* **82**, 3527–40 (1999).

38. Sherman, S. M. & Guillery, R. W. On the actions that one nerve cell can have on another: Distinguishing "drivers" from "modulators." *Proceedings of the National Academy of Sciences* **95**, 7121–6 (1998).

39. Sherman, S. M. & Guillery, R. W. The role of the thalamus in the flow of information to the cortex. *Philosophical Transactions Royal Soc Lond Ser B Biological Sci* **357**, 1695–1708 (2002).

40. Spacek, M. A., Born, G., Crombie, D., Bauer, Y., Liu, X., Katzner, S. & Busse, L. Robust effects of corticothalamic feedback during naturalistic visual stimulation. *Biorxiv* 776237 (2020) doi:10.1101/776237.

41. Andolina, I. M., Jones, H. E. & Sillito, A. M. Effects of cortical feedback on the spatial properties of relay cells in the lateral geniculate nucleus. *Journal of neurophysiology* **109**, 889–99 (2013).

42. Andolina, I. M., Jones, H. E., Wang, W. & Sillito, A. M. Corticothalamic feedback enhances stimulus response precision in the visual system. *Proceedings of the National Academy of Sciences of the United States of America* **104**, 1685–90 (2007).

43. Przybyszewski, A. W., Gaska, J. P., Foote, W. & Pollen, D. A. Striate cortex increases contrast gain of macaque LGN neurons. *Visual neuroscience* **17**, 485–94 (2000).

44. Casanova, C., Savard, T. & Darveau, S. Contribution of Area 17 to Cell Responses in the Striate-recipient Zone of the Cat's Lateral Posterior-Pulvinar Complex. *Eur J Neurosci* **9**, 1026–1036 (1997).

45. Bennett, C., Gale, S. D., Garrett, M. E., Newton, M. L., Callaway, E. M., Murphy, G. J. & Olsen, S. R. Higher-Order Thalamic Circuits Channel Parallel Streams of Visual Information in Mice. *Neuron* **102**, 477-492.e5 (2019).

46. Beltramo, R. & Scanziani, M. A collicular visual cortex: Neocortical space for an ancient midbrain visual structure. *Science* **363**, 64–69 (2019).

47. Bender, D. B. Visual activation of neurons in the primate pulvinar depends on cortex but not colliculus. *Brain Research* **279**, 258–261 (1983).

48. Diamond, M. E., Armstrong-James, M., Budway, M. J. & Ebner, F. F. Somatic sensory responses in the rostral sector of the posterior group (POm) and in the ventral posterior medial nucleus (VPM) of the rat thalamus: Dependence on the barrel field cortex. *J Comp Neurol* **319**, 66–84 (1992).

49. Mease, R. A., Sumser, A., Sakmann, B. & Groh, A. Cortical Dependence of Whisker Responses in Posterior Medial Thalamus In Vivo. *Cerebral Cortex* **26**, 3534–3543 (2016).

Chapter 1. Context-dependent and dynamic functional influence of corticothalamic pathways to first- and higher-order visual thalamus

Abstract

Layer 6 (L6) is the sole purveyor of corticothalamic (CT) feedback to first-order thalamus and also sends projections to higher-order thalamus, yet how it engages the full corticothalamic circuit to contribute to sensory processing in an awake animal remains unknown. We sought to elucidate the functional impact of L6CT projections from primary visual cortex to visual thalamic nuclei dLGN (first-order) and pulvinar (higher-order) using optogenetics and extracellular electrophysiology in awake mice. While sustained L6CT photostimulation suppresses activity in both visual thalamic nuclei *in vivo*, moderate-frequency (10Hz) stimulation powerfully facilitates thalamic spiking. We show that each stimulation paradigm differentially influences the balance between monosynaptic excitatory and disynaptic inhibitory corticothalamic pathways to dLGN and pulvinar as well as the prevalence of burst versus tonic firing. Altogether, our results support a model in which L6CTs modulate first- and higher-order thalamus through parallel excitatory and inhibitory pathways that are highly dynamic and context-dependent.

Introduction

While the flow of information from thalamus to cortex is widely appreciated as a critical step in sensory processing, the significance of a given cortical area's projection back to thalamus is considerably less clear. In the case of first-order nuclei, like the dorsal lateral geniculate nucleus (dLGN) in the visual system, this corticothalamic feedback originates from layer 6. Layer 6 corticothalamic neurons (L6CTs) have been classically described as providing "modulatory" feedback to dLGN[1,2] that may influence response gain[3–8], temporal precision[9,10], spatiotemporal filtering[6,10,11], sensory adaptation[12], and burst versus tonic firing modes[7,8,11,12]. Still, how these L6CTs might perform these various functions is not well understood. Moreover, many L6CTs also project to higher-order thalamus, such as the visual pulvinar (also known as the lateral posterior nucleus, or LP, in rodents)[13]. While anatomical and physiological

similarities between L6CT projections to first- and higher-order thalamus[14–16] suggest they may play similar "modulatory" functions across thalamic nuclei classes, the pathway from cortex to higher-order thalamus has not been investigated *in vivo*. Thus, many questions remain with regards to the nature of corticothalamic feedback as a general feature of sensory circuits and whether these same principles hold across different classes of thalamic nuclei.

One such question is how L6CTs influence their thalamic targets during sensory processing in an awake animal. On one hand, previous observations of dramatically reduced visual responses recorded in dLGN of anesthetized mice during V1 L6CT optogenetic activation[4,5] suggest that L6CT feedback may be fundamentally inhibitory, likely through a disynaptic inhibitory pathway through the GABAergic thalamic reticular nucleus (TRN). However, other studies in the visual as well as other sensory systems disagree, finding no change or even increased activity in first-order thalamus with L6CT photoactivation[10,17,18]. Moreover, optogenetically inactivating L6CTs has mixed effects in dLGN[5], suggesting that their natural function is not to invariably suppress their thalamic targets.

An alternative explanation could be that the level and manner of L6CTs' activation may determine how they influence their thalamic targets. For instance, the effects of L6CT optogenetic stimulation on first-order thalamus VPm in the somatosensory *in vitro* slice preparation have been shown to "switch" from being net-suppressing to net-facilitating with higher-frequency (10Hz) L6CT stimulation[19]. This frequency-dependence has been explained by the different short-term plasticity characteristics at different synapses in the full corticothalamic circuit, since the competing monosynaptic excitatory and disynaptic inhibitory (via TRN) routes to first-order thalamus are net-facilitating and net-depressing, respectively[19]. Previous studies have not used temporally controlled L6CT optogenetic manipulations in awake animals or probed *in vivo* L6CT effects on a higher-order thalamic nucleus. Therefore, it remains to be seen whether L6CT projections can exert flexible, bi-directional influence on thalamic activity in the visual system, in different classes of thalamic nuclei, and *in vivo*.

To address these questions, we have recorded extracellular single-unit activity from dLGN, pulvinar, and TRN in awake mice. We optogenetically manipulated L6CTs in primary visual cortex with

both controlled (photostimulation trains) and uncontrolled (continuous light) methods for photostimulation. While we observe similar influences of L6CTs on dLGN and pulvinar, different photostimulation conditions had strikingly different effects on thalamic firing rates, firing mode, and their balance with activity changes in the TRN. Our results thus provide novel evidence that L6CTs are capable of dynamically influencing activity in both their first-and higher-order thalamic targets.

Results

Sustained L6CT photostimulation suppresses activity in dLGN and pulvinar in vivo

Before turning to more controlled stimulation of L6CT neurons, we first tested whether previous effects observed in dLGN of the anesthetized animal during sustained L6CT photostimulation are also observed in *awake* mice. Additionally, since L6CTs are hypothesized to play similar functional roles in both first- and higher-order thalamic nuclei[1], we wondered whether effects observed in dLGN would also extend to the pulvinar. To address these questions, we injected an AAV encoding Cre-dependent ChR2-eYFP into V1 of Ntsr1-Cre GN220 transgenic mice (Methods). Consistent with prior reports of the specificity of the Ntsr1-Cre transgenic line[20,21], expression of the ChR2-eYFP fusion protein was specific to V1 layer 6 (Figure 1.1B). Corticothalamic axons expressing ChR2-eYFP were readily apparent in both dLGN and pulvinar (Figures 1.1C and 1.S1A), demonstrating that L6CTs labeled by the Ntsr1-Cre line project to both visual thalamic nuclei.

Single-unit activity was recorded in the visual thalamus of awake, head-fixed mice using high-density, multi-shank microelectrode arrays[22]. Probes were coated with lipophilic dye (DiI) in order to visualize electrode tracks and determine which thalamic nucleus was sampled by each shank (Figure 1.1C). Since the mouse pulvinar is not uniformly innervated by V1[23–25], calretinin expression was used to distinguish between pulvinar subdivisions (Figure 1.S1A). Only units recorded from shanks which passed through eYFP-labeled L6CT axons from V1 in the lateral, calretinin-negative zone of the pulvinar[24] were included for pulvinar analyses (e.g., second shank in Figure 1.1C), while units recorded more medially were treated separately (e.g., first shank in Figure 1.1C, Figure 1.S1B-E). While mice viewed square-

Figure 1.1 L6CT photostimulation with continuous light delivery suppresses activity in dLGN and pulvinar *in vivo.* (A) Experimental design. Left: diagram of the experimental setup and trial structure for visual and LED stimulation. Right: schematic of the L6 corticothalamic circuit, indicating recording and LED stimulation locations. (B) Coronal section depicting ChR2-eYFP cell body expression in V1 L6 and apical dendrites in L4 of a Ntsr1-Cre mouse injected with AAV5-DIO-ChR2-eYFP. Scale bar = 500μm. (C) Coronal section of the visual thalamus, depicting ChR2-eYFP-positive axon terminals in dLGN and pulvinar. Recording tracks from a four-shank probe are labeled with DiI (red). Immunohistochemical staining for calretinin (purple) provides borders from lateral pulvinar to dLGN and medial pulvinar. Scale bar = 500μm. (D) Two example dLGN units. Left panels: raster plots with trials organized by LED condition (trials with different conditions were interspersed during the actual experiment). The shaded area indicates photostimulation period (0.5-1.5s following visual stimulus onset). Middle panels: peristimulus time histograms (PSTHs) of average firing rates during visual trials for each condition, shown over time relative to visual stimulus onset. Right panels: PSTHs of average firing rates during blank trials (grey screen). (E) Average firing rates during the 1-second photostimulation period from visual trials, with versus without medium-intensity L6CT photostimulation. Inset: expanded scatter plot from area within the square (0-20 spks/s). Saturated points indicate visually responsive units. (F) Light modulation index (<0 suppressed, >0 activated) by depth (distance from highest channel on the probe with a visually responsive unit). (G) Average normalized PSTH (normalized to each unit's prestimulus firing rate) across all dLGN units. Shading indicates ± 1 standard error of the mean. (H) Proportions of units which were significantly suppressed or activated in two or more conditions (units not passing these criteria considered "other"). (I-M) Same as (D-H) but for units recorded in lateral pulvinar.

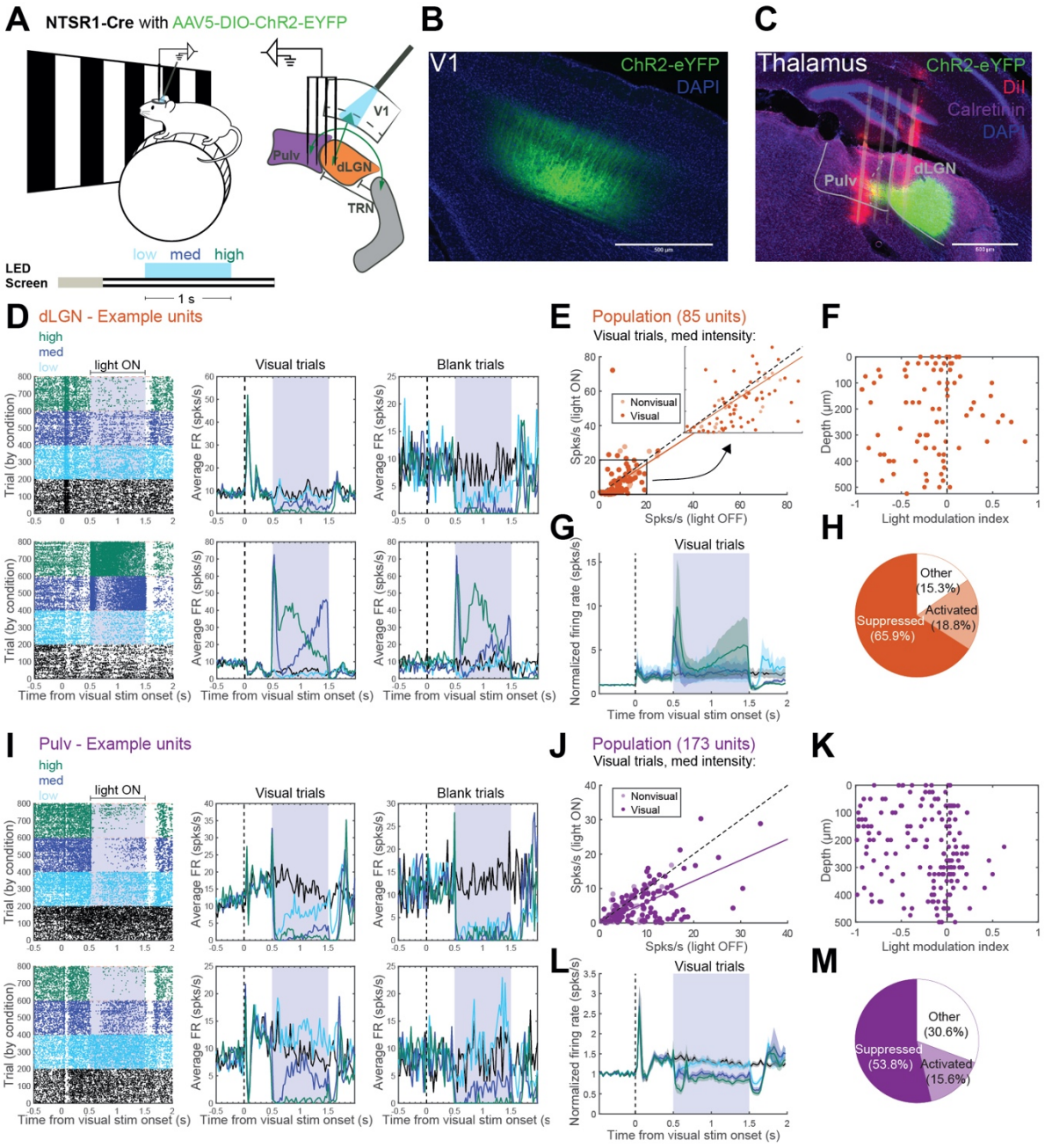
A
NTSR1-Cre with AAV5-DIO-ChR2-EYFP
V1
Pulv
dLGN
TRN
low med high
LED
Screen
1 s
B
V1
ChR2-eYFP
DAPI
C
Thalamus
ChR2-eYFP
DiI
Calretinin
DAPI
Pulv
dLGN
D
dLGN - Example units
high
med
low
light ON
Visual trials
Blank trials
Trial (by condition)
Average FR (spks/s)
Time from visual stim onset (s)
E
Population (85 units)
Visual trials, med intensity:
Nonvisual
Visual
Spks/s (light ON)
Spks/s (light OFF)
F
Depth (µm)
Light modulation index
G
Visual trials
Normalized firing rate (spks/s)
Time from visual stim onset (s)
H
Other (15.3%)
Activated (18.8%)
Suppressed (65.9%)
I
Pulv - Example units
high
med
low
light ON
Visual trials
Blank trials
Trial (by condition)
Average FR (spks/s)
Time from visual stim onset (s)
J
Population (173 units)
Visual trials, med intensity:
Nonvisual
Visual
Spks/s (light ON)
Spks/s (light OFF)
K
Depth (µm)
Light modulation index
L
Visual trials
Normalized firing rate (spks/s)
Time from visual stim onset (s)
M
Other (30.6%)
Suppressed (53.8%)
Activated (15.6%)

wave drifting gratings (“Visual trials”, see Methods) or a gray screen (“Blank trials”), ChR2-expressing cell bodies in V1 were stimulated with one second of sustained blue LED light at three different intensities (“low”, "medium", and “high”, Figure 1.1A; see Methods). This allowed us to further probe the possibility that different degrees of L6CT stimulation might account for the variety of results previously observed with sustained light delivery[4,5,17,18]. We also conducted V1 recordings in a subset of AAV-injected Ntsr1-Cre mice to verify that sustained light delivery was activating L6CTs (Figures 1.S2A-F).

Consistent with prior reports in anesthetized mice[4,5], L6CT photostimulation with sustained light delivery at all intensities significantly suppressed visually evoked firing rates (first example unit, Figure 1.1D; n=85 single-units from 7 shanks in 4 animals, Figures 1.1E-H) in dLGN of awake mice ($p \leq 0.003$ for visual trials with vs. without LED in all light conditions, Wilcoxon signed-rank tests). Suppression of spontaneous dLGN firing rates was also significant with high-level light stimulation (first example unit, Figure 1.1D, right; population, Figures 1.S3A-D; p=0.054, 0.056, 0.008 for low, med, and high LED vs. no LED). We also found that lateral pulvinar activity (first example unit, Figure 1.1I; n=173 single-units from 10 shanks in 6 animals, Figure 1.1J-M) was strongly suppressed by L6CT photostimulation during visual trials as well as blank trials (Figures 1.S3E-G) at all light levels ($p<0.001$ for visual and blank trials in all LED conditions). In contrast, units recorded in the calretinin-expressing, medial area of pulvinar that lacks direct L6CT input from V1[24] were considerably less visually responsive or modulated by LED stimulation (Figure 1.S1). There was some heterogeneity among units in both thalamic nuclei (see second example units in Figures 1.1D and I), but especially in dLGN where a subset of units that tended to be close to each other along the dorsal-ventral axis of dLGN were strongly activated at higher light levels (Figure 1.1F). While these strongly activated units in dLGN obscure the average normalized peristimulus time histograms across units (Figures 1.1G and L), the majority of units in dLGN (56/85, 65.88%) and lateral pulvinar (93/173, 53.76%) were significantly suppressed by L6CT photostimulation (Figures 1.1H and M). Consistent with some prior reports of firing mode changes in first-order thalamus by sustained L6CT photostimulation[4,12], all light intensities significantly decreased the rate of bursting in dLGN (Figure 1.S4D; $p<0.001$, <0.001, $=0.003$ for low, med and high LED vs. no LED). Bursting in pulvinar

also decreased with low-level photostimulation (Figures 1.S4A and E; $p<0.001$) but was unchanged with medium-level and increased with high-level photostimulation ($p=0.911$, <0.001). Light-induced changes in activity were not observed in dLGN or pulvinar units recorded from uninjected control animals (Figures 1.S3H-N), demonstrating that they were due solely to specific manipulation of L6CT activity. Thus, we demonstrate for the first time *in vivo* that visually evoked and spontaneous activity in pulvinar, much like in anesthetized[4,5] and awake dLGN (our data), is suppressed by sustained L6CT photostimulation.

L6CT photostimulation trains reveal frequency-dependent effects in dLGN and pulvinar

While our experiments with continuous light delivery for L6CT activation demonstrate L6CTs' ability to suppress their first- and higher-order thalamic targets, can they also modulate thalamic activity in other ways? Continuous light delivery is a relatively uncontrolled method for photostimulation, and our own V1 recordings demonstrate variable effects of continuous light on L6 units' activity that sometimes exceeded physiologically relevant levels (Figures 1.S2C-F). To overcome some of the shortcomings of continuous LED stimulation and to test for possible frequency-dependent influences that have been described *in vitro*[19], we used a train stimulation paradigm (Figure 1.2A; 10ms LED pulses at 1, 10, and 20 or 40 Hz for 1 second) to stimulate L6CT cell bodies during the same dLGN and pulvinar single-unit recording sessions from Figure 1.1. We hypothesized that subsequent stimulation pulses in a 10Hz stimulation train, and perhaps also at higher frequencies, would produce increasing spike outputs in thalamus as demonstrated in the somatosensory system *in vitro*[19].

Indeed, in both dLGN and pulvinar, we consistently observed facilitating spiking following subsequent pulses in a 10Hz train (example units in Figures 1.2B-C). Whereas a single photostimulation pulse elicited at most a weak and short-lived response, this response increased dramatically with further 10Hz stimulation pulses. The facilitation effect for each unit can be quantified by comparing the number of spikes following any pulse in the train to the number of spikes after the first pulse; thus, spike count ratios greater than 1 indicate facilitating spiking. Of the units recorded in dLGN and pulvinar that

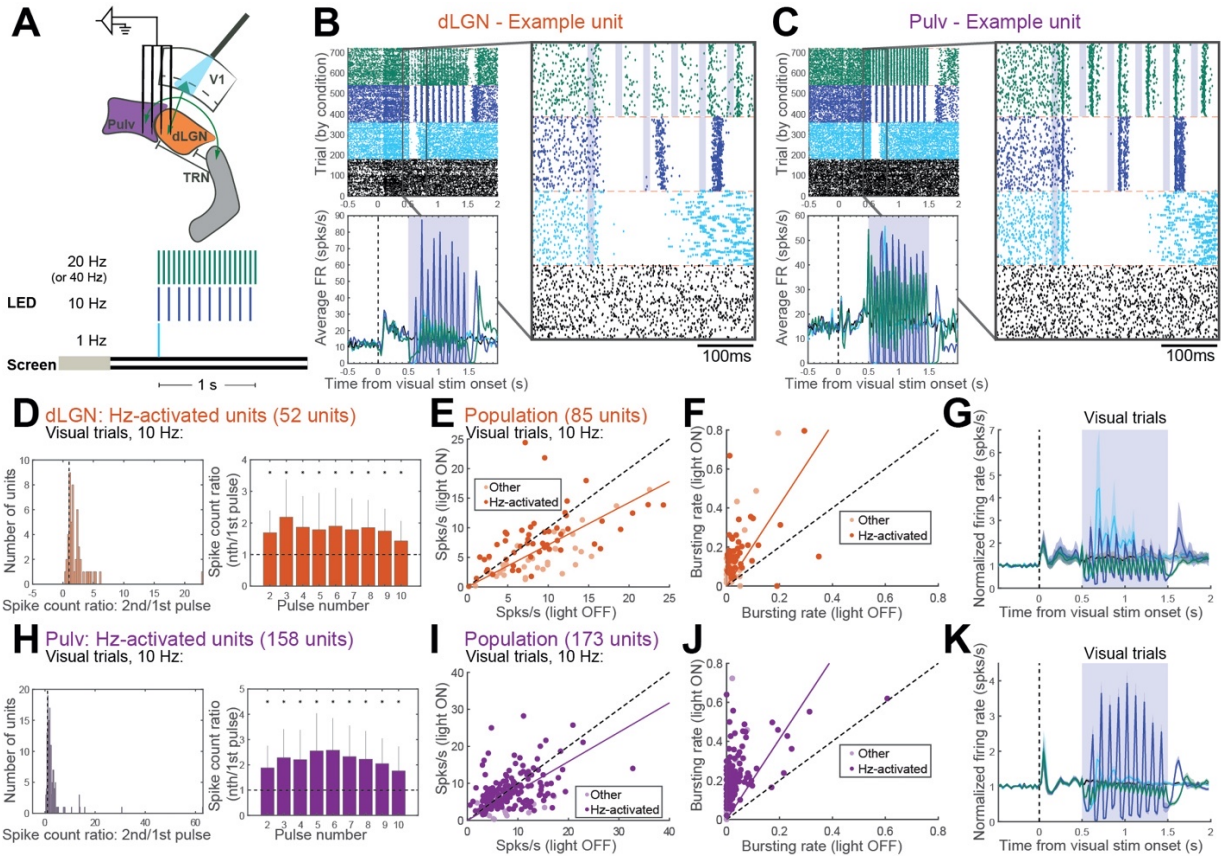

Figure 1.2 10Hz photostimulation of L6CTs facilitates spiking and increases bursting in dLGN and pulvinar. (A) Diagram of photostimulation and dLGN/pulvinar recording configuration and trial structure for visual and LED stimulation. (B) An example unit recorded in dLGN. Left: raster plot (top) and PSTH of average firing rates across visual trials (bottom). Right: zoomed-in image of boxed part of raster plot (100ms before to 300ms after LED photostimulation onset). Shaded rectangles indicate 10ms photostimulation pulses. (C) Same as (B) but for an example unit recorded in lateral pulvinar (same example unit as in Figure 1.1I, top). (D) Quantification of facilitating spiking during 10Hz photostimulation trials across Hz-activated units in dLGN (see Methods for "Hz-activated" unit classification). Left: histogram of spike count ratios (spike outputs following the second photostimulation pulse relative to the first in a 10Hz train). Right: median spike count ratios across Hz-activated units, comparing spike outputs following photostimulation pulses 2-10 relative to the first pulse. Asterisks indicate ratios significantly different from 1 (p's <0.002, sign test), and error bars indicate interquartile range. (E) Average firing rates during the 1-second photostimulation period from visual trials, with versus without 10Hz photostimulation. Saturated points indicate Hz-activated units included in quantification in (D). (F) Average bursting rates (number of spikes that occurred during bursts / total number of spikes during 1s photostimulation period across trials) for all units during visual trials with and without L6CT photostimulation. (G) Average normalized PSTH from visual trials across all dLGN units. Shading indicates ±1 standard error of the mean. (H-K) Same as (D-G) but for pulvinar.

exhibited spiking responses to individual 10Hz light pulses (52/85 and 158/173 units considered "Hz-activated" in dLGN and pulvinar, respectively; Methods), the majority had spike count ratios (pulse 2/pulse 1) much greater than 1, and median spike count ratios were greater than 1 for all subsequent pulses (Figures 1.2D and H; p's<0.002, sign test). These same signatures of facilitating spiking were absent from laminar recordings in V1 (Figures 1.S2J and L), indicating that this phenomenon is particular to L6 corticothalamic (as opposed to intracortical) synapses. Notably, the example pulvinar unit (Figure 1.2C) is the same unit depicted in Figure 1.1I (top); while it was strongly suppressed by sustained photostimulation, it exhibited facilitating spiking when driven by 10Hz photostimulation. In fact, the majority of units in each thalamic nucleus that were significantly suppressed by sustained L6CT photostimulation demonstrated spike facilitation (spike count ratio >1) with 10Hz photostimulation (30/56 and 78/93 in dLGN and pulvinar, respectively). Some thalamic units (like those depicted in Figures 1.2B-C) also exhibited facilitating spiking at 20Hz, but this was less consistent across units (Figures 1.S5A-C).

While facilitatory spiking was observed in both dLGN and pulvinar directly following the photostimulation pulses, the effects of 10-20Hz L6CT photostimulation on average thalamic firing rates across the full photostimulation period were, if anything, significantly suppressive in dLGN (Figure 1.2E; p=0.07, <0.001, <0.001 for 1Hz, 10Hz and 20-40Hz vs. no LED in visual trials, p's≤0.004 in blank trials, Wilcoxen signed-rank tests) and approaching significance in pulvinar (Figure 1.2I; p=0.001, 0.054, <0.001 in visual trials, p<0.001, 0.068 and <0.001 in blank trials) due to the bursting nature of their spike outputs which closely followed the stimulation pulses. In fact, and in contrast to the effects of continuous L6CT photostimulation, the incidence of burst (as opposed to tonic) spikes increased dramatically under each train photostimulation condition in both dLGN (Figures 1.2F and 1.S4H; p's<0.001 for 1Hz, 10Hz and 20Hz) and pulvinar (Figures 1.2J, 1.S4B and 1.S4I; p's ≤0.001). Therefore, moderate-frequency (10Hz) L6CT photostimulation profoundly alters the firing mode and facilitates the spiking responses of their thalamic targets (Figures 1.2G and K) – even among those which are suppressed by the same pathway under different conditions.

L6CT axon terminal stimulation does not suppress dLGN and pulvinar

To begin to explore potential circuit mechanisms underlying the context-dependent effects of L6CT photostimulation, we recorded from dLGN and/or pulvinar using a two-shank "optrode" (Figures 1.3A and F; Methods) that delivers blue light at the same site as the recording contacts[22]. We hypothesized that by directly photostimulating ChR2-expressing L6CT axon terminals within the dLGN and/or pulvinar instead of their cortical cell bodies, the TRN would not be directly engaged and thus inhibition of dLGN and pulvinar would be greatly reduced. Indeed, sustained (1-second) L6CT axon terminal stimulation elicited responses in dLGN and pulvinar that were very different from what we previously observed with L6CT cell body stimulation (example units, Figures 1.3B and G; dLGN and pulvinar populations, Figures 1.3E and J). In experiments that included at least one shank in dLGN (n=88 single-units from 5 shanks in 4 animals), light levels had to be carefully titrated because aberrant activity was observed in dLGN if the light intensity was too high (Methods). This likely reflects the much higher density of L6CT axon terminals in dLGN versus pulvinar[14]. Because of this, lower light levels were used in recordings that included dLGN, and in these instances the ramp-like increase in activity in pulvinar was largely absent (Figures 1.S6A-D). Under these stimulation conditions, effects of terminal stimulation on dLGN activity were variable (Figure 1.3C; p=0.316, 0.003 and 0.498, visual trials with low, ramp to high and high LED vs. no LED; p=0.002, <0.001, 0.752, blank trials). In experiments where both recording shanks were in the pulvinar (Figure 1.3F; n=129 single-units from 6 shanks in 3 animals), higher light levels resulted in significant enhancement of pulvinar activity (Figure 1.3H; p=0.001 (reduced activity), visual trials with low LED vs. no LED; p=0.067, <0.001 (increased activity), visual trials with med and high LED vs. no LED; p=0.185, <0.001, <0.001 (increased activity), blank trials with low, med and high LED vs. no LED). As with the subset of facilitated units in dLGN from cell body stimulation (Figure 1.1F), units that were activated by L6CT axon terminal stimulation in both nuclei were also spatially clustered along the dorsal-ventral axis (Figures 1.3D and I). Similar to the effects of L6CT cell body train stimulation (Figure 1.2), the rate of bursting was also significantly increased by terminal stimulation in both dLGN and pulvinar (Figures 1.S6E-G; p's <0.001). These changes in thalamic activity were not seen

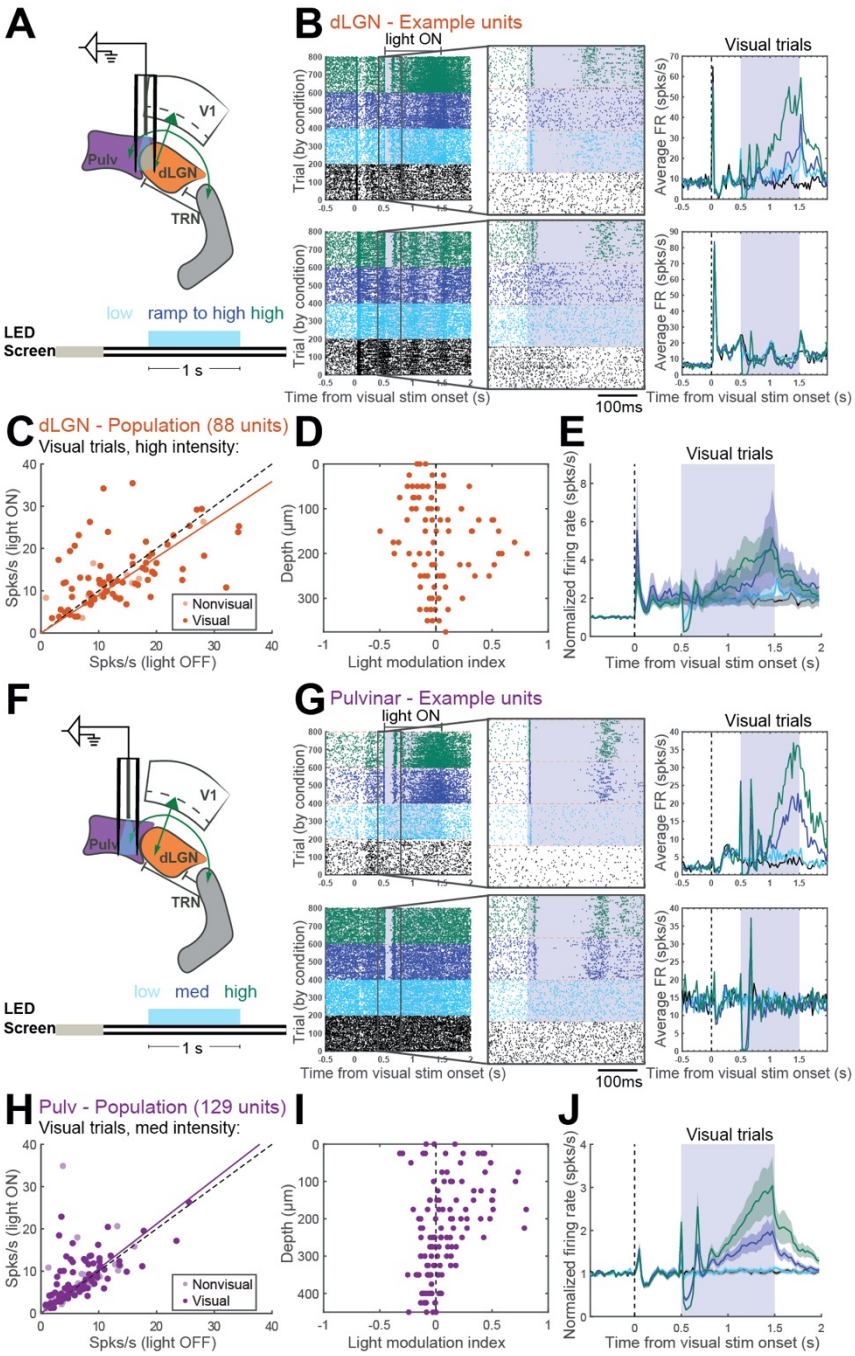

Figure 1.3 Photostimulation of L6CT axon terminals in dLGN/pulvinar does not suppress activity in visual thalamic nuclei. (A) Diagram of optrode configuration and trial structure for visual and LED stimulation. (B) Two example dLGN units. Left panels: raster plots. Middle panels: zoomed-in images of boxed parts of raster plots (from 100ms before to 300ms after LED stimulation onset). Right panels: PSTHs of average firing rates during visual trials. (C) Average firing rates during the 1-second photostimulation period from visual trials, with versus without high-intensity L6CT photostimulation. (D) Light modulation index by depth within dLGN. (E) Average normalized PSTH from visual trials across all dLGN units. Shading indicates ± 1 standard error of the mean. (F-J) Same as (A-E) but for units recorded in lateral pulvinar, during experiments in which the optrode was entirely in the pulvinar and higher light levels were used (see Methods).

in an optrode recording from a control mouse (Figures 1.S6H-K), demonstrating that they were not due to the light itself or to damage from the optrode.

Overall, stimulation of L6CT terminals elicited similar changes to visually evoked and spontaneous activity in dLGN and pulvinar (Figures 1.3E and J), and these changes were qualitatively very different from the activity changes recorded in dLGN and pulvinar following L6CT cell body stimulation (Figure 1.1). Although L6CT terminal stimulation may have antidromically activated L6CT cell bodies[26], the fact that L6CT cell body versus terminal photostimulation evoked very different effects on recorded thalamic activity argues that antidromic activation, if present, was weak. Thus, these results demonstrate that the potent inhibitory effects observed from continuous L6CT cell body photostimulation are a consequence of the larger L6 corticothalamic circuit, likely including the TRN.

Consistent with the known facilitating nature of direct L6CT-dLGN projections[15,27], 10-20Hz train stimulation of L6CT axon terminals also produced spike facilitation and increased bursting in dLGN (Figures 1.S5E-I). The absence of facilitation by terminal stimulation in lateral pulvinar (Figures 1.S5J-N) may be due to multiple factors relating to the lower density of terminals in pulvinar relative to dLGN[14]. First, light levels in these experiments were optimized for dLGN, which may have been sub-optimal for pulvinar. Second, ChR2 delivered to axons has been shown to incompletely recruit axons under moderate-to-high (10-40Hz) stimulation conditions, which can cause decreasing axon activation and post-synaptic responses that resemble short-term depression even at non-depressing synapses[28]. Therefore, these terminal stimulation experiments further point towards both the TRN and local synaptic properties (i.e., facilitation) in mediating the frequency-dependent responses we observed with L6CT cell body stimulation.

L6CT photostimulation activates visTRN and also causes frequency-dependent spike facilitation

To more directly assess the role of the TRN in the L6CT circuit *in vivo*, we recorded single-unit activity in the visual sector of the TRN (visTRN) with the same L6CT cell body stimulation conditions as for dLGN and pulvinar recordings (Figure 1.4A). As one would expect if recordings were well-targeted to

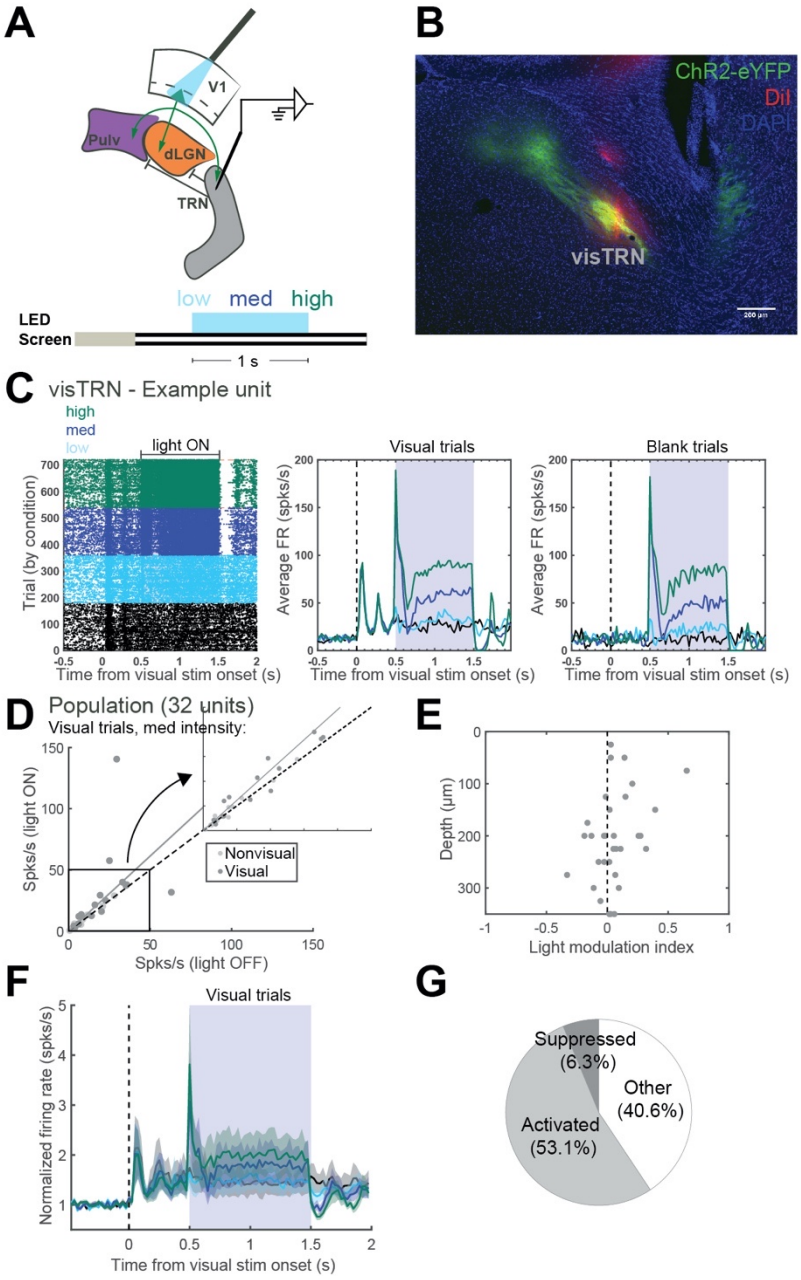

Figure 1.4 L6CT cell body photostimulation with continuous light delivery activates units in visTRN. (A) Diagram of photostimulation and visTRN recording locations and trial structure for visual and LED stimulation. (B) Coronal section depicting ChR2-eYFP-positive axon terminals in the visual sector of the thalamic reticular nucleus (visTRN) from a Ntsr1-Cre mouse injected with AAV-DIO-ChR2-eYFP. The DiI track from the recording probe (red) overlaps with the L6CT axon terminal field (green). Scale bar = 200µm. (C) Raster plot (left) and PSTHs from visual trials (middle) and from blank trials (right) for an example unit recorded in visTRN. (D) Average firing rates during the 1-second photostimulation period from visual trials, with versus without medium-intensity L6CT photostimulation. Inset: expanded scatter plot from area within the square (0-50 spks/s). (E) Light modulation index by depth within visTRN. (F) Average normalized PSTH across all visTRN units. Shading indicates ±1 standard error of the mean. (G) Proportions of units which were significantly suppressed or activated in two or more photostimulation conditions.

visTRN (Figure 1.4B), more than half (59.38%) of units were significantly visually responsive, and the majority (62.50%) exhibited fast-spiking profiles, in contrast to in dLGN (11.76%) and pulvinar (1.73%). Since the GABAergic visTRN receives axon collaterals from L6CTs in V1[13] and thus provides disynaptic inhibition to both dLGN and pulvinar[29], we hypothesized that the dominant effects of sustained L6CT photostimulation on visTRN activity would be opposite of those on dLGN and lateral pulvinar – i.e., excitatory. Moreover, since L6CT-TRN synapses are also facilitating[27,30], we predicted that moderate-frequency L6CT stimulation would cause similar spike facilitation in visTRN as in dLGN and pulvinar. Consistent with a role for disynaptic inhibition through TRN in suppressing dLGN and pulvinar during sustained L6CT cell body stimulation, many units in visTRN were rapidly and strongly activated under these conditions (example unit, Figure 1.4C; population, n=32 single-units from 4 penetrations in 3 animals, Figures 1.4D-G). At the population level, both visually evoked and spontaneous firing rates were significantly increased with L6CT photostimulation at all light levels during visual trials (Figure 1.4D; p=0.029, 0.023, 0.003 for low, med, and high LED vs. no LED) and approached significance in blank trials (p=0.014, 0.050, 0.054). Similar to observations in dLGN and pulvinar, the rate of bursting was also significantly reduced with low- and medium-intensity L6CT stimulation (Figure 1.S4F; p=0.045, 0.024, 0.754 for low, med, and high LED vs. no LED). Average visTRN population activity was increased by L6CT stimulation in a graded manner for the full duration of the photostimulation period (Figure 1.4F), and the majority (17/32, 53.13%) of units were significantly activated (Figure 1.4G). Importantly, the activation latency of the TRN population by L6CT photostimulation (Figure 1.4F) was the same as in dLGN (12ms; Figure 1.1G), which argues that the TRN was engaged monosynaptically rather than indirectly by its reciprocal connections with dLGN and pulvinar. Therefore, since visTRN is rapidly activated during sustained L6CT photostimulation and provides GABAergic input to dLGN and pulvinar, it will provide disynaptic inhibition to suppress dLGN and pulvinar under these sustained stimulation conditions.

We also observed excitatory, and in fact facilitating, responses in visTRN from 10Hz L6CT photostimulation trains (Figures 1.5A-C; p's<0.05). As with dLGN and pulvinar, 20Hz was not as

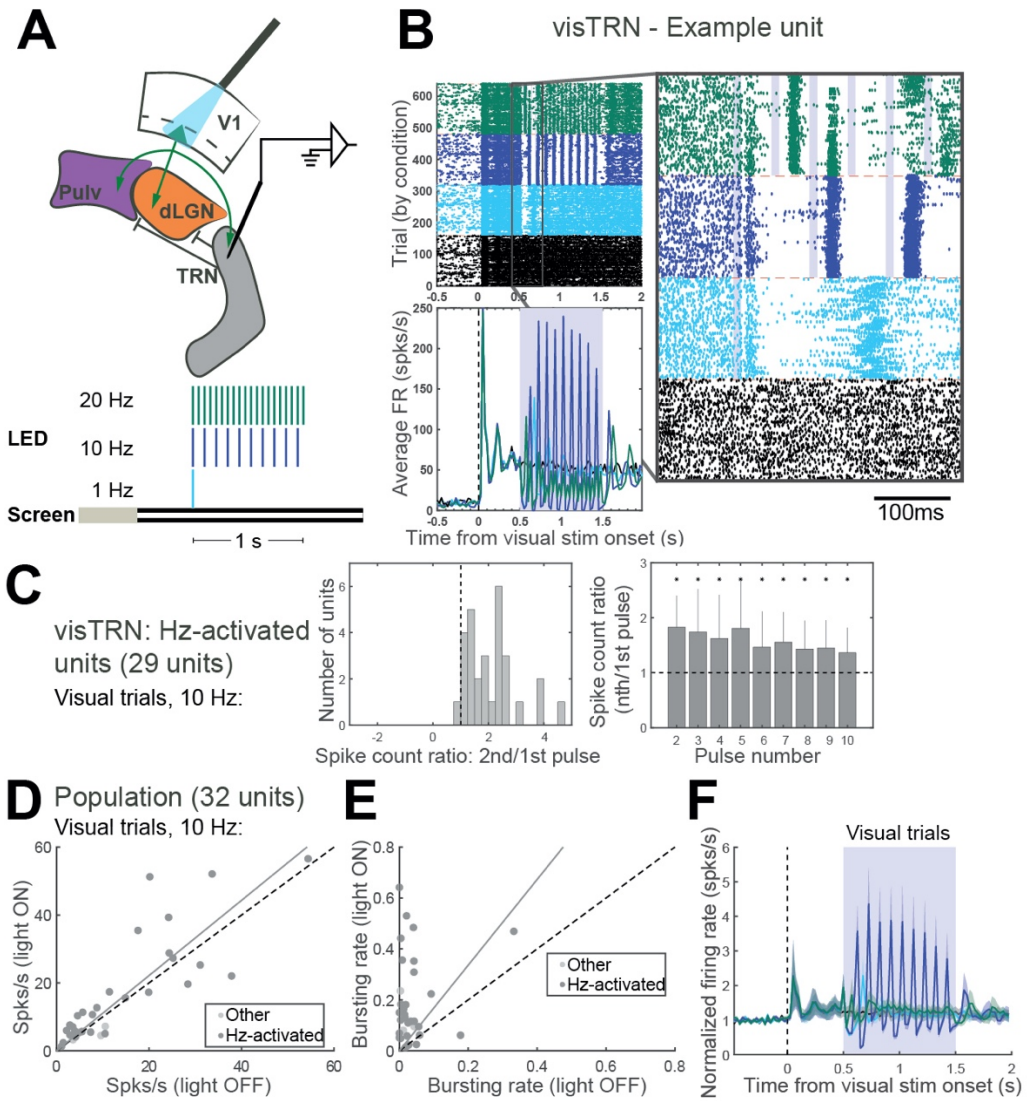

Figure 1.5 10Hz photostimulation of L6CTs also facilitates spiking and increases bursting in visTRN. (A) Diagram of photostimulation and visTRN recording configuration and trial structure for visual and LED stimulation. (B) An example unit recorded in visTRN. Left: raster plot (top) and PSTH of average firing rates across visual trials (bottom). Right: zoomed-in image of boxed part of raster plot (100ms before to 300ms after LED photostimulation onset). Shaded rectangles indicate 10ms photostimulation pulses. (C) Quantification of facilitating spiking during 10Hz photostimulation trials across Hz-activated units in visTRN. Left: histogram of spike count ratios (spike outputs following the second photostimulation pulse relative to the first in a 10Hz train). Right: median spike count ratios across Hz-activated units, comparing spike outputs following photostimulation pulses 2-10 relative to the first pulse. Asterisks indicate ratios significantly different from 1 (p's <0.05, sign test), and error bars indicate interquartile range. (D) Average firing rates during the 1-second photostimulation period from visual trials, with versus without 10Hz photostimulation. Saturated points indicate Hz-activated units included in quantification in (C). (E) Average bursting rates for all units during visual trials with and without L6CT photostimulation. (F) Average normalized PSTH from visual trials across all visTRN units. Shading indicates ±1 standard error of the mean.

effective at facilitating visTRN spiking (Figure 1.S5D), yet all conditions (1-20Hz) strongly increased the rate of bursting (Figures 1.5E and 1.S4J; $p<0.001$, $p<0.001$ and $p=0.016$ for 1Hz, 10Hz, and 20Hz). Overall, the cumulative effect of L6CT train stimulation on visTRN (Figure 1.5F) is virtually identical to that on dLGN (Figure 1.2G) and on the pulvinar (Figure 1.2K). This similarity between dLGN/pulvinar and TRN responses to L6CT train stimulation, compared to their opposite responses (suppression vs. excitation) to sustained cell body stimulation (Figure 1.1 vs. Figure 1.4), suggests that activity in dLGN and pulvinar more closely reflects their direct, excitatory inputs under moderate-frequency (e.g., 10Hz) stimulation conditions whereas the inhibitory pathway through TRN dominates under sustained conditions. In other words, these parallel monosynaptic excitatory and disynaptic inhibitory pathways from L6 to first- and higher-order thalamus are dynamically opposed, which can lead to highly flexible, context-dependent effects.

Discussion

We set out to investigate how layer 6 corticothalamic neurons (L6CTs) influence first- and higher-order thalamus, using the visual system as a model. While these corticothalamic neurons are thought to serve modulatory roles in sharpening sensory responses and enhancing thalamocortical transmission in first-order thalamus[31], how they might accomplish such functions through their different excitatory and inhibitory routes to their thalamic targets is unclear. Moreover, the nature of the pathway from layer 6 to higher-order thalamic nuclei, like the mouse pulvinar, has not previously been explored, leaving many unanswered questions as to how these corticothalamic neurons might exert similar or dissimilar modulatory control over different classes of thalamic nuclei.

Using high-density multielectrode recordings with optogenetics in awake, head-fixed mice, we find very similar effects on both dLGN and pulvinar with L6CT photostimulation, but even within nuclei these effects vary greatly with the manner and degree of stimulation. Sustained optogenetic activation of L6CTs in V1 with different levels of continuous light strongly suppresses visually evoked and spontaneous activity in dLGN and pulvinar, yet controlled 10Hz stimulation of this same population leads

to facilitating spiking in both areas. These activity changes are accompanied by changes in burst versus tonic modes of firing, which is consistent with previous reports that corticothalamic feedback can modulate thalamic firing mode[7,8,11,12,32]. Remarkably, we also observed similar facilitating spiking at 10Hz in TRN, yielding virtually indistinguishable effects between TRN and pulvinar/dLGN with L6CT train photostimulation. This stands in stark contrast to the effects on TRN and pulvinar/dLGN under sustained stimulation conditions, which were opposite in sign. These findings demonstrate the highly dynamic nature of these connections, whereby the relative balance between excitatory and inhibitory input to pulvinar and dLGN and the mode of thalamic firing can shift depending on the context of corticothalamic engagement. Therefore, describing the overall effect of the L6 corticothalamic pathway as simply suppressive or excitatory would fail to capture the functional nuance of this circuit.

Effects of L6CT activation depend on the degree and manner of their activation

Previous optogenetic experiments using Ntsr1-Cre transgenic mice under anesthesia with continuous light delivery describe a net-suppressive influence of L6CT activation on first-order visual thalamus dLGN[4,5]. We replicate these findings in awake mice and show similar effects in the pulvinar. However, other effects of L6CT optogenetic stimulation have been reported in other species and other sensory systems; in particular, no change in dLGN firing rates in anesthetized ferret[10] and increased activity in first-order auditory and somatosensory thalamic nuclei MGBv and VPm, respectively[17,18]. While these discrepant findings could plausibly be attributed to differences between species and/or sensory systems, they could also be caused by methodological incongruities. Since the majority of these studies used continuous light delivery for L6CT photostimulation, the intensity and duration of light stimulation, as well the level of viral expression, could all influence their reported observations. For instance, although we found significant population-level suppression of thalamic activity with each of our chosen light intensities, there was some heterogeneity such that some units' activity changed in opposite directions with different light intensities (e.g., bottom examples unit in Figure 1.1D and I). Thus, in combination with our train stimulation experiments with the same population of neurons, our results can

help reconcile some of these prior conflicting findings by illustrating how the complex nature of L6 corticothalamic circuitry can lead to very different downstream effects under different contexts of L6CT activity. This is particularly relevant in light of the fact that L6CT neurons have very low spontaneous firing rates, are highly orientation tuned[33] and can fire at rates around 10Hz *in vivo* in response to their preferred visual stimuli[34]. Brain states, such as arousal, have also been shown to increase L6CT activity[34]. Therefore, our findings suggest that different degrees of L6CT engagement under normal physiological conditions and in different behavioral contexts could have significant ramifications for cortico-thalamocortical signaling.

Another important factor that may determine how L6CTs influence their thalamic targets is their topographic alignment. A limitation of ours and other rodent L6CT optogenetic studies[4,5,12,17,18] is the use of broad ChR2 expression and photoactivation of many L6CTs across retinotopic, tonotopic, or somatotopic locations. Some evidence suggests that inhibition is broader than topographically aligned excitation in cat dLGN[35] and rat VPm[36]. Thus, it is entirely possible that our broad activation of L6CTs throughout V1, our use of full-field visual stimuli, and simultaneous single-unit recordings from different retinotopic locations in thalamus may have biased us toward observing suppressive effects with sustained L6CT photostimulation in V1. Future studies, perhaps in other species (e.g., ferret, non-human primate) with larger cortices and finer retinotopic maps or with more sophisticated methods for targeted optogenetic stimulation, could directly test the possibility that the relative balance between monosynaptic excitatory and disynaptic inhibitory pathways *in vivo* also depends on the retinotopic alignment between cortical and thalamic cells.

Potential mechanisms underlying the dynamic nature of corticothalamic pathways

A major strength of this study is our investigation of how L6CTs impact activity in their first- and higher-order thalamic targets under a variety of different conditions in an awake animal. Our combination of recordings in dLGN, pulvinar and visTRN have allowed us to explore how these circuit components are recruited under various photostimulation conditions, yet we are limited by our *in vivo* extracellular

recording methodology in capturing all possible mechanisms underlying our observed effects. For instance, the patterns of activity we see are also likely to be influenced by the reciprocal excitatory/inhibitory connections between the TRN and both dLGN and pulvinar[37,38]. Thalamic inhibition could also come from local inhibitory interneurons which, though quite rare in the rodent thalamus and especially in the pulvinar[39], are innervated by L6CTs[27,40]. Nevertheless, the lack of pronounced suppression with axon terminal (Figure 1.3) compared to cell body (Figure 1.1) photostimulation suggests that thalamic interneurons are not sufficient for (but likely contribute to) the suppressive effects we observe under the latter condition.

Meanwhile, the consistency of our findings with prior *in vitro* work[19] allows us to speculate on likely synaptic mechanisms underlying the frequency-dependent effects we observe. First, short-term facilitation in L6CT synapses is a robust and well-described phenomenon and an important component of frequency-dependent spiking observed in the somatosensory slice preparation[19]. Excitatory synaptic inputs from L6CTs to dLGN neurons have also been shown to persistently facilitate with moderate-to-high frequency (up to ~25Hz) electrical stimulation of the corticogeniculate pathway *in vitro*[41,42] and in the anesthetized cat[43], as well as to pulvinar neurons *in vitro*[15]. Based on our observations of spike facilitation in the TRN with 10Hz L6CT photostimulation, which is consistent with the known facilitating nature of these synapses[4,19,27,30], one might have predicted that facilitating inhibition from TRN would balance with facilitating excitation from L6CTs to produce consistent (rather than facilitating) spike outputs in dLGN and pulvinar. Instead, we also observed robust spike facilitation in dLGN and pulvinar with 10Hz stimulation. One possible explanation is that L6CT-TRN facilitation is weaker than at L6CT-relay cell synapses[19,27,30], which would lead to net-facilitation of the monosynaptic excitatory pathway overall. Another potential explanation is that GABAergic synapses from TRN to thalamic relay neurons exhibit prominent synaptic depression[19], which would allow the relative influence of disynaptic inhibition through TRN to weaken overall with higher-frequency L6CT activity. Thus, we suspect that facilitating excitation and depressing inhibition through TRN are both important synaptic mechanisms underlying our frequency-dependent effects.

Still other mechanisms could also be at play that are not mutually exclusive with the previously described circuit and synaptic contributions. For instance, thalamic neurons' intrinsic properties, and in particular the presence of T-type calcium channels which lead to bursting when "deinactivated" at hyperpolarized membrane potentials[44,45], may also contribute to the frequency-dependent effects we see. In fact, we observed a pronounced shift towards increased bursting during train photostimulation experiments (Figures 1.2F, 1.2J, 1.5E, and 1.S4G-J). These intrinsic properties likely account for the characteristic rebound spiking (and increased bursting) we observed in all three thalamic nuclei following ~100ms of silenced activity with 1Hz photostimulation (Figures 1.2B, 1.2C and 1.5B), which corresponds to the approximate time for T-type calcium channels to become deinactivated by hyperpolarizing input (from TRN, for instance) and trigger a shift into burst mode[44,45]. Still, we hypothesize that these intrinsic burst properties are not sufficient on their own for the spike facilitation we observe with 10Hz photostimulation because higher-frequency (20Hz) photostimulation also increased bursting (Figures 1.S4H-J) but did not produce spike facilitation (Figures 1.S5B-D). Moreover, thalamic relay neurons *in vitro* have been shown to exhibit spike facilitation (primarily within the first few L6CT stimulation pulses, as was the case in our experiments) even when held at hyperpolarized membrane potentials to induce a sustained burst mode of firing[19]. To what extent these intrinsic properties contribute to our frequency-dependent effects could be tested directly in mice with T-type calcium channels genetically deleted[46]. Overall, we suggest that multiple mechanisms (intrinsic physiological, synaptic, and circuit) all contribute to the highly dynamic nature of L6CT corticothalamic pathways.

L6CT influences on first- versus higher-order thalamus

This study offers the first investigation of how L6CTs influence their higher-order thalamic targets, such as the pulvinar in the rodent visual system, *in vivo*. We find that, overall, L6CT photostimulation had similar effects on lateral pulvinar as on first-order thalamus dLGN that were highly dynamic and frequency-dependent. These findings are consistent with hypothesized functional similarities between L6CT projections to both classes of thalamic nuclei based on their similar "modulator"-like

morphological and physiological characteristics[1,2]. Nevertheless, there are some differences between L6CT projections to dLGN and pulvinar that could have led to functional disparities. For instance, while many L6CTs that project to dLGN also project to the pulvinar[13], those that project to both classes of thalamic nuclei are only found in lower L6[13,47–49]. The pulvinar receives additional L6 input from other visual cortical areas, and pulvinar-projecting L6CTs in these areas are found throughout L6[47]. Thus, by restricting photostimulation to V1, we are engaging a subset and perhaps even a minority of the pulvinar's L6CT inputs. Moreover, a previous study identified a small population of L6B cells that project exclusively to higher-order thalamus, but not to first-order thalamus or TRN[50]; if and how this population's functional influence on pulvinar differs from that of the traditional L6CT population would be of significant interest. Yet despite these anatomical differences, we see remarkably similar effects of L6CT photostimulation in the pulvinar and dLGN that may be indicative of fundamentally similar functions for these corticothalamic pathways.

Another distinguishing feature of higher-order compared to first-order thalamic nuclei is that L6CTs are not their only source of corticothalamic input. Higher-order nuclei like the pulvinar also receive CT projections from layer 5 (L5), and these are hypothesized to act as the primary "driving" inputs in lieu of strong input from the sensory periphery[1,2]. Given the suppressive influence of L6CTs on other cortical populations within V1[4], it is therefore possible that the inhibitory effects we see in pulvinar with sustained L6CT photostimulation are due not only to the engagement of the visTRN as we describe, but also to indirect suppression of the L5CT "driving" inputs. While we cannot rule out this possibility, we note that L5, including lower L5 ("L5B") where subcortically-projecting L5 neurons in V1 are somewhat biased to reside[51], was not fully inactivated under our light stimulation conditions (Figure 1.S2D). Moreover, the fact that we see such similar and robustly facilitating spiking with moderate-frequency L6CT photostimulation in pulvinar as in dLGN cannot easily be explained by a mechanism involving L5CTs. Instead, we believe our findings provide compelling *in vivo* evidence of functional similarity in L6CT projections to different classes of thalamic nuclei.

Summary

Our results contribute to a broader understanding of the circuit computations underlying L6CTs' functions in both first- and higher-order sensory thalamus. Observations of visual response suppression by L6CTs in dLGN[4,5] has led some to suppose that this is the primary mechanism by which these corticothalamic neurons wield functional influence over their thalamic targets. However, our results suggest that L6CTs take a more nuanced approach. We propose that when only weakly or transiently activated (e.g., 1Hz condition, Figure 1.2), or when TRN is sufficiently recruited to overpower direct excitation (e.g., by sustained L6CT stimulation, Figure 1.1), L6CTs exert net-inhibition over their thalamic targets (Figure 1.6A). However, when activated within an optimal frequency range (e.g., 10Hz, Figure 1.2), L6CTs can facilitate their targets' responses to their inputs (Figure 1.6B). That facilitating spiking was less consistent with 20Hz L6CT stimulation (Figures 1.S5A-D) than with 10Hz suggests that the relative influence of these pathways may shift again to favor disynaptic inhibition at sufficiently high frequencies (which might more closely resemble continuous LED stimulation; Figure 1.S2). Furthermore, these L6CT connections can regulate not only the level but also the mode of thalamic activity, as demonstrated by our observed changes in burst versus tonic firing under different photostimulation conditions. Our data suggest that this functional flexibility is mediated by careful balancing between the parallel excitatory and inhibitory (through TRN) routes from cortical layer 6 to dorsal thalamus, altogether allowing L6CT projections to flexibly control thalamocortical input. Since we see similar L6CT effects in both first- and higher-order visual thalamus, we expect these projections to affect not only thalamocortical transmission to V1, but also cortico-thalamo-cortical transfer through the pulvinar to higher-order visual cortical areas. These dynamic corticothalamic pathways could afford numerous functional and computational advantages, such as for stimulus-specific amplification[31,41] and even higher-level representations, like perceptual decision confidence in the pulvinar as demonstrated by computational modeling of these pathways[52]. With an improved understanding of the highly dynamic nature of these L6CT pathways to first- and higher-order thalamus in an awake animal, future work may

be able to elucidate their role in modulating sensory processing in the context of sensory-guided behaviors.

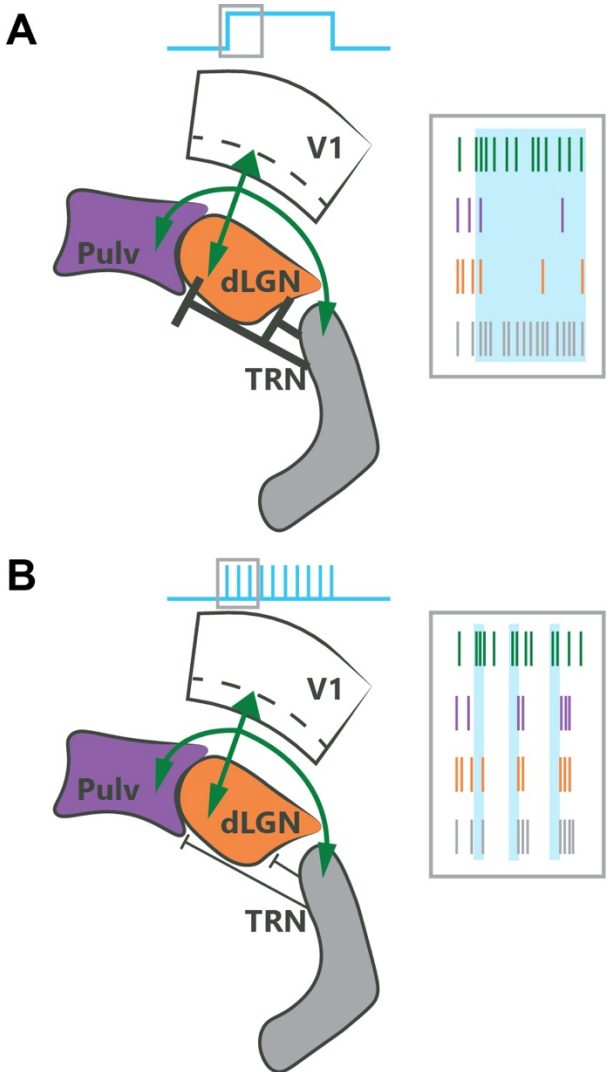

Figure 1.6 Summary of how different L6CT pathways are engaged under different L6CT stimulation conditions. (A) With continuous light stimulation (and perhaps also with high-frequency train stimulation, e.g., ≥20Hz) of L6CTs in V1 (green ticks), TRN is strongly activated (grey) and thus disynaptic inhibition overpowers direct, monosynaptic excitation to result in net-suppression of dLGN (orange) and pulvinar (purple) activity. (B) With moderate-frequency (e.g., 10Hz) photostimulation of L6CTs, responses in dLGN, pulvinar and TRN are all similar, with facilitating and bursting spike outputs following subsequent stimulation pulses. Under these conditions, the monosynaptic excitatory pathway appears to dominate the disynaptic inhibitory pathway. Schematics of spike trains are for illustrative purposes and do not directly reflect recorded spike trains.

Methods

Animals

Male and female Ntsr1-Cre GN220 transgenic mice (GENSAT) aged 8-14 weeks (with the exception of three mice, which were 16-17 weeks old) were used for experiments. Cre-negative animals were used for control experiments. All experimental procedures followed protocols approved by the Salk Institute Animal Care and Use Committee.

Experimental design and procedures

Surgeries

Mice were first anesthetized with a ketamine/xylazine cocktail (100mg/kg of ketamine and 10mg/kg xylazine) via intra-peritoneal injection and then placed in a stereotax (David Kopf Instruments Model 940 series). A small craniotomy was made over primary visual cortex of the left hemisphere (coordinates relative to bregma: 3.20mm posterior, 2.65mm lateral). A total of 100-150nl of AAV5-EF1a-DIO-hChR2(H134R)-eYFP was pressure-injected via Picospritzer (General Valve Corp) or syringe through a 25-30μm pipette at 1-2 depths, 0.3-0.6mm from pial surface. AAVs were injected at an approximate rate of 20nl/min, and the pipette was left in place for at least 5 minutes following injection prior to removal. Mice were returned to their cages and given 2.5-3 weeks before experimentation.

Four to seven days before experimentation, mice underwent an acute surgery for headframe implantation. Skin was cleared away so that a circular headframe (7mm inner diameter) could be attached with dental cement (C&B-Metabond, Parkell). A dull pipette attached to a micromanipulator (MP-285, Sutter Instrument Co) was used to relocate bregma and mark positions with a waterproof pen for targeting thalamus recordings (coordinates relative to bregma: 1.25-2.75mm lateral, 1.8-1.9mm posterior). The skull was covered with a silicone elastomer (Kwik-Cast, World Precision Instruments) and mice were given a carpofen subcutaneous injection (5mg/kg), Ibuprofen in their water bottles and at least 24 hours undisturbed in their cages.

In vivo electrophysiology

Prior to recordings, mice were given 2-4 training sessions to habituate to the running wheel. One day prior and on the day of recordings, mice were given a dilution of dexmethasone (15mg/kg) to alleviate brain swelling. On the day of recording, mice were anesthetized with isoflurane, and a craniotomy was made over the thalamus of the left hemisphere. For cell body stimulation experiments, an additional craniotomy was made over the injection site in V1 (in two animals the cortex was heavily thinned). Mice were then head-fixed on a wheel, where they were free to run at their will and movement was tracked with a rotary encoder. Silicon microprobes[22] were coated with a 2.5-5% solution of DiI (D282, ThermoFisher) in distilled water or ethanol and lowered into thalamus with a micromanipulator (MP-285, Sutter Instrument Co). Probe configurations used for dLGN/pulvinar recordings were 128DN and 128D (128 channels across 4 shanks, 775µm vertical extent of electrodes, 150µm or 330µm separation between shanks, respectively) or 64G (64 channels across 2 shanks, 300µm separation between shanks, 525µm vertical extent of electrodes). A 64D probe (64 channels on one shank, 1.05mm vertical extent of electrodes) was used for visTRN recordings. For cell body stimulation experiments, a 1mm diameter optical fiber (1mm diameter, 0.39 NA, ThorLabs) was positioned at approximately a 50-60° angle from and 0.5-1mm above the surface of the V1 craniotomy. Multi-shank probes for thalamic recordings were oriented horizontally (medial-lateral). After the probe penetrated the cortical surface, agarose (2.5-3.5%; A9793, Sigma-Aldrich) was poured over to fill the well of the headframe holder, thus covering the probe shank(s) and the tip of the optical fiber. The probe was continuously lowered slowly down to ~2.4-2.6mm beneath the cortical surface over the course of approximately 20 minutes. Once the probe was in its final position, it was allowed to sit and settle for 30 minutes before any data acquisition commenced. Data from all but two animals was acquired at 20kHz with an OpenEphys acquisition system[53], connected to an Intan RHD2000 128-channel amplifier board. Data from the remaining two animals was acquired at 20kHz with an Intan RHD2000 USB interface board.

Visual and optogenetic stimulation

Visual stimuli were generated through custom MATLAB code using Psychtoolbox, as described previously[54] and presented on a 24" LED monitor (GL2450-B, BenQ). The monitor screen was positioned 12cm from the mouse's right eye. Visual stimuli consisted of square-wave drifting gratings at four orientations in eight directions, 0.04 cycles/° spatial frequency, and 2Hz temporal frequency (one experiment in one mouse at 1Hz). A full "trial" consisted of a 0.5-second pre-stimulus period (grey screen), 2 seconds of visual stimulus presentation, and 1.5-2 seconds post-stimulus period (grey screen). 20% of trials were "blank" trials, in which the screen remained grey for the full trial duration.

Optogenetic stimulation was controlled via an Arduino Zero microcontroller board with a 12-bit DAC output pin which interfaced with MATLAB through a serial port connection. All experiments consisted of a "no light" condition plus three different light conditions: sustained photostimulation at low, medium, or high light intensities, or trains of 10ms photostimulation pulses at 1, 10, and 20 Hz (40 Hz in two mice). All recorded units underwent both sustained and trains photostimulation experiments (except V1 units from two mice, which only underwent sustained photostimulation experiments). LED stimulation always lasted for 1 second and started 1 second after the trial start (0.5 seconds after visual stimulus onset). For cell body stimulation experiments, blue LED light was delivered through a custom optical fiber patch cord (1mm diameter, 0.39 NA, ThorLabs) connected to an LED driver (PlexBright LED 465nm, Plexon). For axon terminal stimulation experiments, blue light was delivered through a custom "optrode" (64G probe, integrated with a 200μm diameter, 0.22 NA multimode fiber halfway between the two shanks and ending just above the top contacts) connected to an LED driver (470nm fiber-coupled LED with T-Cube LED driver, ThorLabs). Light intensity was controlled by assigning output values for the Arduino DAC 12-bit output pin (0-4095). These output values were typically kept consistent across experiments, but power output was also measured with a power meter (PM100D with 1.S121C power sensor, ThorLabs) as verification of consistency. Output power ranges from the Plexon LED through the 1mm diameter fiber were 0.7-1mW ("low"), 3.5-4.5mW ("med"), and 6.5-8.5mW ("high"). Output powers from ThorLabs LED to optrode with 200μm diameter fiber were estimated with a dummy fiber-optic implant (200μm diameter, 0.22NA). In these optrode experiments, DAC outputs

assigned to “low”, “med” and “high” conditions had to be varied by experiment because it was observed in some experiments, and specifically in experiments in which at least one shank on the probe was in dLGN, too high light power caused a massive ramp-like increase in activity before units went completely silent for >20 seconds. Thus, light levels were titrated during recording so that this seemingly excitotoxic effect did not occur. Consequently, estimated light levels during experiments that included at least one shank in dLGN ranged from 120-152μW (“low”) and 250-560μW (“high”) as measured through the 200μm diameter dummy fiber. In these experiments, the third light condition was a 1 second ramp, in which the Arduino DAC output was linearly increased in bits over 1 second so that it ended at the “high” light level. In pulvinar-only optrode experiments, estimated light levels ranged from 120-152μW (“low”), 250-310μW (“med”) and 500-600μW (“high”).

Histology

After recordings were completed, animals were given an intraperitoneal injection of euthasol dilution (15.6mg/ml) and then perfused with phosphate-buffered saline (PBS) followed by 4% paraformaldehyde. Brains were dissected out from skulls and post-fixed in 2% PFA and 15% sucrose solution at 4°C for ~24 hours before being moved to 30% sucrose at 4°C for another ~24 hours. Brains were frozen in sucrose and sliced on a freezing microtome into 50μm sections, starting from the anterior edge of the hippocampus to the posterior end of cortex. All sections were counterstained with 10μM DAPI in PBS for 10 minutes before being mounted and coverslipped with Polyvinyl alcohol mounting medium containing DABCO. Additional immunohistochemistry was performed on thalamic sections by incubating at 4°C for 16-20 hours with rabbit anti-calretinin primary antibody (1:1000; Swant 7697) in 1% Donkey Serum/.1% Triton-X 100/PBS, followed by donkey anti-rabbit conjugated to Alexa 647 (1:500; A-31573, Life Technologies) before DAPI counterstaining. Imaging was performed on an Olympus BX63 microscope with a 10X objective.

Quantification and statistical analysis

Spike-sorting

Spike-sorting on extracellularly recorded data was performed semi-automatically using Kilosort[55]. Briefly, different recordings from the same recording session (e.g., different intensities experiment followed by trains stimulation experiment) were concatenated together into a single binary file, common average referenced, bandpass filtered (300-2000Hz) and spatially whitened prior to template-matching. Because onset and offset of LED stimulation for optogenetics caused artifacts that could be mistaken for spikes by the algorithm, spikes within 3ms of the light onset and offset were removed, and additional "spikes" were removed whose amplitudes surpassed 20 times the standard deviation of spike amplitudes. Clusters were further curated manually using Phy[56]. Additional optogenetic artifacts were evident as points far outside the cluster of principal component features whose cross-correlograms with their assigned clusters exhibited clear refractory period violations and thus could be manually removed. For a few experiments in which the timing of the ADC input to OpenEphys from the Arduino (for controlling the LED) was not saved properly due to a bug in the OpenEphys GUI, thus prohibiting us from removing optogenetic artifacts based on their timing relative to LED onset and offset, we removed artifacts based only on their large amplitudes in Kilosort and as outliers in their principal component features in Phy. If artifacts were not removed, they were extremely obvious in unit raster plots because they lined up precisely with LED photostimulation onset/offset and thus were readily distinguishable from legitimate spikes, even those with short latency. Thus, we are very confident that we successfully removed the vast majority of optogenetic artifacts, and all short-latency responses that we report come from legitimate spikes. We did our best to also remove optogenetic "hash" from ChR2-expressing axons in our thalamic recordings, which usually manifested as points well outside the main cluster in the principal component features view that exhibited substantial refractory period violations in their cross-correlograms. These "hash"-y units were especially prominent in dLGN and, when analyzed separately, their spikes occurred nearly exclusively during photostimulation periods, further suggesting that they were not true thalamic units (which had high spontaneous firing rates). Spike clusters were manually assigned to noise, multi-unit, and good/single-unit categories, and only good single-units that

had fewer than 0.5% refractory period violations and "unit quality" (isolation distance[57]) greater than 16 were included for analyses.

Assigning units to thalamic nuclei

Prior to *in vivo* recordings, recording probes were coated in DiI and were easily visualized post-mortem. Staining for calretinin (described above) provided a clear border between lateral pulvinar (calretinin-negative) and dLGN (calretinin-positive axons from retinal ganglion cells), thus allowing for definitive assignment of units recorded on different probe shanks to lateral pulvinar or dLGN. In rare instances in which a DiI trace fell ambiguously right on the border between pulvinar and dLGN, units recorded from the corresponding shank were excluded from analyses. Calretinin staining also provided an additional border between lateral pulvinar and rostral-medial and caudal-medial pulvinar, where cell bodies were calretinin-positive. Pulvinar units were assigned to lateral pulvinar if the DiI trace from their corresponding probe shank passed through the calretinin-negative portion of pulvinar and through eYFP-positive axon terminals, whereas shanks passing mainly through calretinin-positive cells and absent or sparse eYFP-expressing axons were considered in medial pulvinar. Similarly, data from one shank in one experiment which passed through dLGN but not through eYFP-expressing axons were excluded from dLGN analyses. Calretinin staining did not allow us to distinguish between rostromedial and caudomedial pulvinar[24].

To approximate where the dorsal/ventral boundaries of thalamic nuclei (dLGN, pulvinar, visTRN) fell on each recording shank, we determined the anatomical boundaries of visually responsive units. To classify visually responsive units, we identified the visual direction which maximally changed each unit's firing rate from baseline and used the spike counts from those preferred visual stimulus trials without LED stimulation to assess whether each unit's activity was significantly different from "blank" trials without LED stimulation (Wilcoxon rank-sum test). We separately compared spike counts between blank and preferred-visual trials during the first 100ms of the visual stimulus (to assess visual onset response) and 0.5-1.5s from the visual stimulus onset (to assess sustained visual stimulus response), and

thus considered units visually responsive if either of these p-values passed the 0.025 threshold (Bonferroni correction for two comparisons). We then estimated the dorsal/ventral boundaries of visual thalamic nuclei as the first and last channels on each probe shank which had visually responsive units. These boundaries were corroborated across experiments from the same recording sessions, and if there were discrepancies the boundaries were set as those channels which had significantly visually responsive units in both experiments. In this way, all units analyzed from sustained photostimulation experiments were also analyzed for the trains experiments and vice versa. For visTRN recordings, we sometimes recorded visually responsive units very far ventral and with very short latency, possibly through the optic tract. Thus, we also included as criteria that channels with visually responsive units that were separated by more than 100μm from the nearest visually responsive channel were excluded, and for visTRN specifically that depth of included channels should not exceed 400μm. Units were considered fast-spiking (FS) whose waveform trough-to-peak times were less than 0.4ms but were not analyzed separately because they were very uncommon in dLGN and extremely rare in pulvinar, consistent with other reports[58].

Analysis

Average firing rates were calculated from the one-second period of photostimulation (0.5-1.5s from visual stimulus onset). Although our mice did not run very often, we exclusively used stationary trials (speed < 2cm/s) for our average firing rate calculations since running has been shown not only to affect firing rates in V1[59], but also in dLGN[60]. Firing rates were calculated separately for visual and blank trials and for each light condition (no light, low, med, high).

For population-level statistics on the effects of L6CT photostimulation on these average firing rates, we pooled together all units from the same experiment type (e.g., trains vs. sustained photostimulation) and from the same thalamic nucleus across animals and recording shanks and compared their firing rates in trials without L6CT photostimulation to firing rates in each photostimulation condition using the Wilcoxon signed-rank test. Population-averaged peristimulus time histograms (PSTHs) were

constructed using individual units' average firing rate across trials (visual and blank trials separately) in 25ms bins across the full trial duration (2.5s). We then normalized to each unit's baseline firing rate (calculated from the 500ms prestimulus period) and averaged these normalized PSTHs across units. Response latencies were estimated from population-averaged PSTHs in 1ms bins from blank trials, and latency was taken as the first time point after the LED onset which surpassed 2 standard deviations above baseline.

Average firing rates were also used to compute a light modulation index for each unit. The light modulation index was computed as the difference between average firing rates in visual trials with and without L6CT photostimulation (separately for each photostimulation condition) divided by their sum. Thus, a positive light modulation index indicates increased activity with L6CT photostimulation while negative indicates decreased activity.

To determine the statistical significance of each unit's response to L6CT photostimulation, we compared spiking responses during the one second photostimulation period on all trials with and without photostimulation (separately for each photostimulation condition) with a Wilcoxon rank-sum test. In order to summarize how individual units were affected by sustained L6CT photostimulation, units were considered "suppressed" if their activity was significantly suppressed ($p<0.05$ and light modulation index < 0) in at least 2/3 conditions, or "activated" if their activity was significantly increased ($p<0.05$ and light modulation index >0) in at least 2/3 conditions.

To analyze frequency-dependent effects, we first sought to identify units that spiked in response to individual photostimulation pulses. This is because it was expected that not every neuron we recorded from should be directly innervated by our ChR2-expressing L6CTs (as demonstrated by non-uniform expression of ChR2-eYFP across each thalamic nucleus). With each unit's peristimulus time histogram of spike counts (in 5ms bins) for visual trials with 10Hz or 20Hz photostimulation, we used the following criteria for so-called "Hz-activated" units: 1) at least one bin surpasses threshold (three standard deviations above the mean visually evoked response, taken from the one-second photostimulation period in no light trials) within 50ms of at least the first or second photostimulation pulse in the train; 2) if there

was no significant response to either of the first two photostimulation pulses, there had to be significant response bins (above threshold) following at least half of all subsequent pulses. Only these "Hz-activated" units were analyzed for spike count ratios, which were calculated as the total number of spikes within 50ms of each photostimulation pulse divided by the total number of spikes within 50ms of the first pulse. Since the distributions of these data were clearly non-normally distributed, we chose to plot the medians and interquartile ranges. The sign test was used to test the null hypothesis that the median of spike count ratios was equal to one (i.e., no change in spike outputs).

To investigate the effects of our different L6CT photostimulation conditions on thalamic bursting, for each unit we analyzed the interspike intervals (ISIs) for all spikes that occurred within the 1-second photostimulation period (.5-1.5s post-visual stimulus onset) across visual trials. To control for possible changes in bursting induced by behavioral state rather than our L6CT manipulations[59], we restricted these analyses to trials in which the mouse was stationary as for our firing rate analyses (speed < 2cm/s). Spikes occurring in bursts were defined per convention[61] as those which were preceded by an ISI $\geq$ 100ms and followed by an ISI $\leq$ 4ms (first spikes in a burst) and all subsequent spikes which were preceded by an ISI $\leq$ 4ms. The bursting rate for each unit was calculated as the ratio of the number of spikes occurring in bursts to the total number of spikes in the 1-second photostimulation period, calculated separately for each photostimulation condition. Changes in bursting under each photostimulation condition compared to the no-photostimulation condition were assessed statistically using the Wilcoxen signed-rank test.

V1 recordings

In two mice, additional experiments were performed to record single-unit activity in primary visual cortex with a single (64D) recording probe, while a few mice (n=3) only underwent V1 recordings with a two-shank (128AN) recording probe. The same optogenetic and visual stimulation conditions were used as for thalamic recordings, but with an additional stimulus protocol consisting of alternating 2-second periods of the screen flashing on and off 2 minutes. From these short recordings, we performed current source density (CSD) analysis by taking the second spatial derivative using CSDPlotter[62] of the

low-pass-filtered (<1000Hz) local field potential during the transitions between screen-off and screen-on periods. For each column of each shank, we assigned channels to layer based on the following criteria: congruent channels which exhibited the fastest current sink (typically 2-3 channels per column, spanning 100-150μm) were assigned to layer 4; those that fell above this initial current sink as layer 2/3; those that exhibited an additional but delayed current sink approximately 150-300μm beneath the bottom of layer 4 as layer 5B; those in between layers 4 and 5B and layer 5A; and those below layer 5B as layer 6. Units were separated into fast-spiking (FS) and regular-spiking (RS) categories based on their waveform trough-to-peak times (<0.475ms considered FS) because this metric appeared to clearly separate all recorded units into two main clusters (Figure 1.S2B). Firing rates and light modulation indices were analyzed as for thalamic units.

To assess how our different photostimulation conditions affected the firing rates of putative L6CT cells, we took two different approaches (Figures 1.S2E-F). First, we used the Stimulus-Associated spike Latency Test[63] to identify L6 RS units with statistically significant responses within 10ms of photostimulation onset. However, because of extensive interconnectivity among cortical pyramidal cells which can lead to short-latency spikes in cells synaptically connected to ChR2-expressing cells, we suspect there are some false positives in this sample. Thus, we took an additional approach of simply identifying L6 RS cells which were positively light-modulated (light modulation index > 0 in at least two photostimulation conditions), based on the observation that L6CTs primarily inhibit other cortical pyramidal cells through their connections with fast-spiking interneurons[4]. Because these two different approaches yielded very similar estimates of putative L6CT firing rates across our different photostimulation conditions, we felt that our phototagging approach using the SALT test provided a reasonable approximation of the L6CT population.

Appendix

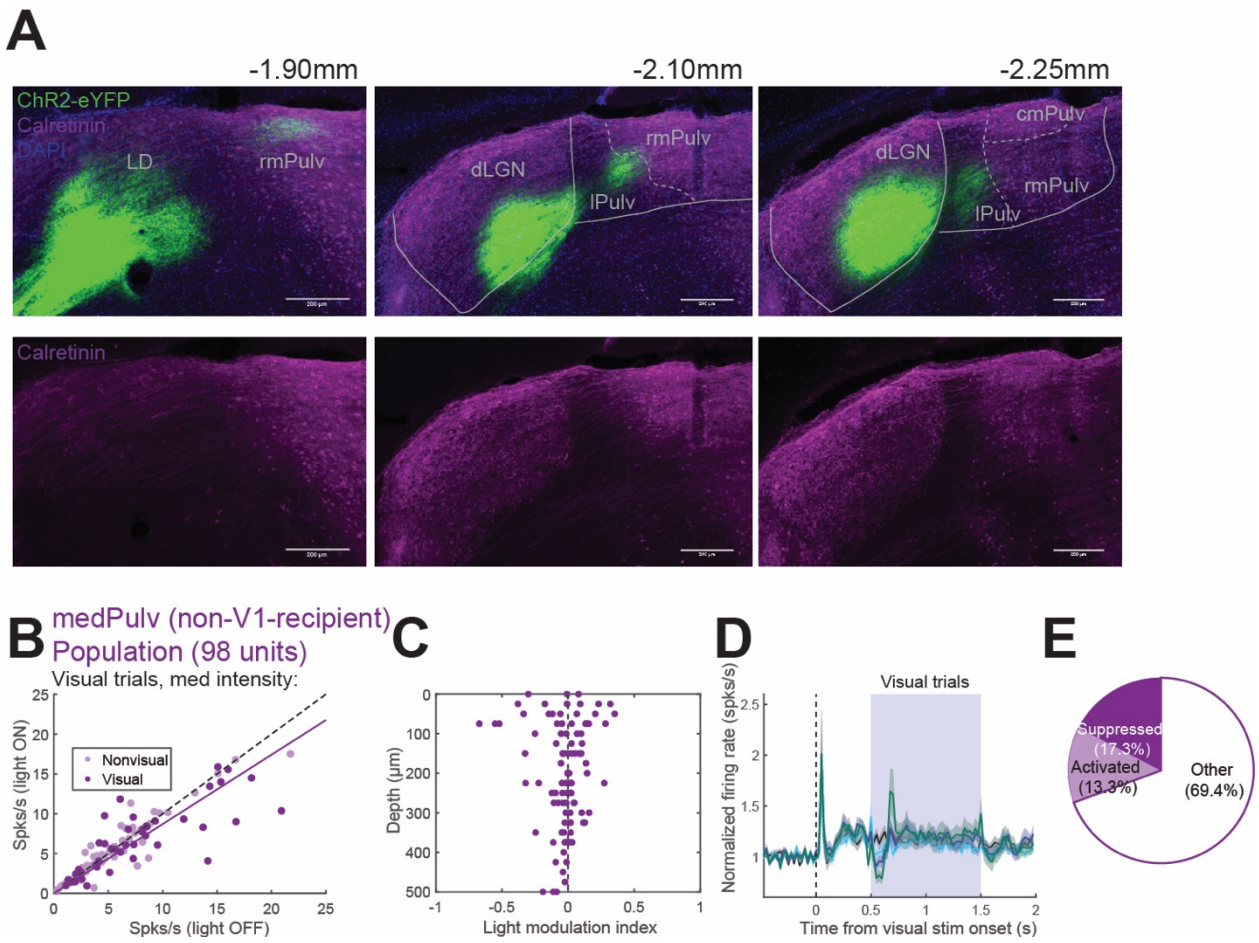

Figure 1.S1 Effects of sustained L6CT photostimulation on different subnuclei of the pulvinar. (A) Calretinin helps distinguish between different pulvinar subnuclei. Images in three columns are from different coronal sections in the same animal, from anterior (left) to posterior (right). Bottom row shows the calretinin channel in isolation. Scale bars are 200μm. (B) Average firing rates during the 1-second photostimulation period from visual trials, with versus without medium-intensity L6CT photostimulation. Saturated points indicate visually responsive units. (C) Light modulation index by depth (distance from highest channel on the same probe shank and in the same experiment with a visually responsive unit). (D) Average normalized PSTH across all units. Shading indicates ±1 standard error of the mean. (E) Proportions of significantly suppressed and activated units recorded in medPulv.

Figure 1.S2 Effects of L6CT optogenetic manipulations on local V1 activity. (A) Schematic of V1 laminar recordings with L6CT photostimulation (left) and determination of which cortical layers correspond to which electrode contacts using current source density (CSD) analysis (right). The CSD plot comes from a single column of electrode contacts on a single probe shank (boxed area). (B) Two distinct groups of units, referred to as fast-spiking (FS) and regular-spiking (RS), are identifiable based on the trough-to-peak times and trough-to-peak ratios of their waveforms. Units with trough-to-peak times less than 0.475ms were considered FS, and others were considered RS. (C) Example L6 RS unit, putatively ChR2-expressing. Left: raster plot organized by photostimulation condition. Middle: zoomed-in image of boxed part of raster plot (from 100ms before to 300ms after LED photostimulation onset), showing short-latency onset of increased activity. Shaded region indicates photostimulation period (1s duration). Right: PSTH averaged across visual trials. (D) Median light modulation index by layer of FS (middle) and RS (right) cells with sustained 1-second L6CT photostimulation at low, medium, and high levels. Error bars indicate interquartile range. (E) Left: average firing rates of L6 RS units during the 1-second photostimulation period from visual trials, with and without medium-intensity photostimulation. Saturated points indicate "phototagged", putative ChR2-expressing L6CT units (see Additional Methods), and crosses indicate mean firing rates across phototagged and non-phototagged units. Inset: proportion of L6 RS units that were phototagged. Right: mean firing rates across all L6 RS "phototagged" units for each light condition. Error bars indicate ± 1 standard error of the mean. (F) Same as (E) but with putative ChR2-expressing L6CT units identified by light modulation index > 0 in L6 RS units. (G) Same example L6 RS unit has in (C) but during the trains experiment, with 1Hz, 10Hz, and 20Hz L6CT photostimulation trains. There was some recoding drift so that more spikes were detected during the trains experiment than in (C). Panel descriptions are same as for (C), although shaded rectangles in left two panels indicate 10ms photostimulation pulses. (H) Like (D) but for trains experiments. (I) Quantification of frequency-dependent spiking of "phototagged" L6 RS units driven at 10Hz. Left: histogram of spike count ratios (comparing spike outputs following the second photostimulation pulse relative to the first) for phototagged units. Right: median spike count ratios across phototagged units, comparing spike outputs following photostimulation pulses 2-10 relative to the first photostimulation pulse. (J) Same as (I) but including all RS and FS units across all layers. (K-L) Same as (I-J) but with 20Hz L6CT photostimulation. Asterisks indicate ratios significantly different from 1 (p's < 0.05, sign test). Error bars indicate interquartile range.

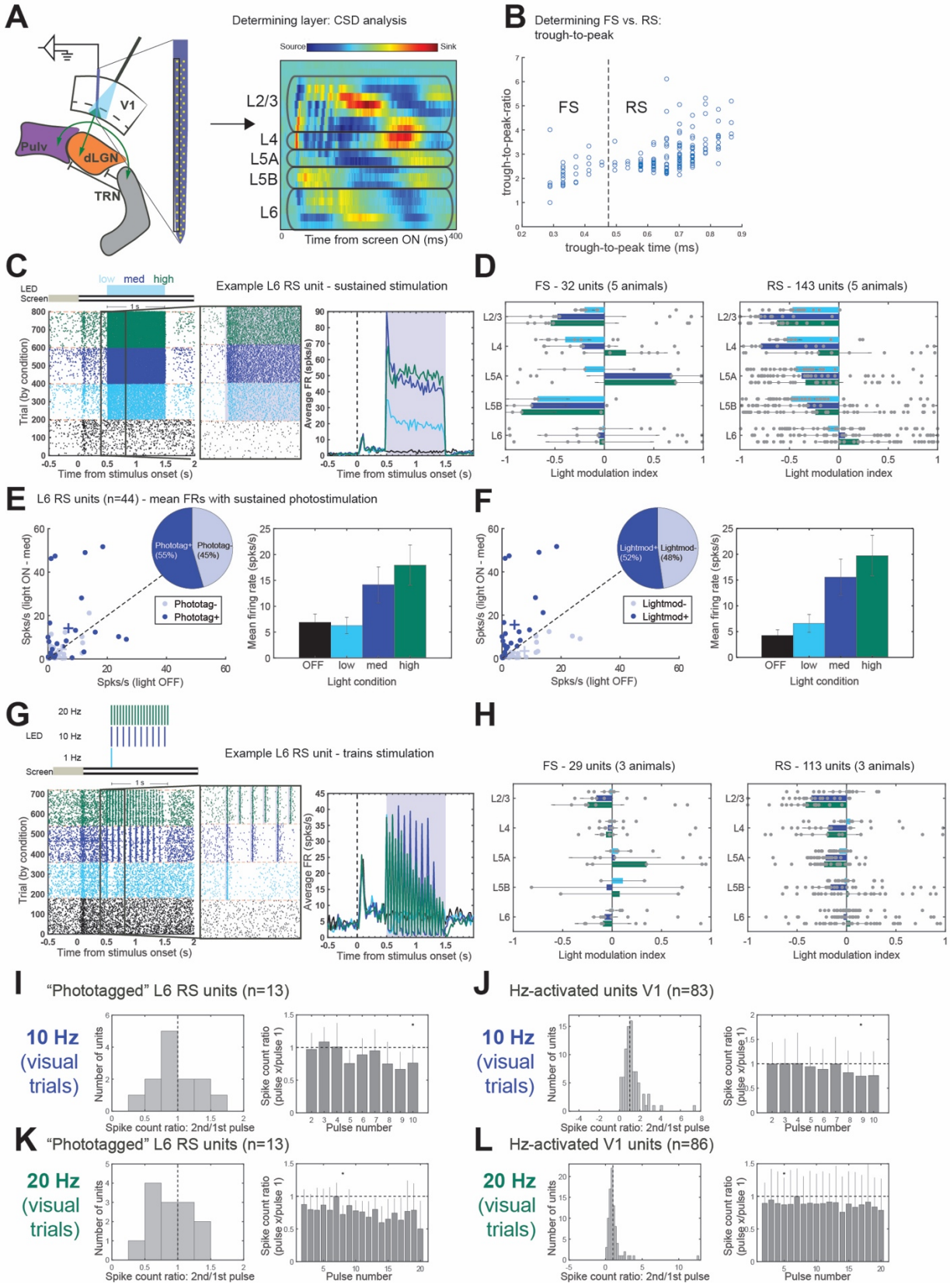
A
Determining layer: CSD analysis
Source
Sink
V1
Pulv
dLGN
TRN
L2/3
L4
L5A
L5B
L6
Time from screen ON (ms)
B
Determining FS vs. RS:
trough-to-peak
FS
RS
trough-to-peak-ratio
trough-to-peak time (ms)
C
Example L6 RS unit - sustained stimulation
LED
Screen
low med high
Trial (by condition)
Average FR (spks/s)
Time from stimulus onset (s)
D
FS - 32 units (5 animals)
RS - 143 units (5 animals)
Light modulation index
E
L6 RS units (n=44) - mean FRs with sustained photostimulation
Phototag+ (55%)
Phototag- (45%)
Spks/s (light ON - med)
Spks/s (light OFF)
Mean firing rate (spks/s)
OFF low med high
Light condition
F
Lightmod+ (52%)
Lightmod- (48%)
G
Example L6 RS unit - trains stimulation
20 Hz
10 Hz
1 Hz
H
FS - 29 units (3 animals)
RS - 113 units (3 animals)
I
"Phototagged" L6 RS units (n=13)
10 Hz (visual trials)
Number of units
Spike count ratio: 2nd/1st pulse
Spike count ratio (pulse x/pulse 1)
Pulse number
J
Hz-activated units V1 (n=83)
K
"Phototagged" L6 RS units (n=13)
20 Hz (visual trials)
L
Hz-activated V1 units (n=86)

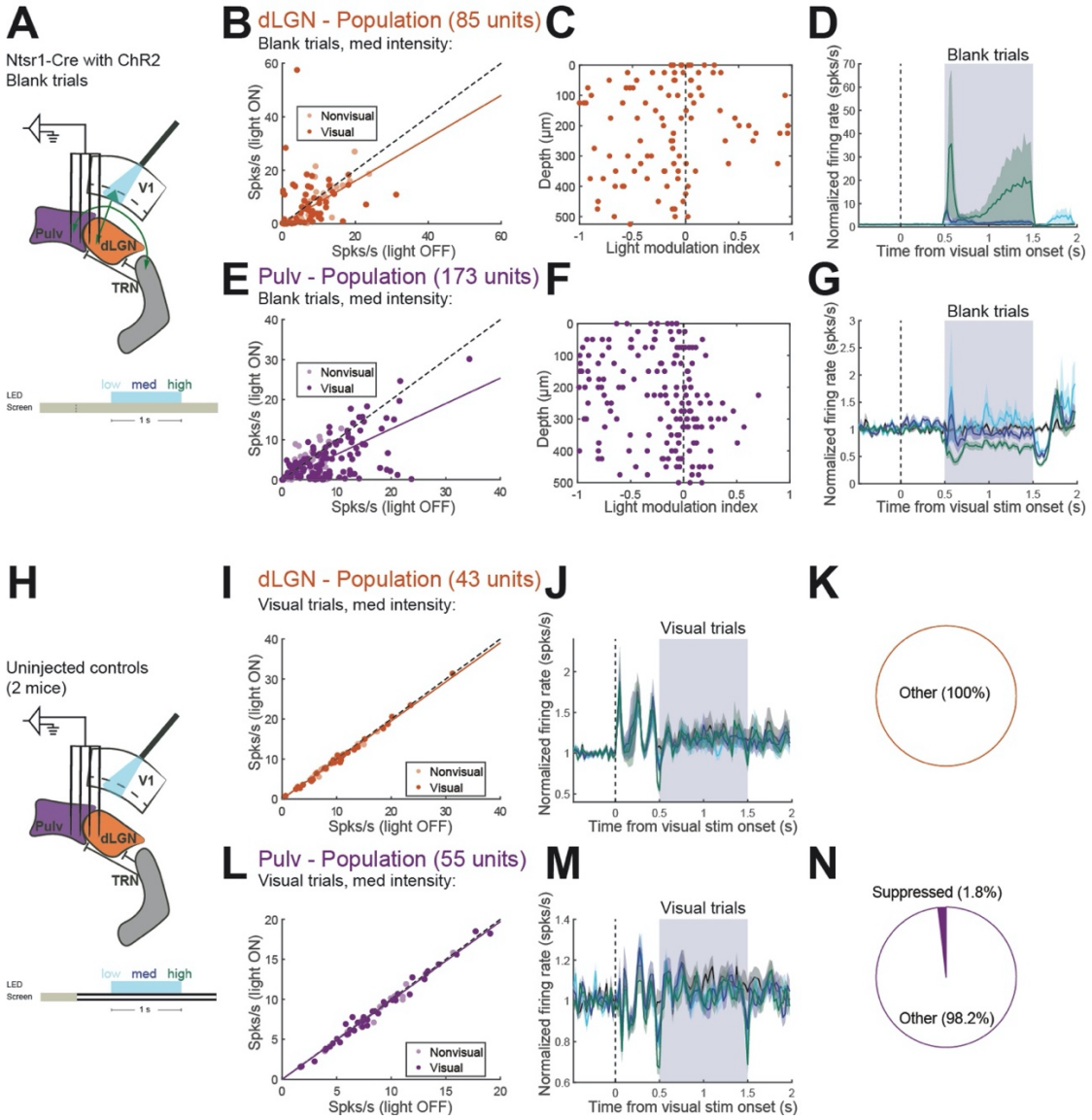

Figure 1.S3 Additional results from L6CT continuous light photostimulation experiments – effects on spontaneous activity and uninjected controls. (A) Schematic of recording and photostimulation setup and trial structure (same experiments as in Figure 1.1). (B) Average firing rates in dLGN during the 1-second photostimulation period from blank trials with versus without medium-intensity L6CT photostimulation. (C) Light modulation index (calculated from blank trials) by depth. (D) Average normalized PSTH across all dLGN units. (E-G) Same as (B-D) but for units recorded in lateral pulvinar. (H) Schematic of recording and photostimulation setup and trial structure during control experiments with uninjected mice. (I) Average firing rates recorded in dLGN from control recordings during the 1-second photostimulation period from visual trials, with versus without medium-intensity photostimulation. (J) Average normalized PSTH of all units recorded in dLGN during control recordings. The dip in firing rate at the start and end of the photostimulation period can be attributed to light artifacts at the onset and offset of the LED that impacted accurate spike detection in a narrow time window (within 3ms of LED onset), and so spikes in this window were excluded in all experiments (see Methods). Shading indicates ±1 standard error of the mean. (K) No units were individually significantly modulated by light. (L-N) Same as (I-K) but for units recorded in lateral pulvinar during control experiments. Only one unit was artifactually considered "suppressed" under our criteria.

Figure 1.S4 Changes in bursting in dLGN, lateral pulvinar and visTRN under different photostimulation conditions. (A) Scatterplots of pre- and post-interspike intervals (ISIs) for all spikes of an example pulvinar unit (the same as in Figure 1.1I, top and Figure 1.2C) that occurred in the 1-second photostimulation period during visual trials without photostimulation (left) and during visual trials with low, medium and high continuous L6CT photostimulation (right three panels, respectively). Dashed lines demarcate the pre- and post-ISI cut-offs for being considered burst spikes (pre-ISI $\geq$ 100ms and post-ISI $\leq$ 4ms, or pre-ISI $\leq$ 4ms; see Methods). Filled black circles indicate spikes classified as burst spikes (notice that some spikes with preISIs $\leq$ 4ms were not considered burst spikes if they were not preceded by another burst spike). (B) Same as (A) but for the same unit during train photostimulation experiments with no light, 1 Hz, 10 Hz and 20 Hz photostimulation. (C) Recording and photostimulation configuration and trial structure for burst analyses in (D-F). (D-F) Average bursting rates (number of spikes that occurred during bursts / total number of spikes during 1-second photostimulation period across trials) for all units recorded in dLGN (D), lateral pulvinar (E), and visTRN (F) during visual trials with and without L6CT photostimulation. Rows correspond to different L6CT photostimulation conditions (low, medium, high). (G) Recording and photostimulation configuration and trial structure of photostimulation trains experiments, used for burst analyses in (H-J). (H-J) Average bursting rates for all units recorded in dLGN (H), lateral pulvinar (I), and visTRN (J) during visual trials with and without L6CT train photostimulation. Insets show zoomed-in images of boxed parts of plots (0-0.2 bursting rates). Plots from 10 Hz photostimulation trials are missing because they are already shown in Figures 1.2 and 1.5.

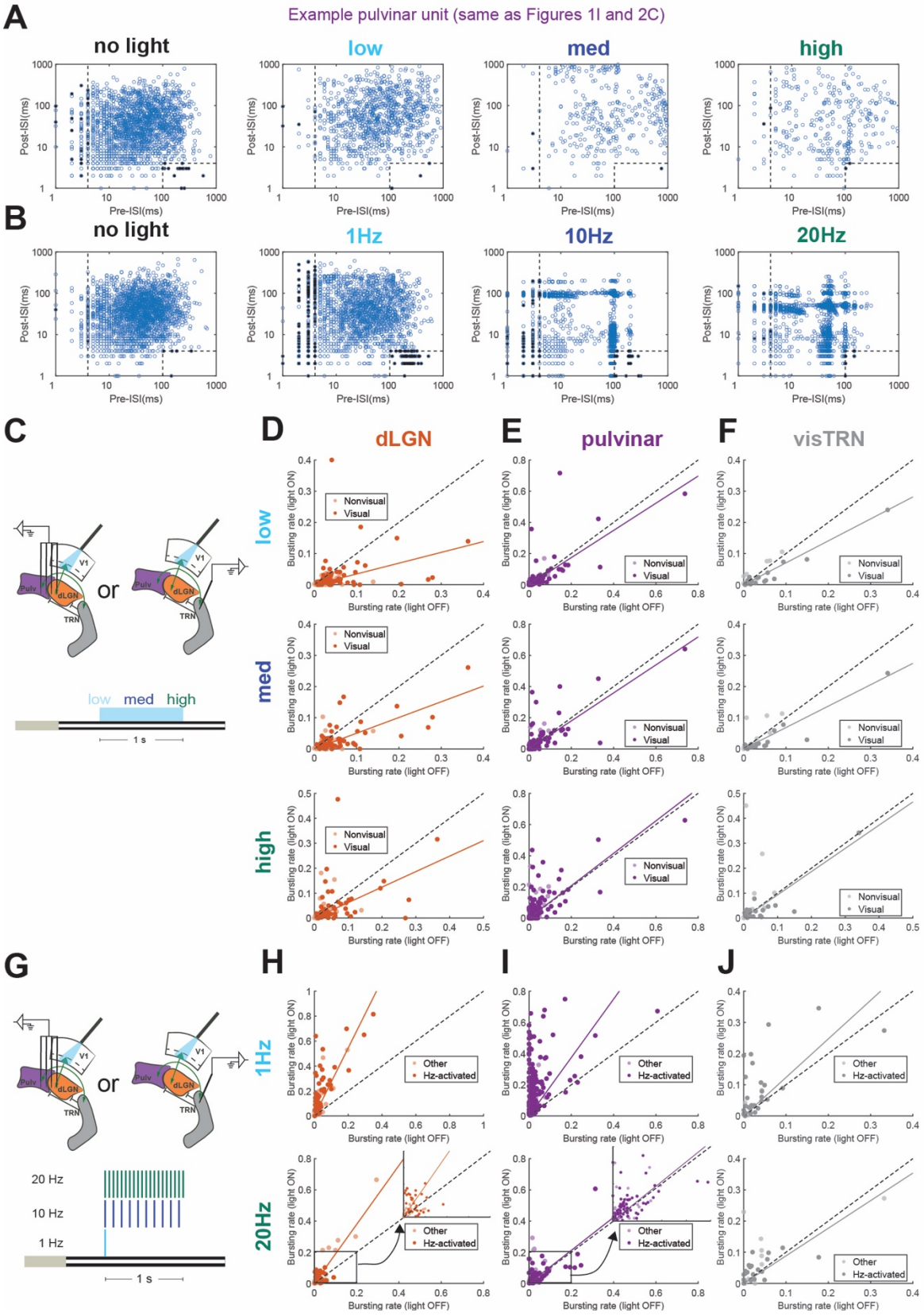
A
Example pulvinar unit (same as Figures 1I and 2C)
no light
low
med
high
B
no light
1Hz
10Hz
20Hz
Post-ISI(ms)
Pre-ISI(ms)
C
V1
dLGN
Pulv
TRN
or
low med high
1 s
D
dLGN
E
pulvinar
F
visTRN
low
med
high
Nonvisual
Visual
Bursting rate (light ON)
Bursting rate (light OFF)
G
20 Hz
10 Hz
1 Hz
1 s
H
I
J
1Hz
20Hz
Other
Hz-activated

Figure 1.S5 Other frequency-dependent effects in thalamus using 20Hz cell body photostimulation and 1-20Hz axon terminal stimulation. (A) Diagram of recording and photostimulation configuration in dLGN/pulvinar and visTRN recordings and trial structure of visual trials with 20Hz L6CT photostimulation. Experiments from two animals in dLGN/pulvinar that were included in the 10Hz photostimulation analysis in Figure 1.2 were excluded from these analyses because the high-frequency condition was 40Hz instead of 20Hz. (B) Quantification of dLGN spiking with 20Hz L6CT photostimulation. Left: histogram of spike count ratios (comparing spike outputs following the second photostimulation pulse relative to the first) for 20Hz-activated units. Right: median spike count ratios across 20Hz-activated units, comparing spike outputs following photostimulation pulses 2-20 relative to the first photostimulation pulse. Asterisks indicate ratios significantly different from 1 (p's < 0.05, sign test). Error bars indicate interquartile range. (C) Quantification of pulvinar spiking with 20Hz L6CT photostimulation. Panel descriptions same as for (B). (D) Quantification of visTRN spiking with 20Hz L6CT photostimulation. Panel descriptions same as for (B). (E) Photostimulation trains experiments during dLGN optrode recordings. Left: diagram of optrode configuration (partially or entirely in dLGN) and trial structure for visual and LED stimulation during trains experiments. Right: average normalized PSTH of dLGN units' activity during visual trials. Shading indicates ± 1 standard error of the mean. (F) Quantification of dLGN spiking with 10Hz axon terminal stimulation. Panel descriptions same as for (B). (G) Average bursting rates for all units with versus without 10Hz L6CT photostimulation in visual trials. (H) Quantification of dLGN spiking with 20Hz axon terminal stimulation. Panel descriptions as for (B). (I) Photostimulation trains experiments during pulvinar optrode recordings. Left: diagram of optrode configuration in the pulvinar and trial structure for visual and LED stimulation during trains experiments. Right: average normalized PSTH of pulvinar units' activity during visual trials. Shading indicates ± 1 standard error of the mean. (K-N) Same as (F-I) but for units recorded from the optrode in the pulvinar.

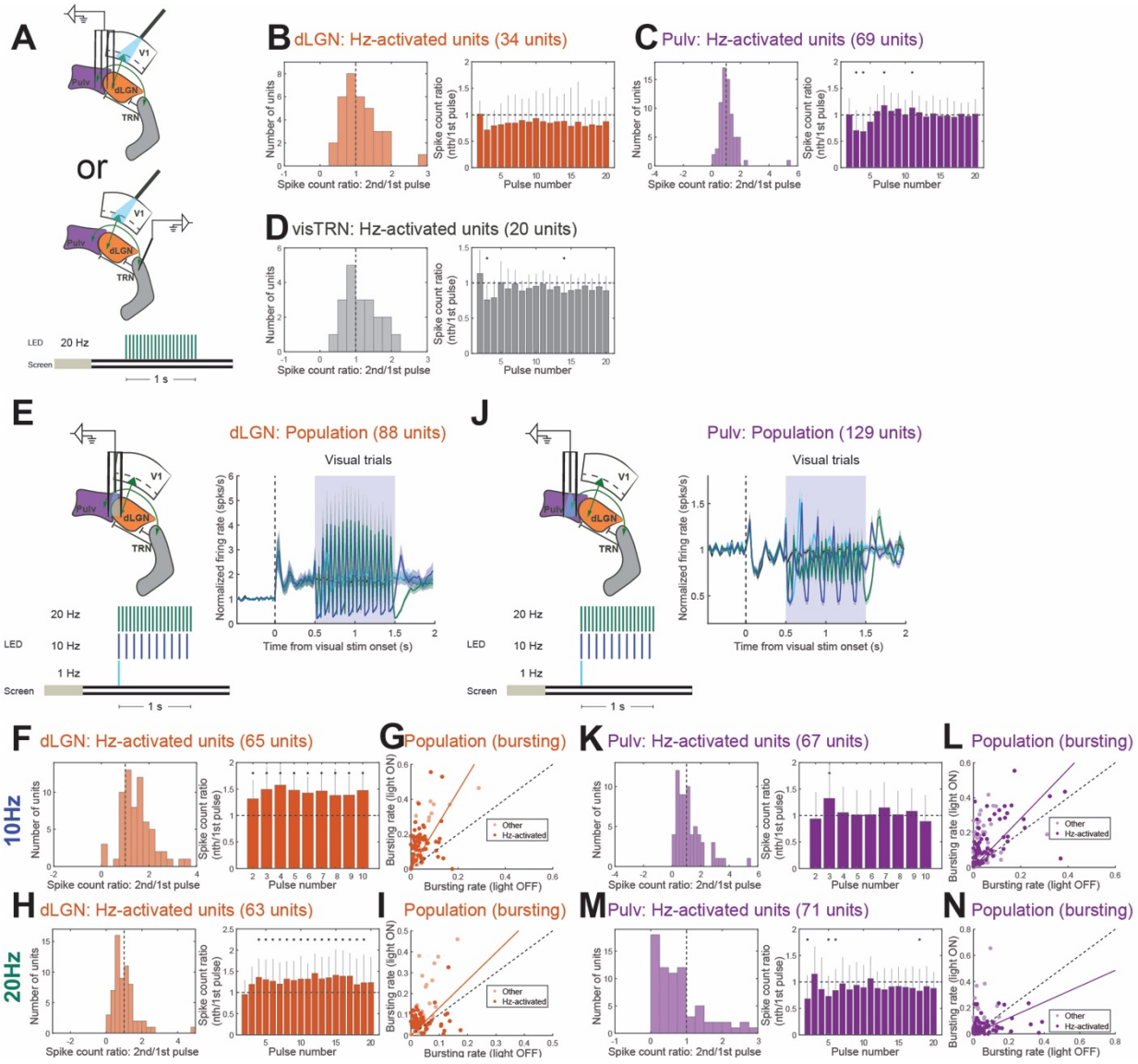
A
V1
Pulv
dLGN
TRN
or
LED
20 Hz
Screen
1 s
B dLGN: Hz-activated units (34 units)
C Pulv: Hz-activated units (69 units)
D visTRN: Hz-activated units (20 units)
Number of units
Spike count ratio (nth/1st pulse)
Spike count ratio: 2nd/1st pulse
Pulse number
E
dLGN: Population (88 units)
J
Pulv: Population (129 units)
Visual trials
Normalized firing rate (spks/s)
Time from visual stim onset (s)
20 Hz
10 Hz
1 Hz
F dLGN: Hz-activated units (65 units)
G Population (bursting)
K Pulv: Hz-activated units (67 units)
L Population (bursting)
10Hz
H dLGN: Hz-activated units (63 units)
I Population (bursting)
M Pulv: Hz-activated units (71 units)
N Population (bursting)
Bursting rate (light ON)
Bursting rate (light OFF)
Other
Hz-activated
20Hz

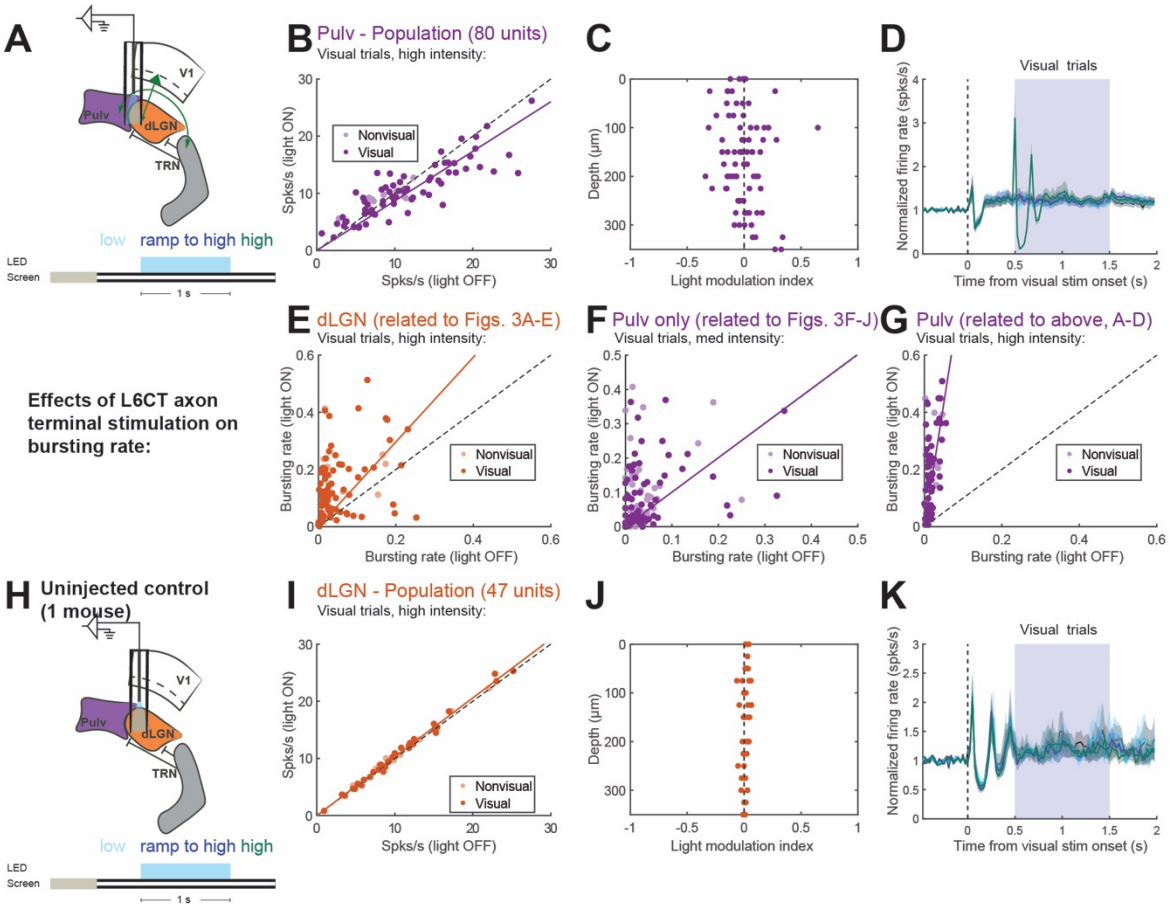

Figure 1.S6 Increased activity with axon terminal stimulation is absent from the pulvinar in experiments using lower light levels and in an uninjected control animal. (A) Diagram of optrode location (half in lateral pulvinar, half in dLGN) and trial structure for visual and LED stimulation. Exact light levels used for "high" photostimulation conditions were titrated per experiment and thus should be interpreted as a relative rather than an absolute value (see Methods). (B) Average firing rates during the 1-second photostimulation period from visual trials, with versus without photostimulation. (C) Light modulation index by depth. (D) Averaged normalized PSTH (visual trials) from all units recorded in the pulvinar during split pulvinar-dLGN optrode recordings. Shading indicates ±1 standard error of the mean. (E-G) Average bursting rates from visual trials, with versus without axon terminal stimulation for: (E) dLGN units during optrode recordings (same experiments as in Figures 1.3A-E); (F) pulvinar units from optrode recordings in which the optrode was entirely in pulvinar (same experiments as in Figures 1.3F-J); (G) pulvinar units from optrode recordings in which probe was split between dLGN and pulvinar and lower light levels were used (same experiments as above in B-D). (H) Diagram of optrode location in dLGN and trial structure during a control experiment in an uninjected wild-type mouse. (I) Average firing rates from control experiment during the 1-second photostimulation period from visual trials, with versus without photostimulation. (J) Light modulation index by depth. (K) Average normalized PSTH (visual trials) from all units during the dLGN control optrode recording. Shading indicates ±1 standard error of the mean.

Acknowledgements

We thank Ashley Juavinett and Pamela Reinagel for comments on the manuscript, Sotiris Masmanidis and Kwang Lee for help with optrode assembly, and other members of the Callaway lab for helpful discussions. This work was supported by NIH grants F31 EY028853 (M.A.K.), R01 MH063912 and R01 EY022577 (E.M.C.).

Chapter 1, in full, is a reprint of the material as it appears in: Kirchgessner, MA, Franklin, AD, & Callaway, EM (2020). Context-dependent and dynamic functional influence of corticothalamic pathways to first- and higher-order visual thalamus. *Proceedings of the National Academy of Sciences*, *117*(23), 13066. The dissertation author was the primary investigator and author of this paper.

References

1. Sherman, S. M. & Guillery, R. W. On the actions that one nerve cell can have on another: Distinguishing "drivers" from "modulators." *Proceedings of the National Academy of Sciences* **95**, 7121–6 (1998).

2. Sherman, S. M. Thalamus plays a central role in ongoing cortical functioning. *Nature Neuroscience* **16**, (2016).

3. Przybyszewski, A. W., Gaska, J. P., Foote, W. & Pollen, D. A. Striate cortex increases contrast gain of macaque LGN neurons. *Visual neuroscience* **17**, 485–94 (2000).

4. Olsen, S. R., Bortone, D. S., Adesnik, H. & Scanziani, M. Gain control by layer six in cortical circuits of vision. *Nature* **483**, 47–52 (2012).

5. Denman, D. J. & Contreras, D. Complex Effects on In Vivo Visual Responses by Specific Projections from Mouse Cortical Layer 6 to Dorsal Lateral Geniculate Nucleus. *The Journal of neuroscience : the official journal of the Society for Neuroscience* **35**, 9265–80 (2015).

6. Wang, W., Andolina, I. M., Lu, Y., Jones, H. E. & Sillito, A. M. Focal Gain Control of Thalamic Visual Receptive Fields by Layer 6 Corticothalamic Feedback. *Cerebral cortex (New York, N.Y. : 1991)* **28**, 267–280 (2018).

7. Wang, W., Jones, H. E., Andolina, I. M., Salt, T. E. & Sillito, A. M. Functional alignment of feedback effects from visual cortex to thalamus. *Nature neuroscience* **9**, 1330–6 (2006).

8. Spacek, M. A., Born, G., Crombie, D., Bauer, Y., Liu, X., Katzner, S. & Busse, L. Robust effects of corticothalamic feedback during naturalistic visual stimulation. *Biorxiv* 776237 (2020) doi:10.1101/776237.

9. Andolina, I. M., Jones, H. E., Wang, W. & Sillito, A. M. Corticothalamic feedback enhances stimulus response precision in the visual system. *Proceedings of the National Academy of Sciences of the United States of America* **104**, 1685–90 (2007).

10. Hasse, J. M. & Briggs, F. Corticogeniculate feedback sharpens the temporal precision and spatial resolution of visual signals in the ferret. *Proceedings of the National Academy of Sciences of the United States of America* **114**, E6222–E6230 (2017).

11. Andolina, I. M., Jones, H. E. & Sillito, A. M. Effects of cortical feedback on the spatial properties of relay cells in the lateral geniculate nucleus. *Journal of neurophysiology* **109**, 889–99 (2013).

12. Mease, R. A., Krieger, P. & Groh, A. Cortical control of adaptation and sensory relay mode in the thalamus. *Proceedings of the National Academy of Sciences of the United States of America* **111**, 6798–803 (2014).

13. Bourassa, J. & Deschênes, M. Corticothalamic projections from the primary visual cortex in rats: a single fiber study using biocytin as an anterograde tracer. *Neuroscience* **66**, 253–63 (1995).

14. Li, J., Wang, S. & Bickford, M. E. Comparison of the ultrastructure of cortical and retinal terminals in the rat dorsal lateral geniculate and lateral posterior nuclei. *The Journal of comparative neurology* **460**, 394–409 (2003).

15. Li, J., Guido, W. & Bickford, M. E. Two distinct types of corticothalamic EPSPs and their contribution to short-term synaptic plasticity. *Journal of neurophysiology* **90**, 3429–40 (2003).

16. Reichova, I. & Sherman, S. M. Somatosensory corticothalamic projections: distinguishing drivers from modulators. *Journal of neurophysiology* **92**, 2185–97 (2004).

17. Guo, W., Clause, A. R., Barth-Maron, A. & Polley, D. B. A Corticothalamic Circuit for Dynamic Switching between Feature Detection and Discrimination. *Neuron* **95**, 180-194.e5 (2017).

18. Pauzin, F. P. P. & Krieger, P. A Corticothalamic Circuit for Refining Tactile Encoding. *Cell reports* **23**, 1314–1325 (2018).

19. Crandall, S. R., Cruikshank, S. J. & Connors, B. W. A corticothalamic switch: controlling the thalamus with dynamic synapses. *Neuron* **86**, 768–82 (2015).

20. Gong, S., Doughty, M., Harbaugh, C. R., Cummins, A., Hatten, M. E., Heintz, N. & Gerfen, C. R. Targeting Cre recombinase to specific neuron populations with bacterial artificial chromosome constructs. *The Journal of neuroscience : the official journal of the Society for Neuroscience* **27**, 9817–23 (2007).

21. Bortone, D. S., Olsen, S. R. & Scanziani, M. Translaminar inhibitory cells recruited by layer 6 corticothalamic neurons suppress visual cortex. *Neuron* **82**, 474–85 (2014).

22. Yang, L., Lee, K., Villagracia, J. & Masmanidis, S. C. Open source silicon microprobes for high throughput neural recording. *J Neural Eng* **17**, 016036 (2020).

23. Beltramo, R. & Scanziani, M. A collicular visual cortex: Neocortical space for an ancient midbrain visual structure. *Science* **363**, 64–69 (2019).

24. Zhou, N. A., Maire, P. S., Masterson, S. P. & Bickford, M. E. The mouse pulvinar nucleus: Organization of the tectorecipient zones. *Visual neuroscience* **34**, E011 (2017).

25. Bennett, C., Gale, S. D., Garrett, M. E., Newton, M. L., Callaway, E. M., Murphy, G. J. & Olsen, S. R. Higher-Order Thalamic Circuits Channel Parallel Streams of Visual Information in Mice. *Neuron* **102**, 477-492.e5 (2019).

26. Williamson, R. S. & Polley, D. B. Parallel pathways for sound processing and functional connectivity among layer 5 and 6 auditory corticofugal neurons. *eLife* **8**, (2019).

27. Jurgens, C. W., Bell, K. A., McQuiston, R. A. & Guido, W. Optogenetic Stimulation of the Corticothalamic Pathway Affects Relay Cells and GABAergic Neurons Differently in the Mouse Visual Thalamus. *PLoS ONE* **7**, e45717 (2012).

28. Hass, C. A. & Glickfeld, L. L. High-fidelity optical excitation of cortico-cortical projections at physiological frequencies. *Journal of Neurophysiology* **116**, 2056–2066 (2016).

29. Pinault, D. & Deschênes, M. Projection and innervation patterns of individual thalamic reticular axons in the thalamus of the adult rat: a three-dimensional, graphic, and morphometric analysis. *The Journal of comparative neurology* **391**, 180–203 (1998).

30. Cruikshank, S. J., Urabe, H., Nurmikko, A. V. & Connors, B. W. Pathway-specific feedforward circuits between thalamus and neocortex revealed by selective optical stimulation of axons. *Neuron* **65**, 230–45 (2010).

31. Briggs, F. & Usrey, W. M. Emerging views of corticothalamic function. *Current opinion in neurobiology* **18**, 403–7 (2008).

32. McCormick, D. A. & Krosigk, M. von. Corticothalamic activation modulates thalamic firing through glutamate "metabotropic" receptors. *Proc National Acad Sci* **89**, 2774–2778 (1992).

33. Vélez-Fort, M., Rousseau, C. V., Niedworok, C. J., Wickersham, I. R., Rancz, E. A., Brown, A. P., Strom, M. & Margrie, T. W. The stimulus selectivity and connectivity of layer six principal cells reveals cortical microcircuits underlying visual processing. *Neuron* **83**, 1431–43 (2014).

34. Stoelzel, C. R., Bereshpolova, Y., Alonso, J.-M. & Swadlow, H. A. Axonal conduction delays, brain state, and corticogeniculate communication. *J Neurosci Official J Soc Neurosci* **37**, 6342–6358 (2017).

35. Tsumoto, T., Creutzfeldt, O. D. & Legéndy, C. R. Functional organization of the corticofugal system from visual cortex to lateral geniculate nucleus in the cat (with an appendix on geniculo-cortical mono-synaptic connections). *Experimental brain research* **32**, 345–64 (1978).

36. Li, L. & Ebner, F. F. Cortical modulation of spatial and angular tuning maps in the rat thalamus. *The Journal of neuroscience : the official journal of the Society for Neuroscience* **27**, 167–79 (2007).

37. Conley, M. & Diamond, I. T. Organization of the Visual Sector of the Thalamic Reticular Nucleus in Galago. *The European journal of neuroscience* **2**, 211–226 (1990).

38. Jones, E. G. *The Thalamus*. (Plenum Press, 1985). doi:10.1007/978-1-4615-1749-8_15.

39. Evangelio, M., García-Amado, M. & Clascá, F. Thalamocortical Projection Neuron and Interneuron Numbers in the Visual Thalamic Nuclei of the Adult C57BL/6 Mouse. *Frontiers in Neuroanatomy* **12**, 27 (2018).

40. Augustinaite, S., Yanagawa, Y. & Heggelund, P. Cortical feedback regulation of input to visual cortex: role of intrageniculate interneurons. *The Journal of physiology* **589**, 2963–77 (2011).

41. Granseth, B. Dynamic properties of corticogeniculate excitatory transmission in the rat dorsal lateral geniculate nucleus in vitro. *The Journal of physiology* **556**, 135–46 (2004).

42. Krosigk, M. von, Monckton, J. E., Reiner, P. B. & McCormick, D. A. Dynamic properties of corticothalamic excitatory postsynaptic potentials and thalamic reticular inhibitory postsynaptic potentials in thalamocortical neurons of the guinea-pig dorsal lateral geniculate nucleus. *Neuroscience* **91**, 7–20 (1999).

43. Lindström, S. & Wróbel, A. Frequency dependent corticofugal excitation of principal cells in the cat's dorsal lateral geniculate nucleus. *Experimental Brain Research* **79**, 313–318 (1990).

44. Jahnsen, H. & Llinás, R. Electrophysiological properties of guinea-pig thalamic neurones: an in vitro study. *The Journal of physiology* **349**, 205–26 (1984).

45. Jahnsen, H. & Llinás, R. Ionic basis for the electro-responsiveness and oscillatory properties of guinea-pig thalamic neurones in vitro. *The Journal of physiology* **349**, 227–47 (1984).

46. Anderson, M. P., Mochizuki, T., Xie, J., Fischler, W., Manger, J. P., Talley, E. M., Scammell, T. E. & Tonegawa, S. Thalamic Cav3.1 T-type Ca2+ channel plays a crucial role in stabilizing sleep. *P Natl Acad Sci Usa* **102**, 1743–1748 (2005).

47. Roth, M. M., Dahmen, J. C., Muir, D. R., Imhof, F., Martini, F. J. & Hofer, S. B. Thalamic nuclei convey diverse contextual information to layer 1 of visual cortex. *Nature neuroscience* **19**, 299–307 (2016).

48. Chevée, M., Robertson, J. D. J., Cannon, G. H., Brown, S. P. & Goff, L. A. Variation in Activity State, Axonal Projection, and Position Define the Transcriptional Identity of Individual Neocortical Projection Neurons. *Cell reports* **22**, 441–455 (2018).

49. Bourassa, J., Pinault, D. & Deschênes, M. Corticothalamic Projections from the Cortical Barrel Field to the Somatosensory Thalamus in Rats: A Single-fibre Study Using Biocytin as an Anterograde Tracer. *Eur J Neurosci* **7**, 19–30 (1995).

50. Hoerder-Suabedissen, A., Hayashi, S., Upton, L., Nolan, Z., Casas-Torremocha, D., Grant, E., Viswanathan, S., Kanold, P. O., Clasca, F., Kim, Y. & Molnár, Z. Subset of Cortical Layer 6b Neurons Selectively Innervates Higher Order Thalamic Nuclei in Mice. *Cerebral cortex (New York, N.Y. : 1991)* **28**, 1882–1897 (2018).

51. Groh, A., Meyer, H. S., Schmidt, E. F., Heintz, N., Sakmann, B. & Krieger, P. Cell-Type Specific Properties of Pyramidal Neurons in Neocortex Underlying a Layout that Is Modifiable Depending on the Cortical Area. *Cerebral Cortex* **20**, 826–36 (2010).

52. Jaramillo, J., Mejias, J. F. & Wang, X.-J. Engagement of Pulvino-cortical Feedforward and Feedback Pathways in Cognitive Computations. *Neuron* **101**, 321-336.e9 (2019).

53. Siegle, J. H., López, A. C., Patel, Y. A., Abramov, K., Ohayon, S. & Voigts, J. Open Ephys: an open-source, plugin-based platform for multichannel electrophysiology. *J Neural Eng* **14**, 045003 (2017).

54. Marshel, J. H., Garrett, M. E., Nauhaus, I. & Callaway, E. M. Functional Specialization of Seven Mouse Visual Cortical Areas. *Neuron* **72**, 1040–54 (2011).

55. Pachitariu, M., Steinmetz, N., Kadir, S., Carandini, M. & D., H. K. Kilosort: realtime spike-sorting for extracellular electrophysiology with hundreds of channels. *Biorxiv* 061481 (2016) doi:10.1101/061481.

56. Rossant, C., Kadir, S. N., Goodman, D. F., Schulman, J., Hunter, M. L., Saleem, A. B., Grosmark, A., Belluscio, M., Denfield, G. H., Ecker, A. S., Tolias, A. S., Solomon, S., Buzsáki, G., Carandini, M. & Harris, K. D. Spike sorting for large, dense electrode arrays. *Nature neuroscience* **19**, 634–41 (2016).

57. Schmitzer-Torbert, N., Jackson, J., Henze, D., Harris, K. & Redish, A. D. Quantitative measures of cluster quality for use in extracellular recordings. *Neuroscience* **131**, 1–11 (2005).

58. Durand, S., Iyer, R., Mizuseki, K., Vries, S. de, Mihalas, S. & Reid, C. R. A Comparison of Visual Response Properties in the Lateral Geniculate Nucleus and Primary Visual Cortex of Awake and Anesthetized Mice. *Journal of Neuroscience* **36**, 12144–12156 (2016).

59. Niell, C. M. & Stryker, M. P. Modulation of visual responses by behavioral state in mouse visual cortex. *Neuron* **65**, 472–9 (2010).

60. Erisken, S., Vaiceliunaite, A., Jurjut, O., Fiorini, M., Katzner, S. & Busse, L. Effects of locomotion extend throughout the mouse early visual system. *Current biology : CB* **24**, 2899–907 (2014).

61. Reinagel, P., Godwin, D., Sherman, S. M. & Koch, C. Encoding of visual information by LGN bursts. *Journal of neurophysiology* **81**, 2558–69 (1999).

62. Pettersen, K. H., Devor, A., Ulbert, I., Dale, A. M. & Einevoll, G. T. Current-source density estimation based on inversion of electrostatic forward solution: Effects of finite extent of neuronal activity and conductivity discontinuities. *J Neurosci Meth* **154**, 116–133 (2006).

63. Pi, H.-J. J., Hangya, B., Kvitsiani, D., Sanders, J. I., Huang, Z. J. & Kepecs, A. Cortical interneurons that specialize in disinhibitory control. *Nature* **503**, 521–4 (2013).

Chapter 2. Distinct "driving" versus "modulatory" influences of different visual corticothalamic pathways

Abstract

Higher-order (HO) thalamic nuclei interact extensively with the cerebral cortex and are innervated by excitatory corticothalamic (CT) populations in layers 5 and 6. While these distinct CT projections have long been thought to have different functional influences on the HO thalamus, this has never been directly tested. By optogenetically inactivating different CT populations in the primary visual cortex (V1) of awake mice, we demonstrate that layer 5, but not layer 6, CT projections drive visual responses in the HO visual pulvinar, even while both pathways provide retinotopic, baseline excitation to their thalamic targets. Inactivating the superior colliculus also affected visual responses in the pulvinar, demonstrating that cortical layer 5 and subcortical inputs both contribute to HO visual thalamic activity - even at the level of putative single neurons. Altogether, these results indicate a functional division of driver and modulator CT pathways from V1 to the visual thalamus *in vivo.*

Introduction

The thalamus and its interactions with the cortex are increasingly appreciated as essential for sensory-guided behaviors and complex cognition[1]. Yet, the nature of these interactions – how the content and manner of communication through cortico-thalamo-cortical pathways are controlled – has been difficult to decipher. This is especially true as it pertains to "higher-order" (HO) thalamic nuclei, such as the pulvinar in the visual system (also sometimes referred to as "LP" in rodents). The pulvinar has been implicated in synchronizing activity across visual cortical areas to support visual attention[2,3] and in integrating sensory signals with behavioral context[4,5]. Still, a mechanistic understanding of the complex interactions between cortex and HO nuclei like the pulvinar has been hindered by incomplete knowledge of the functional impact of their cortical inputs in vivo.

While critical questions remain, decades of research into the anatomy and physiology of corticothalamic (CT) circuitry across systems and species have revealed a number of common motifs. For

instance, most glutamatergic synapses in the thalamus fall into two major categories, characterized by differences in synapse strength, size, number, post-synaptic receptor type, short-term plasticity, and more[6,7] (Figure 2.1a). Their distinctions are noteworthy because these different synapse classes arise from different inputs. For example, "type 1" synapses in first-order (FO) thalamic nuclei, like the dorsolateral geniculate nucleus (dLGN), come from layer 6 corticothalamic feedback neurons (L6CTs, e.g., in V1), whereas "type 2" come from the sensory periphery (e.g., retinal ganglion cells, RGCs). Because visual responses in the dLGN – where these classes were first described[8,9] - are driven by RGC input[10,11], type 2 inputs are considered "drivers". In contrast, because CT feedback is not responsible for visual responses in the dLGN but appears to exert more subtle influences[12], type 1 synapses are called "modulators".

Meanwhile, the functional contributions of different inputs to HO nuclei like the pulvinar is much less clear. HO nuclei (like FO) are also innervated by L6CTs with type 1, "modulator" synapses, but uniquely receive an additional cortical input from a CT subpopulation of layer 5 extratelencephalic neurons (L5ETs) with type 2, "driver"-like characteristics[13–18] (Figure 2.1a). L5CTs are thus frequently referred to as "drivers" and L6CTs as "modulators" of HO nuclei[6,19], but whether these parallel CT projection pathways are functionally distinct has never been directly tested[7]. Experiments demonstrating V1 driving influences on the pulvinar, as well as other HO thalamic nuclei, have relied on inferences following complete (chronic or transient) cortical inactivation[20–25], as opposed to layer-specific manipulations of the putative L5CT driving pathway. However, these non-specific approaches would be expected to affect activity in both L5CTs and L6CTs, as well as activity in other cortical areas and subcortical structures. Therefore, while prior studies would suggest that at least parts of the pulvinar receive driving input from V1, the hypothesized "driving" versus "modulatory" functions of L5CT versus L6CT pathways to the pulvinar, and HO nuclei more broadly, have yet to be dissociated.

Moreover, a distinguishing feature of HO compared to FO nuclei is their diversity of excitatory input sources. The pulvinar, for instance, receives L5CT and L6CT projections from extrastriate cortical areas in addition to V1[4,5,26,27], as well as subcortical excitation from the superior colliculus (SC)[28]. Notably, these SC projections display a mix of "type 1" and "type 2" characteristics[7] and have even been

shown to drive activity in the caudomedial subdivision of the rodent pulvinar (cmPulv)[21,22]. In the lateral subdivision that receives both cortical and ipsilateral SC input (lPulv)[28], it is unclear whether SC projections are still drivers or how (and if) they might interact with cortical afferents to shape visual responses. Perhaps these diverse cortical and subcortical projections could support the pulvinar's proposed roles in multisensory and sensorimotor integration and conveying both visual and contextual signals to downstream cortical areas[4,5,29–31]. Yet how these different inputs – L5CT versus L6CT, cortical versus subcortical – interact in the pulvinar *in vivo* is not presently known.

Here, we utilize a variety of viral and transgenic approaches to selectively inactivate L5 versus L6 CT projections from the primary visual cortex to the pulvinar and dLGN in awake mice and assess their contributions to thalamic activity and visual responses. We find that inactivating L6CTs in V1 can suppress thalamic activity in topographically aligned neurons, most prominently in the dLGN, but this effect is limited to spontaneous as opposed to visually evoked activity. In contrast, L5ET inactivation profoundly suppresses visual activity and receptive field properties in addition to spontaneous activity in some, yet not all, topographically aligned pulvinar units. Further experiments using dual color optogenetics confirmed that individual pulvinar neurons' visual responses are suppressed by L5CT, but not L6CT, inactivation in V1. Thus, while L6CTs can suppress thalamic neurons' baseline activity, they are not necessary for visual responses in the thalamus and are therefore modulatory. Meanwhile, L5CTs are drivers of visual in addition to baseline activity in a subset of pulvinar neurons, whereas others may receive their driving input from outside V1. We thus further investigated the effects of SC inactivation on pulvinar activity, either alone or combined with L5ET inactivation in V1. We find that the pulvinar contains a variety of neurons whose visual responses are driven by V1 L5CTs, by the SC, or even by both, as well as neurons with undetermined driving sources. Altogether, our findings confirm a longstanding but untested hypothesis regarding the dissociable functions of distinct CT projection populations, and also highlight the role of the rodent HO visual thalamus in integrating inputs from both cortical and subcortical sources as opposed to a strictly feed-forward trans-thalamic pathway.

Results

Selective optogenetic inactivation of L5 vs. L6 corticothalamic pathways using different Cre transgenic mouse lines

The mouse pulvinar receives cortical input from two excitatory cell types in V1: corticothalamic (CT) neurons in L6, and a CT subpopulation of extratelencephalic (ET) projection neurons in L5. Consistent with prior studies[4,5,35,36], we confirmed that injections of a cholera toxin subunit B (CTB) retrograde tracer into the pulvinar labeled many L6CTs – primarily in the lower half of L6 - and fewer L5CTs in V1, as well as in surrounding extrastriate cortical areas (Figure 2.1b). We also observed more prominent L5CT labeling when using a self-complimenting retrograde AAV (scAAVretro) injected into pulvinar to retrogradely express a fluorophore without infecting L6CTs[37] (Figure 2.1c).

To target each of these CT populations in V1 for specific optogenetic manipulations, we took advantage of two Cre driver lines. For L6CTs, we utilized the Ntsr1-Cre GN220 BAC transgenic mouse line[38], which has been shown to label L6CTs projecting to the dLGN with near-perfect efficiency and specificity[39,40] and which we previously used to optogenetically stimulate L6CT projections to the dLGN and pulvinar[20]. As expected, following injection of Cre-dependent AAV in V1, axons with "type 1" morphology were observed in both the pulvinar and dLGN (Figure 2.1c). However, not all L6CTs also project to pulvinar. L6CTs in V1 that were retrogradely labeled from the pulvinar were largely restricted to lower L6[4,5,36] (Figure 2.1b,e) and were still a relative minority of all L6CT cells (34.71% in lower L6, 21.5% in all of L6). These proportions are likely underestimates of the full pulvinar-projecting L6CT population, as we had to make smaller and slightly medial injections to avoid the dLGN. Nevertheless, nearly all (87.49% in lower L6, 86.31% in all of L6) pulvinar-projecting L6CTs were labeled by the Ntsr1-Cre line (Figure 2.1e), thus validating the use of this line for reliably targeting the L6CT projection pathway for optogenetic manipulation.

In contrast to the widely used Ntsr1-Cre line, a transgenic mouse line that specifically labels L5ETs with sufficient coverage in V1 has been largely elusive. The most commonly used L5 excitatory mouse line, Rbp4-Cre, labels L5ETs as well as L5 cortico-cortical (CC) neurons[41,42] (Figure 2.S1), which

Figure 2.1 The mouse pulvinar receives V1 input from two distinct corticothalamic (CT) populations that are selectively targeted by different Cre mouse lines. a) Schematic of the visual CT circuit and different glutamatergic synapse classes. Bottom: cartoons of thalamocortical neurons in first-order (FO; e.g., dLGN) and higher-order (HO; e.g., pulvinar) thalamic nuclei which receive type 1 inputs from L6CTs and type 2 from retinal ganglion cells and L5ETs, respectively. These different synapse types exhibit different anatomical and physiological properties (e.g., size, number and location of boutons, left, and short-term plasticity dynamics, right). b) Retrograde tracing with CTB-647 from the pulvinar reveals prominent L6 (primarily lower L6) and fewer, weakly labeled L5 cells (middle), whereas a self-complimenting (sc)AAVretro-mCherry results in more robust L5 labeling but none in L6. 100µm scale bars. c) AAV injection of Cre-dependent GFP into V1 of Ntsr1-Cre transgenic mice results in specific labeling in L6. As expected from the known circuitry (see a), prominent L6 axons are visible in both dLGN and pulvinar with small, diffuse terminals (right; higher magnification view of boxed region). 100µm and 25µm scale bars in full and zoom images, respectively. d) AAV injection of Cre-dependent eYFP into V1 of Npr3-IRES-Cre-neo mice results in specific labeling in L5. L5 axons are only present in the pulvinar (not dLGN) and exhibit larger and sparser terminals compared to those from L6 (right). e) Retrograde labeling (using CTB) from the pulvinar in Ntsr1-Cre/Ai14 mice. 100µm scale bar. Individual and composite channel images are from the boxed region. Right: Quantification of double-labeled cells out of all tdTomato+ cells (Cre+) and out of all CTB+ (CT) cells in L6upper, L6lower, and all of L6. Points are individual animals (n=3 mice), bars represent the mean across animals. h) Retrograde labeling (using scAAVretro-mCherry) from the pulvinar in Npr3-Cre mice with AAV injection of Cre-dependent eYFP into V1. 100µm scale bar. Individual and composite channel images are from the boxed region. Right: quantification of double-labeled cells out of all eYFP+ cells (Cre+) and out of all mCherry+ cells (CT; n=4 mice).

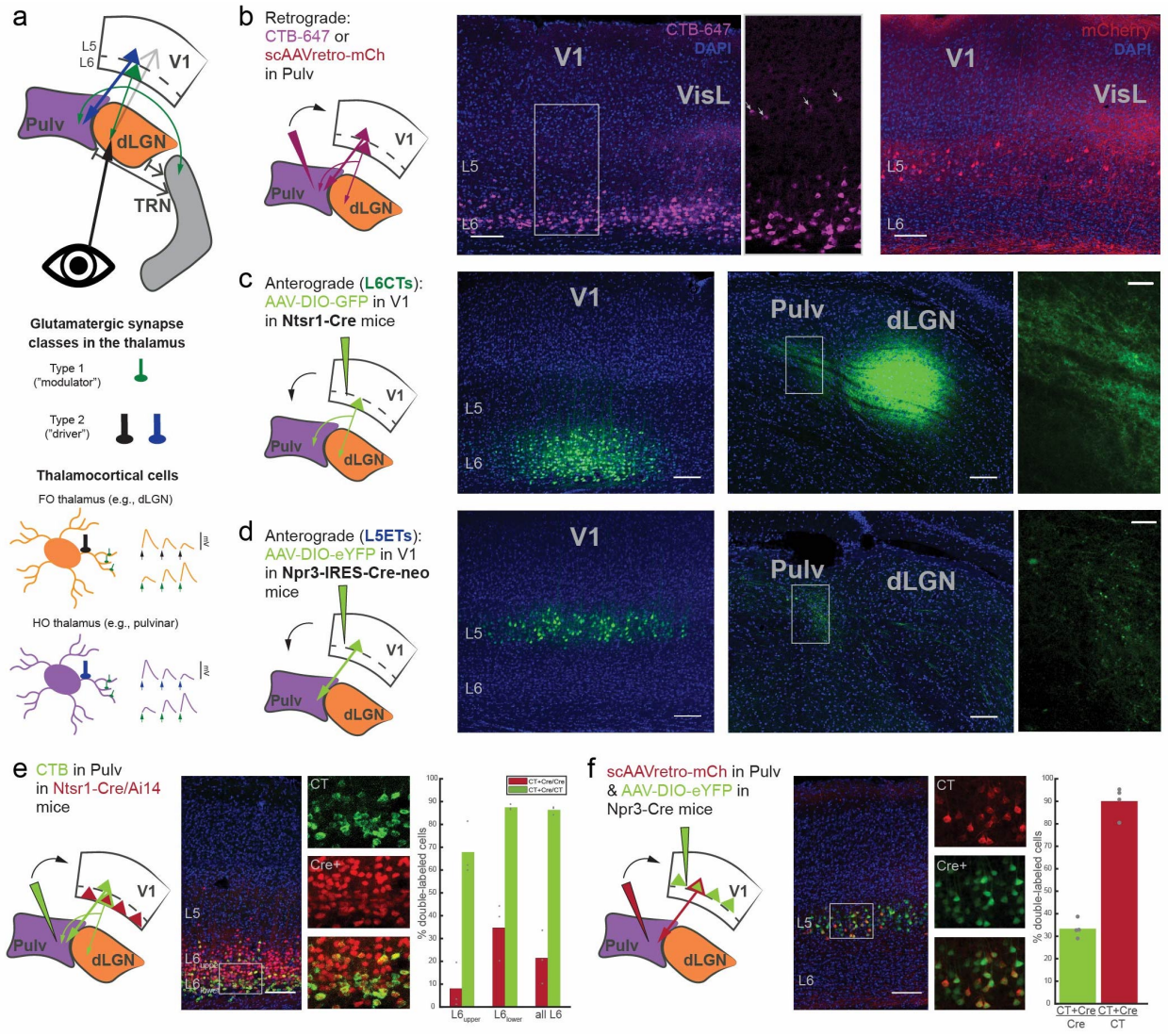
a
L5
L6
V1
Pulv
dLGN
TRN
Glutamatergic synapse classes in the thalamus
Type 1 ("modulator")
Type 2 ("driver")
Thalamocortical cells
FO thalamus (e.g., dLGN)
HO thalamus (e.g., pulvinar)
b Retrograde: CTB-647 or scAAVretro-mCh in Pulv
CTB-647
DAPI
VisL
mCherry
c Anterograde (L6CTs): AAV-DIO-GFP in V1 in Ntsr1-Cre mice
d Anterograde (L5ETs): AAV-DIO-eYFP in V1 in Npr3-IRES-Cre-neo mice
e CTB in Pulv in Ntsr1-Cre/Ai14 mice
CT
Cre+
% double-labeled cells
CT+Cre/Cre
CT+Cre/CT
L6upper
L6lower
all L6
f scAAVretro-mCh in Pulv & AAV-DIO-eYFP in Npr3-Cre mice
CT+Cre
Cre
CT

may play considerable roles in direct inter- and intra-cortical signaling that could confound interpretations about the L5ET-specific CT pathway from V1. Thus, we characterized and used a new knock-in transgenic mouse line, Npr3-IRES-Cre-neo[43] (hereto referred to as Npr3-Cre) that showed considerable efficiency and specificity for L5ETs (Figure 2.1d,f). Anterograde tracing from this line yielded axons specifically in the pulvinar, but not the dLGN, with relatively large and sparse "type 2" terminals – as expected from the known anatomy of L5 CT projections[16]. Indeed, we found that virtually all (90.08%) L5CT neurons retrogradely labeled from the pulvinar co-expressed a Cre-dependent fluorophore following AAV injection (Figure 2.1f) and were completely non-overlapping with retrogradely labeled CC neurons (Figure 2.S1). Precisely a third (33.33%) of Cre+ neurons projected to the pulvinar, which is expected given the heterogeneity of L5ETs' subcortical projection targets (Figure 2.S2). Therefore, the Npr3-Cre line allows for privileged access to L5ET neurons, including the putative "driving" pathway from V1 to the pulvinar.

Having verified the specificity of these mouse lines, we preceded to inject Ntsr1-Cre and Npr3-Cre mice with an AAV encoding Cre-dependent halorhodopsin into V1 to allow for selective inactivation of L6CTs or L5ETs (Figure 2.2a,b). We then used high-density silicon microprobes[44] to record extracellular single-unit activity from V1 in awake, headfixed mice viewing full-field square-wave drifting gratings to verify the efficacy and specificity of our inactivation approach. Current source density analysis was used to determine the laminar location of each recorded unit in an unbiased manner (Figure 2.2c). Strikingly, red light used to stimulate halorhodopsin in each of these mouse lines resulted in potent and highly layer-specific inactivation (Figure 2.2d,g). Because each of these lines only labels subpopulations of excitatory neurons within a particular layer (L6CT or L5ET), not all regular-spiking (i.e., excitatory) units were silenced, as expected. At least 47/223 (21.08%) and 64/108 (59.26%) regular-spiking units in layers 6 and 5, respectively, putatively expressed halorhodopsin (>50% reduction in visually evoked firing rates, Figure 2.2e,h, and example "inactivated" units in Figure 2.2f,i). While those in L6 were fewer than would have been expected given the known proportions of excitatory cell types in L6[39], L6CTs are likely undersampled in our recordings as they are relatively small pyramidal cells with

Figure 2.2 Selective inactivation of L6CTs or L5ETs in primary visual cortex of awake mice. a) Experiment schematic. Mice were awake and headfixed on a wheel and viewing full-field drifting gratings during laminar V1 recordings. b) An AAV encoding Cre-dependent halorhodopsin (eNpHR3.0-eYFP) was injected into V1 in Ntsr1-Cre (L6CTs, left) or Npr3-Cre (L5ETs, right) mice. c) Left: schematic of a 64ch silicon probe typically used for V1 recordings. Right: current source density plot for the right column of channels in an example recording. Layers corresponding to each channel's location were defined by an initial current sink in L4 and a delayed sink in L5B. d) Light modulation index $((FR_{lightON} - FR_{lightOFF}) / (FR_{lightON} + FR_{lightOFF}))$ from visual trials (LMI_{vis}) for all units by depth relative to the L4-5 border. e) Left: LMI_{vis} by layer for regular-spiking units (RS). Boxplots display the median and quartiles, and putative inactivated units (L6 RS and LMI_{vis} <-.33) are colored dots. Right: proportion of all L6 RS units that were putatively directly inactivated. f) An example inactivated L6 unit. Left: raster plot of all trials organized by condition (green=light ON trials for L6CT inactivation). Right: peristimulus time histogram (PSTH) of average firing rates across visual light OFF (black) or light ON (green) trials. Red shading corresponds to the period of light stimulation. g-i) Same as d-f) but for L5ET inactivation experiments.

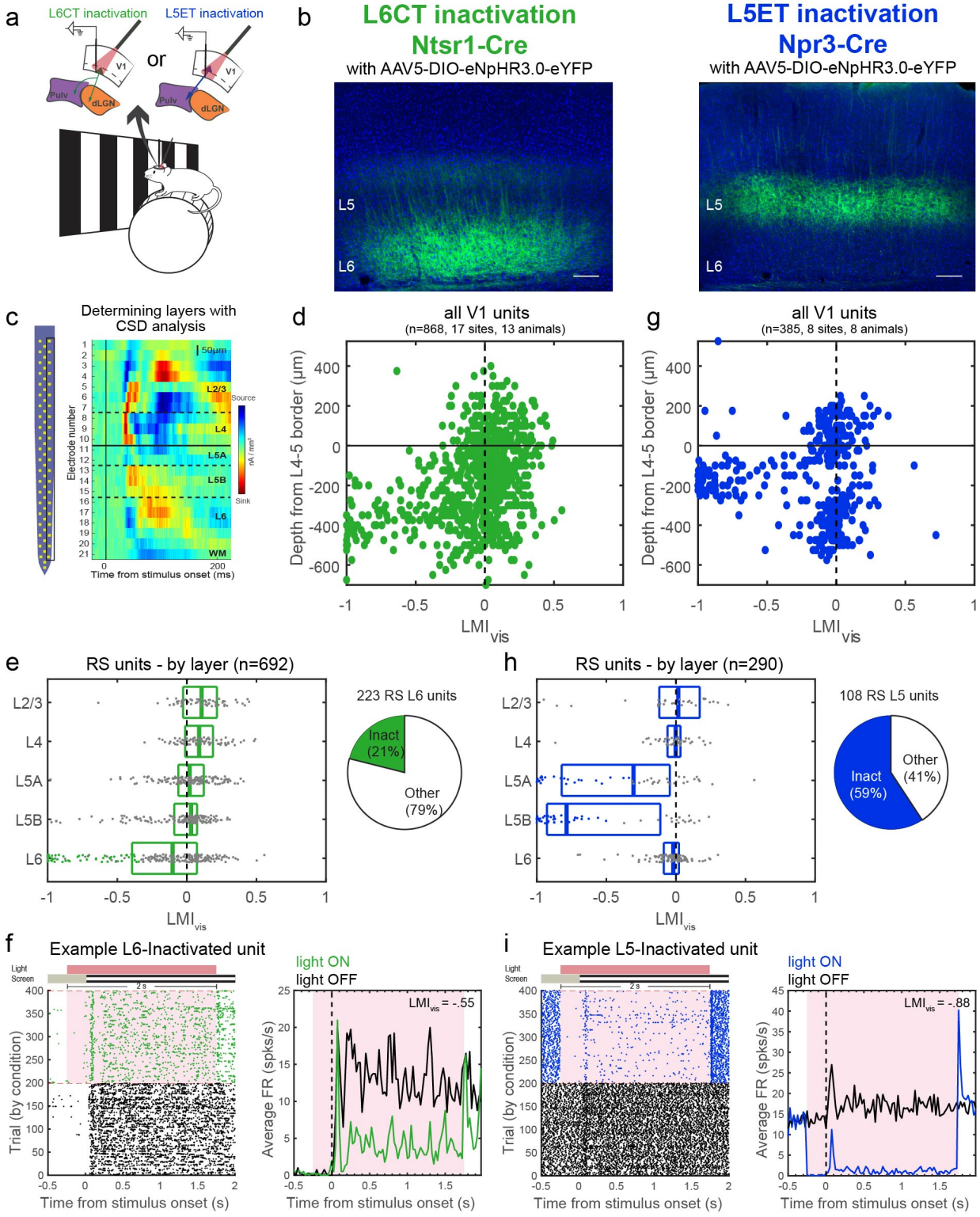
a
L6CT inactivation
L5ET inactivation
or
V1
Pulv
dLGN
b
L6CT inactivation
Ntsr1-Cre
with AAV5-DIO-eNpHR3.0-eYFP
L5ET inactivation
Npr3-Cre
with AAV5-DIO-eNpHR3.0-eYFP
L5
L6
c
Determining layers with CSD analysis
50μm
L2/3
L4
L5A
L5B
L6
WM
Source
Sink
nA / mm³
Electrode number
Time from stimulus onset (ms)
d
all V1 units
(n=868, 17 sites, 13 animals)
Depth from L4-5 border (μm)
LMI vis
g
all V1 units
(n=385, 8 sites, 8 animals)
Depth from L4-5 border (μm)
LMI vis
e
RS units - by layer (n=692)
L2/3
L4
L5A
L5B
L6
LMI vis
223 RS L6 units
Inact (21%)
Other (79%)
h
RS units - by layer (n=290)
L2/3
L4
L5A
L5B
L6
LMI vis
108 RS L5 units
Inact (59%)
Other (41%)
f
Example L6-Inactivated unit
Light Screen
2 s
Trial (by condition)
Time from stimulus onset (s)
light ON
light OFF
LMI vis = -.55
Average FR (spks/s)
Time from stimulus onset (s)
i
Example L5-Inactivated unit
Light Screen
2 s
Trial (by condition)
Time from stimulus onset (s)
light ON
light OFF
LMI vis = -.88
Average FR (spks/s)
Time from stimulus onset (s)

exceptionally sparse and tuned activity[45], compared to L5ETs which are large cells with high (~10Hz) spontaneous firing rates and considerably less tuning selectivity (Figure 2.S3). The fact that we observed increased activity across other layers upon L6CT inactivation, which has been previously reported in mouse V1[39], provides additional evidence that our suppression was effective (Figure 2.S3). Altogether, we have therefore identified Cre-driver mouse lines, including a L5ET-specific line, which allow for layer- and cell type-specific optogenetic inactivation of distinct CT projection populations.

L5 vs. L6 CT pathways differ in their effects on visually evoked activity in the visual thalamus

We next turned to the thalamus to determine how inactivating L6CT versus L5ET projections affected activity and visual processing in the lateral pulvinar (lPulv) of awake mice (Figure 2.3). Because the L6CT projections to the dLGN are a known "modulatory" pathway[9], we also probed the effects of L6CT inactivation on activity in the dLGN. There, L6CT inactivation had disparate effects on spontaneous versus visually evoked activity. In line with another recent study in awake mice[22], we observed considerable suppression of spontaneous activity in a number of units ("Suppressed": e.g., Figure 2.3c) and across the population as a whole (Figures 2.3d and 2.S4). However, the presence of a visual stimulus greatly reduced – and in most cases eliminated – any suppression of dLGN activity induced by L6CT inactivation (e.g., Figure 2.3c,d), and even subtly increased the temporally modulated ("F1") response (Figure 2.S4). This was also observed in an additional set of experiments in which V1 was inactivated non-specifically (Figure 2.S5). Because of the distinct effects on spontaneous versus visually evoked activity, "suppressed" cells here and throughout this study (unless otherwise indicated) are those whose *spontaneous* activity was significantly reduced by the optogenetic manipulation (see Methods). While fewer instances of suppressed units were observed in the pulvinar (although some exhibited transient suppression in the first ~200ms of light onset; e.g., Figure 2.3e), L6CT inactivation had no discernable effect on visually evoked activity, similar to the dLGN. This suggests that L6CT innervation is not necessary for visual responses in the dLGN or pulvinar, consistent with a fundamentally modulatory role for these projections in both FO and HO nuclei. They can, however, contribute to baseline activity,

Figure 2.3 L6CT vs. L5ET inactivation has distinct effects on spontaneous and visually evoked activity in the dLGN and lateral pulvinar (lPulv). a) Experiment schematic - thalamus recordings in the same animals as in Figure 1.2. b) Histological verification of lPulv recording locations (probe shanks coated in DiI, red) in L6CT (left) and L5ET (right) inactivation experiments. Immunohistochemical staining for calretinin (purple) delineates borders between cmPulv (Calr+ cell bodies), lPulv (Calr-), and dLGN (Calr+ axons). Scale bars = 200µm. c) Example of a dLGN unit whose spontaneous (right), but not visually evoked (left), activity is suppressed by L6CT inactivation. Plots are PSTHs of average firing rates (spks/s) across all visual (left) or blank (right) trials with (green) or without (black) L6CT inactivation. d) LMIs of visually evoked (left) or spontaneous (right) activity from all recorded units in dLGN, arranged dorsal-ventral. Units are colored according to whether their spontaneous activity was significantly suppressed or enhanced by L6CT inactivation. Far-right: proportion of visually responsive units suppressed, enhanced, or non-modulated ("other"). e) Example of a lPulv unit unaffected by L6CT inactivation except at the onset of inactivation in both visual and blank trials (indicated by arrows). f) Same as d) but for lPulv units. g) Example of a lPulv unit whose visually evoked and spontaneous activity is suppressed by L5ET inactivation. h) Same as d) but for lPulv units in L5ET inactivation experiments. i) Median visual LMIs for suppressed and enhanced dLGN and lPulv units under L6CT vs. L5ET inactivation conditions. $p<.0001$ for L5ET-Pulv vs. L6CT-dLGN, suppressed units, and $p=.044$ for L5ET-Pulv vs L6CT-Pulv, enhanced units; all other comparisons n.s. (Kruskal-Wallis non-parametric test with the Dunn–Šidák post-hoc test for multiple comparisons). j) Average visually evoked changes in FR ($abs(FR_{vis}-FR_{spont})$) in Light-OFF vs. Light-ON trials for dLGN units in L6CT inactivation experiments ($p=0.016$), lPulv units in L6CT inactivation experiments ($p=0.5$), and lPulv units in L5ET inactivation experiments ($p=0.012$), Wilcoxon signed-rank tests. k) Distribution of visual (-) and spontaneous (- -) LMIs for visually responsive dLGN units in L6CT inactivation experiments (orange), lPulv units in L6CT (green) and L5ET (blue) inactivation experiments, and combined lPulv and dLGN units in control experiments (grey).

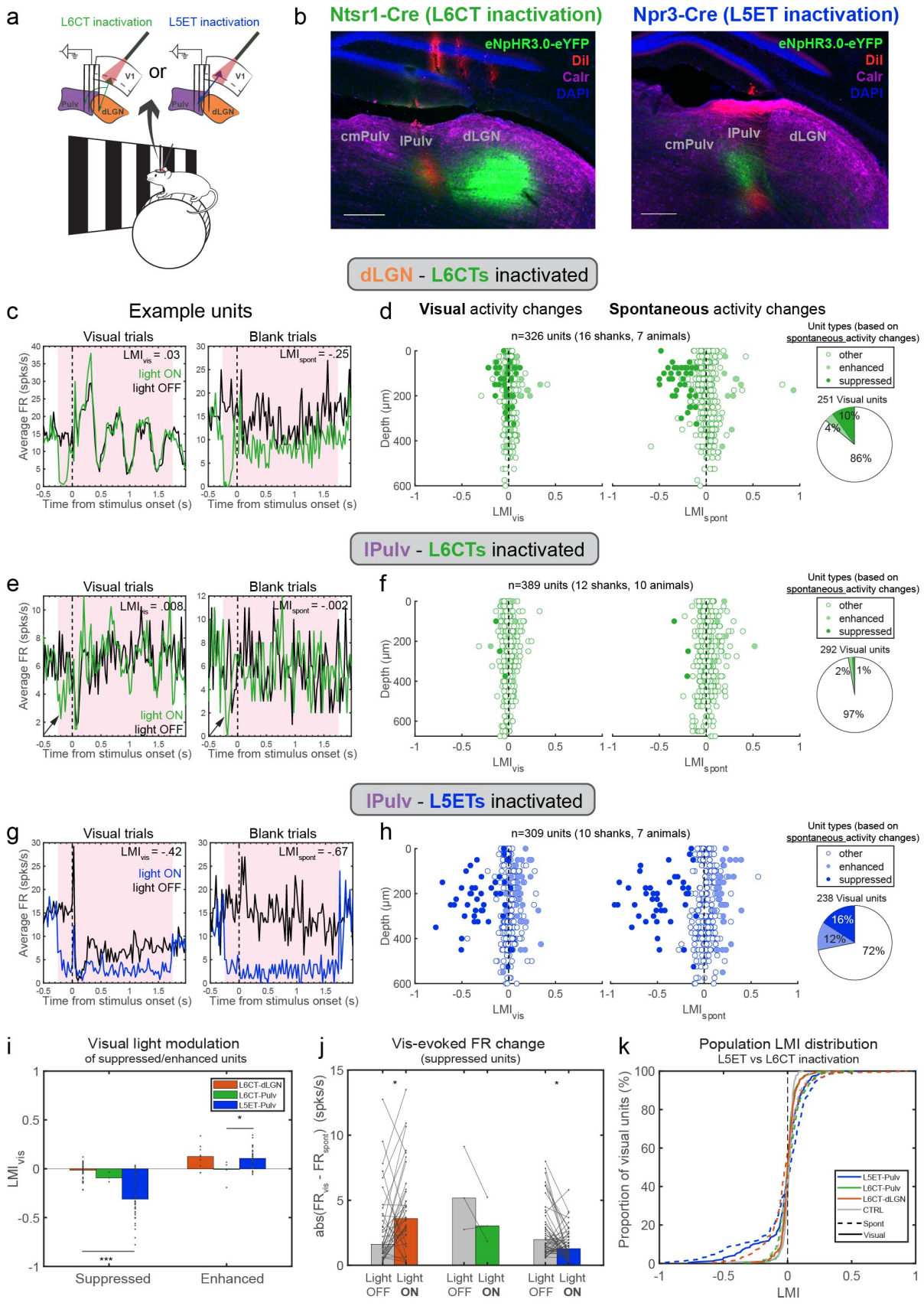
a
L6CT inactivation
L5ET inactivation
or
V1
lPulv
dLGN
b
Ntsr1-Cre (L6CT inactivation)
Npr3-Cre (L5ET inactivation)
eNpHR3.0-eYFP
DiI
CaIr
DAPI
cmPulv
lPulv
dLGN
dLGN - L6CTs inactivated
c
Example units
Visual trials
Blank trials
LMIvis = .03
LMIspont = -.25
light ON
light OFF
Average FR (spks/s)
Time from stimulus onset (s)
d
Visual activity changes
Spontaneous activity changes
n=326 units (16 shanks, 7 animals)
Depth (µm)
LMIvis
LMIspont
Unit types (based on spontaneous activity changes)
other
enhanced
suppressed
251 Visual units
10%
4%
86%
lPulv - L6CTs inactivated
e
LMIvis = .008
LMIspont = -.002
f
n=389 units (12 shanks, 10 animals)
292 Visual units
2%
1%
97%
lPulv - L5ETs inactivated
g
LMIvis = -.42
LMIspont = -.67
h
n=309 units (10 shanks, 7 animals)
238 Visual units
16%
12%
72%
i
Visual light modulation
of suppressed/enhanced units
L6CT-dLGN
L6CT-Pulv
L5ET-Pulv
Suppressed
Enhanced
j
Vis-evoked FR change
(suppressed units)
Light OFF
Light ON
k
Population LMI distribution
L5ET vs L6CT inactivation
Proportion of visual units (%)
L5ET-Pulv
L6CT-Pulv
L6CT-dLGN
CTRL
Spont
Visual
LMI

particularly in the dLGN.

L5ET inactivation, on the other hand, had substantial effects not only on baseline activity, but also on visual responses in lPulv neurons (e.g., Figure 2.3g). Units whose spontaneous activity was significantly suppressed by L5ET inactivation also exhibited considerably reduced activity in the presence of the drifting grating stimulus (Figure 2.3h). Consequently, the degree of L6CT/L5ET modulation of visual responses (visual light modulation index, LMI_{vis}) was greater in L5ET-suppressed lPulv neurons compared to L6CT-suppressed neurons in either the dLGN or the few in the pulvinar (Figure 2.3i). Considered another way, L5ET inactivation reduced the effect of the visual stimulus on activity (magnitude of difference between visual and spontaneous firing rates) in suppressed lPulv units, suggesting that some degree of visual information is conveyed to these pulvinar neurons through the L5ET pathway (Figure 2.3j). In contrast, visually induced activity changes somewhat increased in L6CT-suppressed dLGN units, as a consequence of their reduced baseline but unchanged visually evoked firing rates (Figure 2.3j). These differences cannot be attributed to differences in firing mode induced by L6CT versus L5ET inactivation because we observed increased bursting activity in both cases (Figure 2.S4). They are also not exclusive to lPulv, as we also observed suppressed visual activity during L5ET but not L6CT inactivation in the rostromedial pulvinar (rmPulv), which also receives direct V1 input (Figure 2.S6); we therefore combine data from lPulv and rmPulv (collectively referred to as "pulvinar") for all further analyses unless indicated otherwise. Altogether, we have observed a striking dissociation between the effects of L6CT versus L5ET inactivation on visual activity in the thalamus. This distinction is consistent with the predicted "driving" function of the L5CT pathway, as opposed to "modulatory" CT feedback from L6[9].

Nevertheless, it is notable that even the "driving" effects of L5ET inactivation were observed in a minority of visually responsive pulvinar units (Figure 2.3h,k). This contrasts with some expectations from the proposed models of L5 "drivers" mediating a trans-thalamic feedforward pathway from primary to higher-order cortical areas[8,19,46–48]. We therefore sought to gain further insight into the functional organization of these distinct CT "driving" and "modulatory" pathways.

Retinotopic organization of both L6CT and L5ET excitatory projections to the dLGN and pulvinar

The pulvinar is topographically organized – both in terms of its representations of visual space (i.e., retinotopy[4,28,49,50]) and its connections with various visual cortical areas[51,52]. V1 projections to the pulvinar[28], as well as pulvinar projections back to V1[4], are also coarsely retinotopic. Even though we limited our pulvinar analyses to recordings in which the recording shank passed through CT terminals from V1, nearby pulvinar neurons can have RFs separated by more than 20 degrees[28,53]. Thus, pulvinar neurons that were not modulated by L5ET suppression might simply have not been retinotopically aligned to the cortical inactivation area, causing us to underestimate the "driving" influence of V1 L5ET projections on the pulvinar. Additionally, given recent findings of spatially organized effects of L6CT activation[42], we wondered whether retinotopy might also explain some of the effects of L6CT inactivation on spontaneous activity that we observed in the dLGN, and more modestly in the pulvinar.

To identify receptive field (RF) locations of V1 and thalamic neurons, we utilized a sparse noise stimulus protocol (Methods). This allowed us to identify both "on" and "off" subfields (in response to luminance increases and decreases, respectively) and to precisely coordinate each stimulus presentation with the presence or absence of light stimulation to determine the effects of L6CT or L5ET inactivation on receptive field properties (Figure 2.4a). An example L6CT inactivation experiment, in which V1, dLGN and lPulv were all recorded from simultaneously, is depicted in Figure 2.4b, and a L5ET inactivation experiment with consecutive V1 and lPulv recordings is shown in Figure 2.4c. As expected, V1 neurons recorded across layers were all retinotopically aligned, whereas thalamus penetrations yielded units whose RFs moved along the elevation and/or azimuth axes according to recording depth. For units whose RFs could be confidently identified (see Methods for criteria), their RF information was then related to their responses to drifting grating stimuli and their degrees of light modulation.

In both L6CT and L5ET inactivation experiments, the largest suppressive effects (whether on spontaneous and/or visually evoked activity) were observed in thalamic units whose RFs were closely aligned to those recorded in V1, while units from the same recording penetration whose RF centers were displaced by 20° or more were typically unaffected (Figure 2.4b,c). Thus, when considering thalamic

Figure 2.4 Corticothalamic excitation by both V1 L6CTs and L5ETs is retinotopically organized. a) Schematics of: V1 and thalamus recording configuration (recorded simultaneously in majority of experiments, top) and visual stimulation protocols: sparse noise stimuli (for receptive field mapping - presented at 4Hz; middle) and drifting gratings (temporal frequency=2Hz) with and without light for optogenetic CT inactivation (bottom). b) Example L6CT inactivation experiment in which V1, dLGN and lPulv were recorded from simultaneously. Top: overlayed ON-field RFs (see Methods) from recording shanks in V1, dLGN and lPulv. Sparse noise stimuli (8° squares) were presented in a 12x14 grid. RFs are colored according to their dorsal-ventral location relative to other RFs recorded on the same shank. Middle: Example dLGN (first two columns) and lPulv (third column) units' RFs without (top) and with (bottom) L6CTs inactivated, shown as baseline-subtracted FRs at the same peak timepoint at all possible stimulus positions. Overlayed perimeters and dots indicate estimated RF outline and centroids (see Methods). Note that the first dLGN unit and the lPulv unit's RFs overlap with the retinotopic location of V1 recording; the second dLGN unit does not. Bottom: PSTHs of the same units in response to drifting grating stimuli. Note that the retinotopically aligned dLGN and lPulv units' prestimulus (spontaneous), but not visually evoked, activity was suppressed by L6CT inactivation. c) Same as b) but for a L5ET-inactivation experiment in which V1 and pulvinar were recorded from consecutively (10x12 grid for V1 recording, 12x14 for pulvinar). d) Relationship between light modulation (in drifting grating experiments) and retinotopic displacement from V1 recording site (i.e., the retinotopic locus of L6CT inactivation) from experiments in which sparse noise stimulation was used for both LGN and V1 recordings. Dots indicate LMI_{vis} (right y-axis) of enhanced, suppressed, and other cells (same as Figure 3: classified from blank trials). Pink-outlined dots are the example units from b). Bars indicate proportion of units significantly suppressed or enhanced (left y-axis), binned by retinotopic distance (10° bins). 'Other Vis' are all other units from the same experiments whose RFs could not be determined. White bars reflect means of 1000 shuffled distributions (shuffled separately for each experiment). Asterisks indicate where actual proportions fell beyond either tail (2.5%) of shuffled distributions. e) Same as d) but for pulvinar units defined as "suppressed" from the prestimulus period following light onset (e.g., example pulvinar unit in b). f) Same as d) but for pulvinar units during L5ET inactivation experiments. g) Percent of all pairs of units from each recording shank consisting of at least one suppressed unit in which the second unit was also suppressed or enhanced, binned by vertical distance between units in a pair. White bars reflect means of 1000 shuffled distributions (shuffled separately for each recording shank). Asterisks indicate where actual proportions fell beyond either tail (2.5%) of shuffled distributions. h-i) Same as g) but for pulvinar units in L6CT inactivation experiments (h; "onset suppressed" cells as in e) and pulvinar units in L5ET inactivation experiments (i).

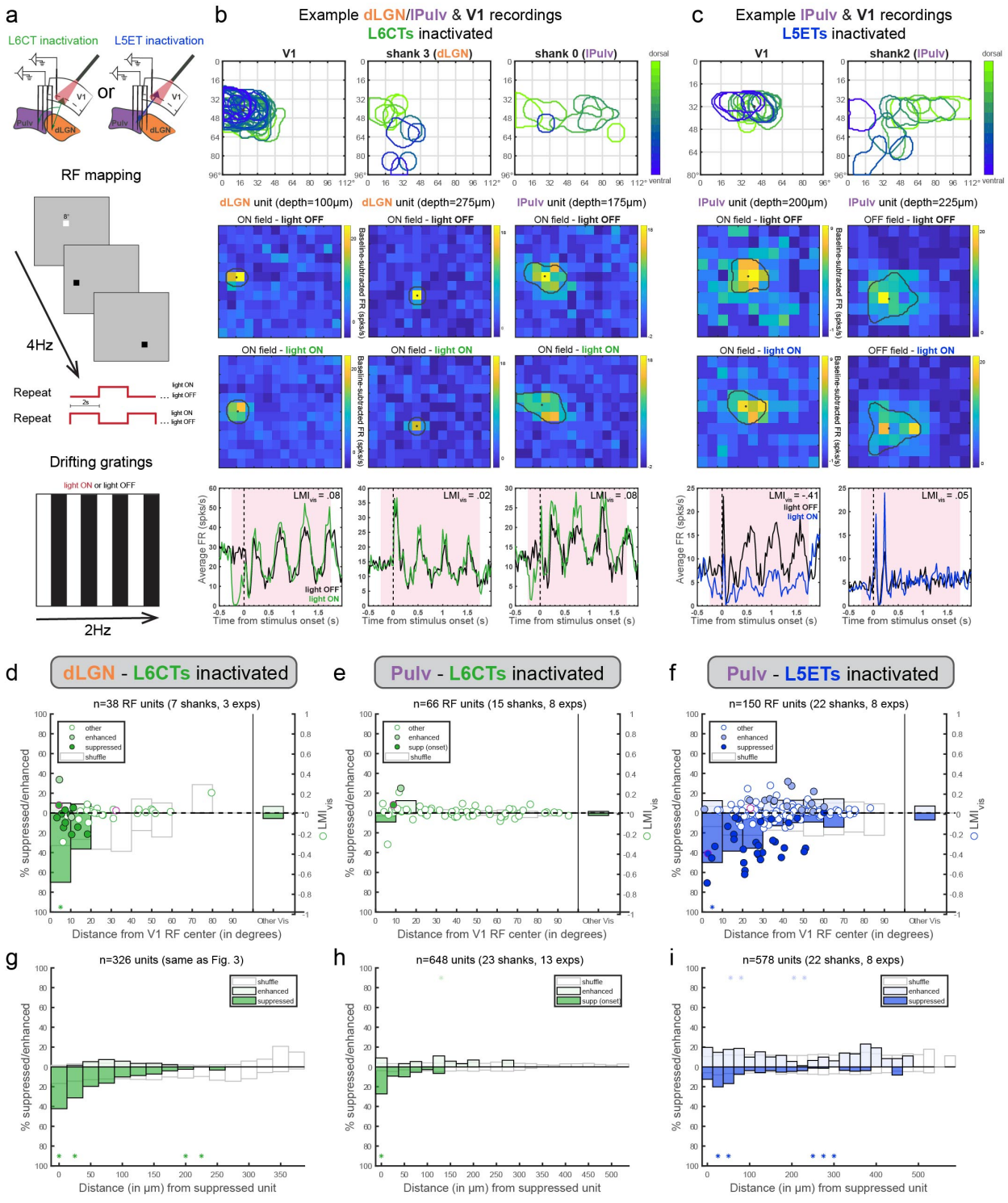
a
L6CT inactivation
L5ET inactivation
or
V1
Pulv
dLGN
RF mapping
8°
4Hz
Repeat
2s
light ON
light OFF
Drifting gratings
light ON or light OFF
2Hz
b
Example dLGN/lPulv & V1 recordings
L6CTs inactivated
V1
shank 3 (dLGN)
shank 0 (lPulv)
dorsal
ventral
dLGN unit (depth=100µm)
dLGN unit (depth=275µm)
lPulv unit (depth=175µm)
ON field - light OFF
ON field - light ON
Baseline-subtracted FR (spks/s)
Average FR (spks/s)
light OFF
light ON
Time from stimulus onset (s)
c
Example lPulv & V1 recordings
L5ETs inactivated
shank2 (lPulv)
lPulv unit (depth=200µm)
lPulv unit (depth=225µm)
OFF field - light OFF
OFF field - light ON
d
dLGN - L6CTs inactivated
n=38 RF units (7 shanks, 3 exps)
other
enhanced
suppressed
shuffle
% suppressed/enhanced
LMIvis
Other Vis
Distance from V1 RF center (in degrees)
e
Pulv - L6CTs inactivated
n=66 RF units (15 shanks, 8 exps)
supp (onset)
f
Pulv - L5ETs inactivated
n=150 RF units (22 shanks, 8 exps)
g
n=326 units (same as Fig. 3)
Distance (in µm) from suppressed unit
h
n=648 units (23 shanks, 13 exps)
i
n=578 units (22 shanks, 8 exps)

units retinotopically aligned (within 10°) to our V1 recordings (and thus confirmed V1 inactivation), at least 50% of dLGN and pulvinar units were classified as "suppressed" based on effects of L6CT or L5ET inactivation to their spontaneous activity during the drifting grating experiments (as in Figure 2.3), compared to 10% and 16% across all visually responsive units (Figure 2.3d,h). This was indeed due to retinotopy as opposed to some other difference among experiments, as this relationship was not observed when we randomly reassigned RF distances among all units recorded within the same experiment (Figure 2.4d-f, "shuffle" = means of 1000 shuffles). Because of the thalamus' retinotopic organization, one would also expect suppressed cells to physically neighbor other suppressed cells. Indeed, we found that in dLGN with L6CT inactivation and pulvinar with L5ET inactivation, units recorded from the same or nearby channels as a suppressed cell were more likely to also be suppressed, and at significantly greater rate than would be expected from a shuffled distribution (Figure 2.4g,i). This trend was also true for pulvinar cells whose onset response (first 200ms) was significantly suppressed by L6CT inactivation (like the example lPulv unit in Figure 2.4b; Figure 2.4h). This relationship was most striking in the dLGN, where cells' physical and retinotopic distances are more closely linked than in the pulvinar[28]. It is notable that dLGN units whose spontaneous activity was facilitated by L6CT inactivation were typically 50-150μm away from their nearest suppressed cell (Figure 2.4g), which is consistent with recent reports of L6CTs exerting inhibitory influence over non-retinotopically matched cells[22]. Taken together, these findings show that direct CT excitation, whether from V1 L6CTs or L5ETs to dLGN or pulvinar, is retinotopically organized, even while its influence on visual versus baseline activity depends critically on the CT source (Figure 2.3).

Complete L5ET silencing confirms L5 "driving" influence of visual response properties in the pulvinar

Our results thus far demonstrate that V1 L5 and L6 projections to the thalamus, while both retinotopic, differ considerably in the extent to which they "drive" or "modulate" visual activity in their thalamic targets. Nevertheless, L5ET inactivation did not completely abolish visual responses in the pulvinar, even in retinotopically aligned cells (e.g., the first unit in Figure 2.4c, though suppressed by

L5ET inactivation, maintained its RF properties). This could mean that V1 L5ETs contribute to but are not wholly necessary for visual responsivity in the pulvinar. Alternatively, L5ETs in V1 may be necessary drivers but were incompletely inactivated by our optogenetic approach. In fact, we noticed that halorhodopsin was more effective at silencing L5ETs' spontaneous than visually evoked activity; this could even result in a sharpening, rather than an ablation, of RFs in "inactivated" L5 cells (Figure 2.S7). We thus sought another optogenetic approach to specifically silence L5ETs with even greater efficacy to more definitively determine the extent to which the pulvinar is driven by V1 L5.

Light-activated chloride channels, such as the blue light-activated, soma-targeted GtACR2 (stGtACR2), have been shown to exhibit enhanced photocurrents relative to other available inhibitory opsins[54]. They also have the advantage of providing shunting inhibition as opposed to hyperpolarization[55] and thereby, potentially, more effective suppression of depolarization caused by visual stimulation. We therefore conducted additional L5ET inactivation experiments using Npr3-Cre mice injected with an AAV encoding Cre-dependent stGtACR2 in V1 (Figure 2.5). While we recorded a similar proportion of inactivated regular-spiking L5 cells in V1 (Figure 2.5c), those cells were inactivated to a greater degree than when using halorhodopsin. In fact, the majority of these cells were completely silenced (Figure 2.5d), and this was equally true of their visual responses, including their orientation tuning and RF properties (e.g., Figure 2.5a), as well as their spontaneous activity (Figure 2.S7).

This pronounced improvement in L5ET inactivation resulted in only marginally greater suppression of a subset of pulvinar neurons (Figure 2.5g,h). Some, such as the example unit in Figure 2.5e (see also unit #808 in Figure 2.7c), were deprived of their orientation tuning and RF integrity; this provides definitive evidence of V1 L5ETs "driving" visual response properties in certain retinotopically aligned pulvinar neurons. Still, a similarly small and even reduced proportion of all visual pulvinar cells were impacted by complete L5ET silencing with stGtACR2 (Figure 2.5f) in comparison to silencing with halorhodopsin (Figure 2.3g). This reduction is likely related to the reduced spread of the stGtACR2-encoding AAV, as when considering retinotopically aligned units, the proportion of suppressed cells was about 50%, similar to our halorhodopsin experiments (Figure 2.S8). Therefore, using the potent blue-

Figure 2.5 Soma-targeted GtACR2 allows greater L5ET silencing than with halorhodopsin and further demonstrates L5ET "driving" influence over a subset of pulvinar units. a) stGtACR2-inactivation of L5ETs in V1. Left: schematic of V1 recordings (although V1 and pulvinar recordings were conducted simultaneously in all experiments). Right: an example inactivated regular-spiking L5 unit whose spontaneous and visually evoked responses are entirely suppressed by blue light. Its orientation tuning and receptive field are also abolished. Dotted lines in tuning plots indicate average spontaneous FRs (from blank trials). b) Light modulation index from visual trials (LMI_{vis}) of all recorded V1 units by their depth through cortex relative to the end of L4. c) LMI_{vis} of regular-spiking units, by layer. Putative inactivated units are blue dots. Overlay: proportion of all RS L5 units putatively inactivated. d) Histogram of putatively inactivated units from halorhodopsin and stGtACR2 experiments. Triangles indicate medians. p=0.0022, Wilcoxon rank-sum test. e) Pulvinar recordings with L5ET inactivation with stGtACR2. Left: recording and light stimulation configuration. Right: an example pulvinar unit whose spontaneous and visually evoked activity, tuning and receptive field were dramatically suppressed by L5ET inactivation using stGtACR2. f) LMI_{vis} by depth for all recorded pulvinar units (combining lPulv and rmPulv units), colored according to whether their spontaneous activity was significantly suppressed or enhanced or non-modulated ("other"). Overlay: proportion of all visually responsive units in each category. g). Comparing LMI_{vis} of suppressed and enhanced units between halorhodopsin and stGtACR2 inactivation experiments (no significant difference in either suppressed or enhanced cells, $p>0.1$ Wilcoxon rank-sum tests). h) Visually induced change in FR in Light OFF versus Light ON (L5ET inactivated) trials in different inactivation experiments (same groups as in g). ***$p<0.0001$, *$p=0.0128$, Wilcoxon signed-rank tests.

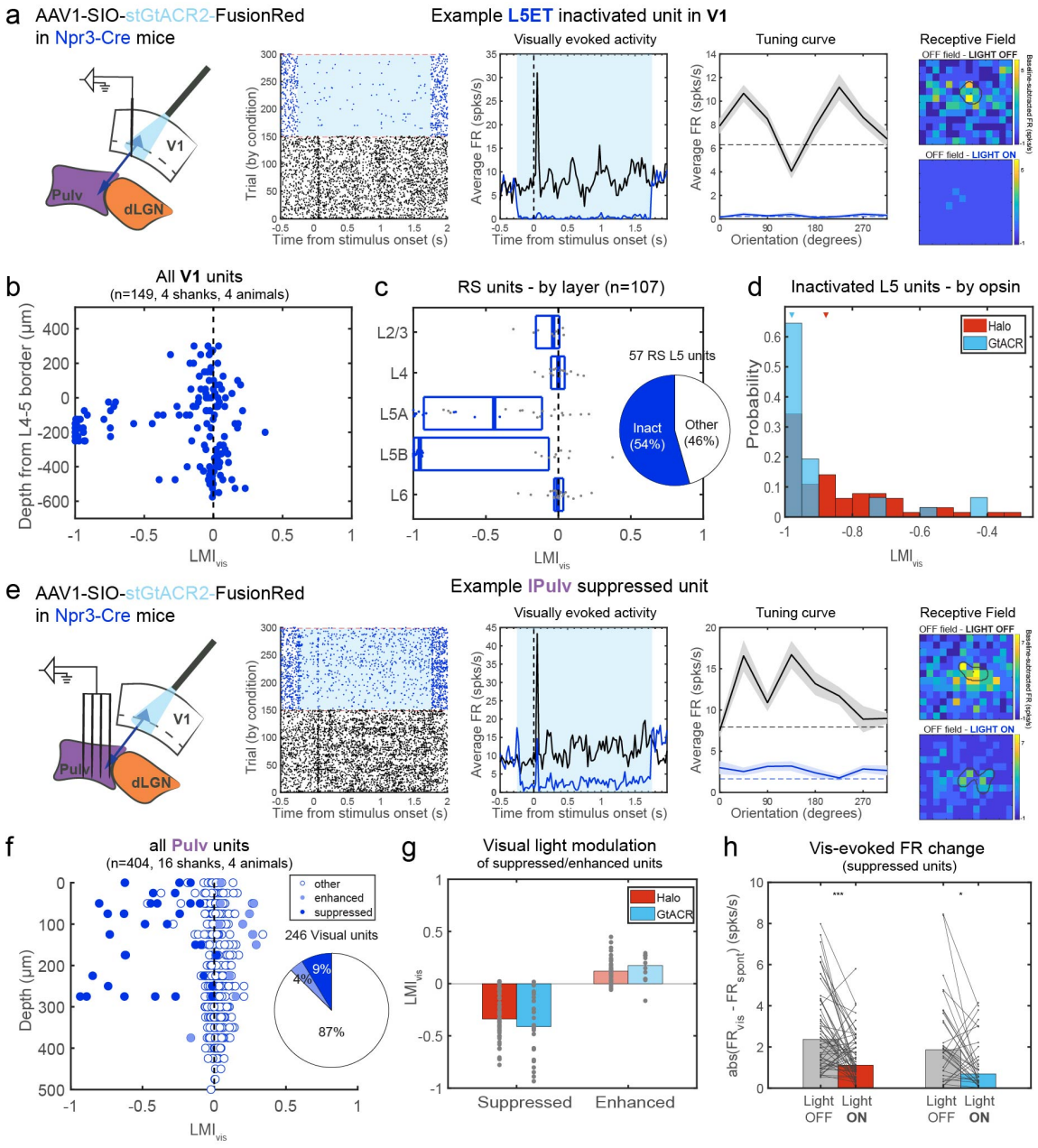
a
AAV1-SIO-stGtACR2-FusionRed
in Npr3-Cre mice
Example L5ET inactivated unit in V1
V1
Pulv
dLGN
Trial (by condition)
Time from stimulus onset (s)
Visually evoked activity
Average FR (spks/s)
Tuning curve
Orientation (degrees)
Receptive Field
OFF field - LIGHT OFF
OFF field - LIGHT ON
b
All V1 units
(n=149, 4 shanks, 4 animals)
Depth from L4-5 border (µm)
LMI vis
c
RS units - by layer (n=107)
L2/3
L4
L5A
L5B
L6
57 RS L5 units
Inact (54%)
Other (46%)
d
Inactivated L5 units - by opsin
Halo
GtACR
Probability
e
AAV1-SIO-stGtACR2-FusionRed
in Npr3-Cre mice
Example lPulv suppressed unit
f
all Pulv units
(n=404, 16 shanks, 4 animals)
other
enhanced
suppressed
246 Visual units
9%
4%
87%
Depth (µm)
g
Visual light modulation
of suppressed/enhanced units
Suppressed
Enhanced
h
Vis-evoked FR change
(suppressed units)
Light OFF
Light ON

light-activated chloride channel stGtACR2 to silence V1 L5ETs increased the potency but not the prevalence of suppression in the pulvinar. In contrast, L6CT silencing with stGtACR2 did not have any more profound effects on dLGN or pulvinar activity and were still clearly "modulatory" (Figure 2.S9). These experiments thus more conclusively demonstrate the "driving" influence of L5CT projections on pulvinar neurons' visual activity and response properties.

Combined inactivation of different CT populations shows that individual pulvinar neurons are driven by L5CT, but not L6CT, inputs from V1

Although we have demonstrated different effects of L6CT versus L5ET inactivation on activity in the pulvinar that are consistent with their hypothesized "driving" and "modulatory" roles, the degree of suppression we observed from specific L5ET inactivation – even when L5ETs were essentially completely silenced (Figure 2.5) - was less complete than in other studies that broadly inactivated all of V1[27,28] (or in our own nonspecific cortical inactivation experiments; Figure 2.S10). We thus considered the possibility that while L6CT inactivation on its own had minimal effects on pulvinar activity (Figure 2.3f), perhaps they could exert more influence when in concert with the L5ET pathway.

To address this possibility, we took advantage of the fact that AAVretro injected into the pulvinar infects only L5, but not L6, CT neurons[37] (Figure 2.1b), thus allowing us to selectively express Flp recombinase in corticothalamic L5 neurons (L5CTs). These injections were made in Ntsr1-Cre mice, where Cre is already present in L6CTs, so that a mixture of AAVs encoding Flp-dependent stGtACR2 and Cre-dependent halorhodopsin injected to V1 resulted in separable opsin expression in each CT population (Figure 2.6a,b). V1 recordings confirmed that blue (455nm) LED light to activate stGtACR2 specifically silenced units in L5 (Figure 2.6c), whereas red (617nm) LED light for halorhodopsin inactivated units in L6 (Figure 2.6d). Fewer L5 units were putatively inactivated in these experiments than when using Npr3-Cre mice, which was expected since opsin expression was restricted to thalamus-projecting L5ETs (i.e., L5CTs). Across the full depth of V1, combined blue and red LED stimulation reduced activity in cells across the infragranular layers, while each LED alone only suppressed units in its

Figure 2.6 Individual pulvinar neurons are suppressed by V1 L5CT, but not L6CT, inactivation. Experimental schematic. Ntsr1-Cre mice were injected to express Cre-dependent halorhodopsin in L6CTs and Flp-dependent stGtACR2 in L5CTs. Right: four different LED stimulation conditions (randomly interspersed). b) Confocal image (maximum intensity projection) of stGtACR2-FusionRed-expressing L5CTs and eNpHR3.0-eYFP-expressing L6CTs in V1. Scale bar = 200µm. c) Example L5CT and d) L6CT inactivated units in V1. Raster plots (left) and average PSTHs of firing rates across visual trials (right). Grey shading indicates the period of LED stimulation. e) Visual light modulation (LMI_{vis}) calculated from L5CT&L6CT-inactivation (left), L5CT-inactivation (middle), L6CT-inactivation (right) trials. Colored units are those whose FRs were significantly suppressed by at least 50% in visual trials with combined L5CT&L6CT-inactivation, and dots outlined in pink are the example units in c) and d). f) Example lPulv and g) rmPulv units which were suppressed by L5CT, but not L6CT, inactivation. f) LMI_{vis} of all pulvinar units across light stimulation conditions of significantly suppressed, enhanced and non-modulated units (classified from blank trials with combined L5CT&L6CT-inactivation). Dots outlined in pink are the example units in f) and g).

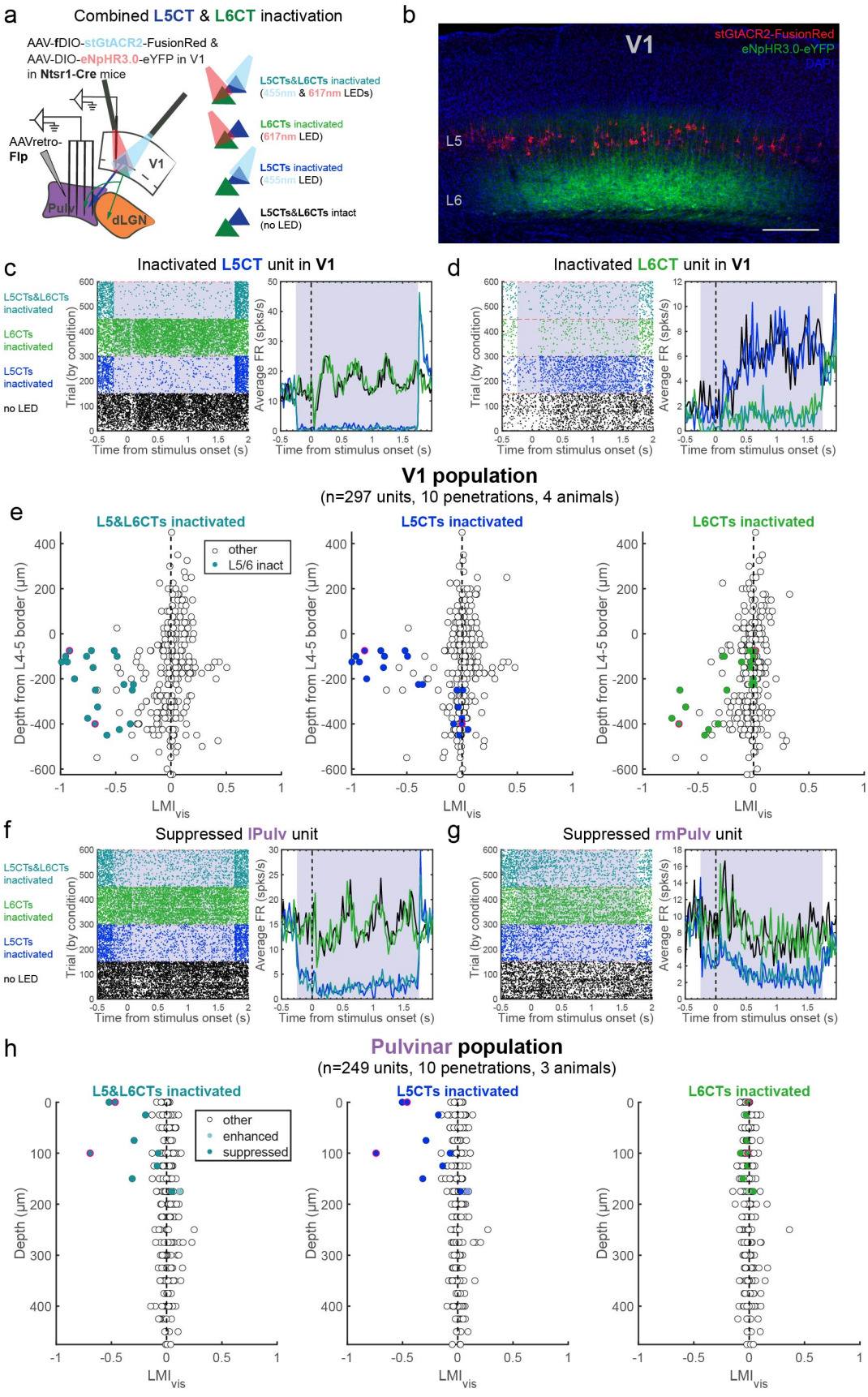
a
Combined L5CT & L6CT inactivation
AAV-fDIO-stGtACR2-FusionRed &
AAV-DIO-eNpHR3.0-eYFP in V1
in Ntsr1-Cre mice
AAVretro-
Flp
V1
Pulv
dLGN
L5CTs&L6CTs inactivated
(455nm & 617nm LEDs)
L6CTs inactivated
(617nm LED)
L5CTs inactivated
(455nm LED)
L5CTs&L6CTs intact
(no LED)
b
V1
stGtACR2-FusionRed
eNpHR3.0-eYFP
DAPI
L5
L6
c
Inactivated L5CT unit in V1
L5CTs&L6CTs inactivated
L6CTs inactivated
L5CTs inactivated
no LED
Trial (by condition)
Average FR (spks/s)
Time from stimulus onset (s)
d
Inactivated L6CT unit in V1
V1 population
(n=297 units, 10 penetrations, 4 animals)
e
L5&L6CTs inactivated
L5CTs inactivated
L6CTs inactivated
other
L5/6 inact
Depth from L4-5 border (μm)
LMIvis
f
Suppressed lPulv unit
g
Suppressed rmPulv unit
h
Pulvinar population
(n=249 units, 10 penetrations, 3 animals)
other
enhanced
suppressed
Depth (μm)

corresponding layer (Figure 2.6e). We confirmed in control animals expressing only one opsin that halorhodopsin was unaffected by our blue LED stimulation, nor was stGtACR2 affected by the red LED (Figure 2.S11).

Using this approach to inactivate L5CTs or L6CTs separately or in combination, we once again observed a subset of pulvinar units that were suppressed by L5CT inactivation with blue light (Figure 2.6f,g). Importantly, however, these units were unaffected by L6CT inactivation with red light, and the effect of combined L5CT and L6CT inactivation was indistinguishable from that of L5CT inactivation alone (Figure 2.6h). While we cannot definitively prove that these same neurons receive input from L6CTs in V1 since they were not affected by suppressing that pathway, our prior demonstration of the retinotopic organization of both L5CT and L6CT projections (Figure 2.4) would support this inference. Thus, these experiments conclusively show that individual pulvinar neurons can be driven by specifically L5CT, but not L6CT, inputs from V1.

So far, we have demonstrated that L5ETs provide a functional "driving" influence on a subset of retinotopically aligned pulvinar cells. Still, the full extent of visual activity observed in the pulvinar is not accounted for. When we virally ablated L5ETs (or L6CTs) in V1 to further ensure the complete inactivation of these populations, we still observed robust visual responses in the pulvinar – even in some neurons whose RFs aligned with the area of L5ET ablation (Figure 2.S12). Although chronic ablation has the potential to induce compensatory mechanisms, these results are consistent with our optogenetics experiments, where we achieved virtually complete and transient L5ET inactivation and still observed residual visual responses (Figure 2.5) and even some unaffected yet retinotopically aligned pulvinar cells (Figure 2.S8). We were therefore interested whether inputs other than from V1 might also play prominent roles in shaping pulvinar activity.

Cortical and subcortical "driving" pathways converge in the lateral pulvinar

In the lateral pulvinar in particular, an important source of additional input may come from the superior colliculus (SC)[30]. Tectopulvinar synapses exhibit morphological and physiological "driver-like"

properties with intermediate type 1 “modulator” and type 2 “driver” characteristics[7,56,57]. Moreover, recent studies have shown that the SC, but not the cortex, drives activity in the caudomedial region of the pulvinar (cmPulv)[27,28]. While our experiments with V1 CT manipulations did not concern this region because it does not receive direct V1 input[30], the lateral pulvinar (lPulv), which we did record from, is innervated by both V1 and SC. Although axons emanating from topographically aligned regions of V1 and SC are largely segregated within lPulv (Figure 2.7a), cortical and tectal terminals have been found in close proximity at the electron microscopic level[57,58]. Moreover, pulvinar neurons have wide-reaching dendrites that can even stretch across pulvinar subdivisions[30], and short-latency effects of either V1 or SC stimulation on single pulvinar cells have been described[29]. Therefore, we were interested: a) whether the visually responsive cells we recorded in lPulv that were unaffected by L5ET inactivation would be suppressed instead by SC inactivation; and b) whether individual neurons in lPulv might receive convergent L5ET and SC “driver” or “driver-like” input.

To address these questions, we recorded single-unit activity from lPulv in awake mice expressing stGtACR2 in L5ETs (using Npr3-Cre mice) and halorhodopsin in the SC, thereby allowing us to use different LEDs to inactivate L5ETs and/or SC (Figure 2.7b). We also made recordings from V1 (data in Figure 2.5a-d) and the SC (Figure 2.S13) to verify the efficacy of our optogenetic manipulations. Not only were there individual units in lPulv which were strongly suppressed by L5ET inactivation with or without SC inactivation, but we also found units, even in the same recording penetration, which were instead suppressed specifically by SC inactivation (Figure 2.7c). These example units were, in fact, “driven” by V1 L5ETs or SC, as their responses to sparse noise stimuli presented within their RFs were abolished by optogenetic silencing of their cortical or subcortical inputs, respectively (Figure 2.7d). Interestingly, the L5ET-driven unit’s (#808) response to its preferred direction stimulus was exclusively suppressed by SC inactivation, even with L5 intact (Figure 2.7c). This suggests that even while this unit’s baseline firing and receptive field is determined by its V1 L5 input, the SC may provide additional input that bestows direction tuning.

Figure 2.7 Subsets of neurons in the lateral pulvinar (lPulv) are driven by V1 L5ETs, the superior colliculus, or both. a) Anterograde tracing of V1 and collicular projections to the pulvinar. AAV injection of eNpHR3.0-eYFP overlaps with V1 axons in the SC (middle), yet cortical and collicular axons are largely segregated with minor overlap in lPulv (right, with higher magnification of boxed area in each channel at far right). Scale bars = 200μm. b). Schematic of experiment for dual-optogenetic inactivation of V1 L5ETs and SC during pulvinar recordings. Bottom: four different inactivation conditions. c) Two example lPulv units, recorded on the same shank in the same experiment. From left to right: raster plots with trials organized by inactivation condition; PSTHs of average visually evoked FRs; and average FRs in response to different drifting grating orientations (dashed lines indicate spontaneous FRs). The first unit (#808) was suppressed by L5ET inactivation conditions, whereas #205 was suppressed by SC-inactivation conditions. d) Receptive fields of units from c) under different inactivation conditions. #808's RF was abolished by L5ET but not SC inactivation, while the opposite was true of #205. RF maps depict average baseline-subtracted firing rates at the peak time point across all OFF stimulus (black square) positions. Outlines depict estimated RF boundaries (see Methods) under each condition. Right: overlayed RFs of V1 (upper) and SC (lower) units recorded in the same animal. e) Example units that exhibit combined effects of L5ET and SC inactivation. f) Unit #378's (from e) RF under different inactivation conditions. Right: Overlayed RFs of simultaneously recorded V1 units. SC was not recorded from in this animal. g) Light modulation of visually evoked activity (LMI_{vis}) from combined L5ET & SC inactivation trials, by depth. Units are colored according to whether they were significantly suppressed by SC inactivation, L5ET inactivation, or both (see Methods for details). Color-outlined dots correspond to example units in c) and e). Right: proportion of different suppressed unit classes out of all visually responsive units. h) LMI_{vis} for each unit in L5ET inactivation versus SC inactivation conditions (same unit classification as in g). Units which fall in the lower left quadrant were inactivated by both L5ET and SC inactivation. Crosses indicate medians of each unit class.

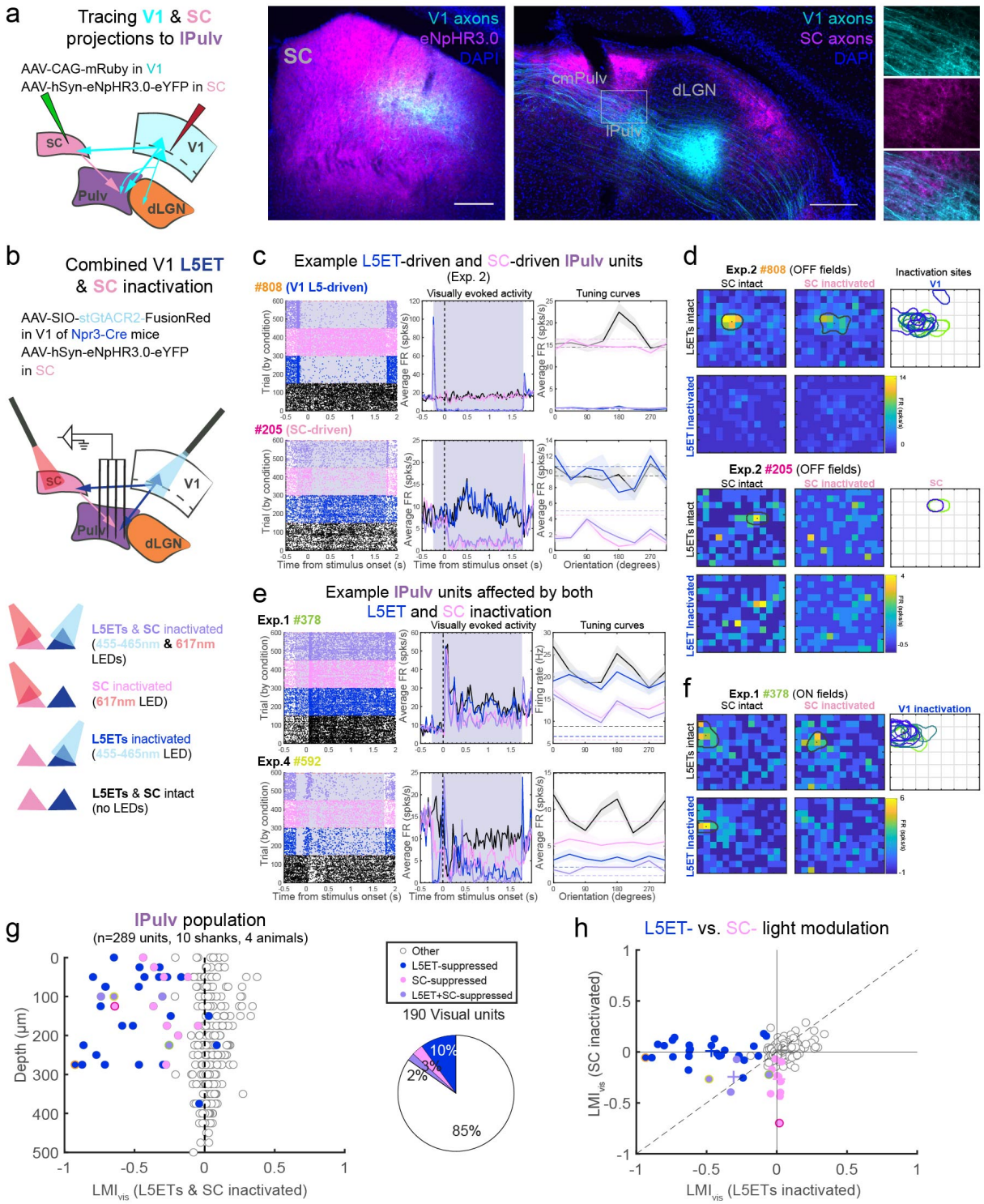
a
Tracing V1 & SC projections to lPulv
AAV-CAG-mRuby in V1
AAV-hSyn-eNpHR3.0-eYFP in SC
SC
V1
Pulv
dLGN
V1 axons
eNpHR3.0
DAPI
SC axons
cmPulv
lPulv
b
Combined V1 L5ET & SC inactivation
AAV-SIO-stGtACR2-FusionRed in V1 of Npr3-Cre mice
AAV-hSyn-eNpHR3.0-eYFP in SC
L5ETs & SC inactivated (455-465nm & 617nm LEDs)
SC inactivated (617nm LED)
L5ETs inactivated (455-465nm LED)
L5ETs & SC intact (no LEDs)
c
Example L5ET-driven and SC-driven lPulv units (Exp. 2)
#808 (V1 L5-driven)
#205 (SC-driven)
Visually evoked activity
Tuning curves
Trial (by condition)
Average FR (spks/s)
Time from stimulus onset (s)
Orientation (degrees)
d
Exp.2 #808 (OFF fields)
Exp.2 #205 (OFF fields)
SC intact
SC inactivated
Inactivation sites
V1
SC
L5ETs intact
L5ET inactivated
e
Example lPulv units affected by both L5ET and SC inactivation
Exp.1 #378
Exp.4 #592
Firing rate (Hz)
f
Exp.1 #378 (ON fields)
V1 inactivation
g
lPulv population
(n=289 units, 10 shanks, 4 animals)
Depth (μm)
LMI vis (L5ETs & SC inactivated)
Other
L5ET-suppressed
SC-suppressed
L5ET+SC-suppressed
190 Visual units
10%
3%
2%
85%
h
L5ET- vs. SC- light modulation
LMI vis (SC inactivated)
LMI vis (L5ETs inactivated)

Indeed, we found a number of intriguing instances of combinatorial effects of L5ET and SC silencing on individual units. The first example in Figure 2.7e was mainly impacted by SC, but not L5ET silencing in its response to drifting grating stimuli. However, this unit's RF appeared to be influenced by both its SC and V1 L5 inputs. Only the portion of its RF that overlapped with the area of L5ET inactivation was suppressed by L5ET silencing, whereas its full RF was suppressed by combined L5ET and SC inactivation (Figure 2.7f; SC was not recorded from in this animal). Similarly, the second example unit in Figure 2.7e exhibited suppressed spontaneous and visually evoked responses from either SC or L5ET inactivation alone and was even more suppressed by combined inactivation (no RF information was available from experiment). This unit would therefore appear to also receive some degree of "driving" input from both L5ET cortical and subcortical sources.

Across our recorded population, we observed a wide range of effects of V1 L5ET versus SC silencing, including relatively small proportions of units which were suppressed (in their visually evoked and/or spontaneous firing rates) by L5ET inactivation only, by SC inactivation only, or by both (Figure 2.7g). Despite the dorsal-ventral distribution of SC and V1 axons in lPulv (Figure 2.7a), we found these different effects to be fairly dispersed (Figure 2.7g). While most of the modulated units were suppressed by either L5ET or SC inactivation but not both (i.e., points falling along either axis in Figure 2.7h), a handful of units (including those in Figure 2.7e) showed significant negative LMI_{vis} values (i.e., suppression) under both L5ET- and SC-inactivation conditions (lower left quadrant of Figure 2.7h). We made similar observations of cortical versus subcortical inactivation having varied and sometimes combinatorial effects on individual units from additional experiments in which V1 (rather than L5ETs specifically) was inactivated (Figure 2.S14).

We have therefore shown that, while certain units of the lateral pulvinar are driven by L5 inputs from V1, these inputs are not the only ones to influence visual activity in this region of the HO visual thalamus. Indeed, other units are driven by subcortical inputs arising from SC, and some even appear to receive input from both sources that convey varying degrees of visual "drive." Given our previous demonstration of the retinotopic specificity of L5ET excitation (Figure 2.4), we may well underestimate

the extent of combined cortical and subcortical influences. For instance, in Figure 2.7d, unit #205's RF aligned with the SC- but not L5ET-inactivation centers; had L5ET inactivation been more widespread to encompass this unit's RF area, perhaps an additional impact of L5ET inactivation would have been observed. Regardless, we have shown that while V1 CT projections from L5 – but not L6 – provide retinotopic, visual driving input to the pulvinar, the SC can also provide some degree of visual drive. These cortical L5 and subcortical inputs thereby converge within the lateral pulvinar - and even onto individual neurons – to shape visual responses in the HO visual thalamus.

Discussion

What roles do two, seemingly parallel corticothalamic pathways originating from different layers of the primary visual cortex play in thalamic processing in an awake animal? The distinct characteristics of L5CT versus L6CT inputs have for decades led to the idea that these are not redundant pathways but rather distinct feedforward, "driving" versus feedback, "modulatory" projections, respectively[8,9,48]. While this idea has been highly influential to the study of corticothalamic circuit organization and function, it has never been directly tested. This is largely due to technical limitations in selectively silencing one or the other CT population and assessing downstream thalamic effects in an awake animal. Taking advantage of cell type-specific transgenic mouse lines, optogenetics and high-density, multielectrode recordings of single-unit activity in awake mice, we find pronounced differences in how these populations influence sensory responses in the visual thalamus. While both L5 and L6 CT projections from V1 provide retinotopic excitation onto their thalamic targets, the extent to which that excitation imparts visual information differs considerably. Our inactivation studies demonstrate that V1 L6CTs can provide some degree of baseline drive, mainly onto retinotopically aligned cells of the dLGN, yet are not necessary for visual responses in either first- or higher-order visual thalamus. In contrast, silencing the L5CT pathway from V1 suppressed visually evoked as well as baseline activity in many retinotopically matched pulvinar neurons, some of which relied entirely on that input for their tuning and/or receptive field properties (e.g., Figure 2.5e and Figure 2.7c-d #808). Therefore, our results affirm a longstanding hypothesis that the L5,

but not the L6, CT pathway from V1 constitutes a functionally "driving" pathway that conveys visual information to the rodent pulvinar.

While we were able to selectively inactivate L5ET versus L6CT subpopulations by using different transgenic mouse lines, there were still some limitations to the specificity of our approach. For instance, although the Ntsr1-Cre line is selective for L6CTs that project to the dLGN[40], not all project to the pulvinar (Figure 2.1e). If anything, this might have led us to overestimate the influence of V1 L6CTs in the pulvinar (e.g., through indirect circuit effects), and yet we still saw minimal impact of their inactivation. On the other hand, many L6CT projections to the pulvinar come from extrastriate areas[4,5,35,36] (Figure 2.1b), which were not targeted by our injections. Our findings of fundamentally similar "modulatory" influences of V1 L6CTs in the dLGN and pulvinar (from our present inactivation and prior activation studies[20]) would lead us to expect that the cumulative effect of L6CT inactivation across cortical areas on the pulvinar would be similar to what we observed in this study in the dLGN (which gets the majority of its L6CT input from V1[59,60]) – namely, suppressed spontaneous but not visual activity. Since L6CTs themselves have exceptionally low spontaneous firing rates (Figure 2.S3), we attribute their effect on baseline thalamic activity to the high degree of convergence of many L6CTs onto single thalamic cells[6,13] and to the fact that our recordings were conducted in awake animals as opposed to under anesthesia, which reduces spontaneous firing rates in the thalamus[61]. Additionally, our approach most likely excluded L6b cells that exclusively project to HO thalamus and exhibit type 2 ("driver"), rather than type 1 ("modulator"), characteristics[62,63]. Although we did not observe many pulvinar-projecting L6CT neurons that might fall within this category (retrogradely labeled tdT-negative cells in Ntsr1-Cre/Ai14 mice, Figure 2.1e), whether they would more closely resemble L5 "drivers" or other L6 "modulators" in terms of their contributions to functional response properties in the pulvinar in vivo is an open question.

Meanwhile, our primary strategy for inactivating L5CT projections was to inactivate extratelencephalic L5 excitatory neurons (L5ETs) using the Npr3-Cre mouse line. This offers a marked improvement in specificity from other studies that have relied on non-specific cortical

inactivation[27,28,32,33], which would be expected to also suppress activity in other cortical areas[64] and thus confound the driving influence of V1, specifically L5ETs, on the pulvinar with that of extrastriate cortex. Indeed, we observed somewhat more widespread pulvinar inactivation when we non-specifically inactivated cortex, even when that inactivation was confined to V1 through AAV injection (Figure 2.S10). Still, not all of our inactivated L5ETs project to the pulvinar (Figure 2.1f), as this heterogenous population can innervate any combination of multiple subcortical areas (pons and SC, Figure 2.S2; also striatum[65]). In fact, in light of ours (Figure 2.7) and others' demonstrations of SC influence onto the pulvinar[27,28], it is possible that some of the suppression we observed in the pulvinar from L5ET inactivation could be mediated indirectly by the SC. However, we still observed suppressed pulvinar activity when we restricted our L5 inactivation to L5CTs (Figure 2.5). We also found largely separable effects of SC and L5ET inactivation in the lateral pulvinar (Figure 2.7, Figure 2.S14) and even within the SC itself (Figure 2.S13), which altogether demonstrate that L5 does not rely on an indirect pathway through the SC to drive visual responses in the pulvinar. Another caveat to our L5ET silencing approach is that our area of inactivation was limited by the spread of our AAVs (Figure 2.S8) and likely did not encompass all of V1. However, this limitation was addressed by assessing the effects of L5ET inactivation on retinotopically aligned pulvinar neurons (Figure 2.4, Figure 2.S8). The fact that half of those cells were still unmodulated by V1 L5ET inactivation suggests that there may be other "driving" inputs to the pulvinar.

Indeed, the pulvinar is innervated by a number of other cortical and subcortical inputs whose in vivo functional influences are not yet known. First, it receives inhibitory input from areas like the ventral LGN (vLGN), the zona incerta and the anterior pretectal nucleus – all of which receive collaterals from L5ETs[5,16,66–68]. These inhibitory pathways might underlie some of the excitatory effects we observed in the pulvinar with L5ET inactivation (Figure 2.3h). Meanwhile, the rodent pulvinar also receives excitatory L5CT input not just from V1, but also from extrastriate areas[4,5,35,36] (Figure 2.1b). Based on our observations of some retinotopically aligned pulvinar units that were unaffected by L5ET inactivation (Figure 2.4f, Figure 2.S8) or ablation (Figure 2.S12) – similar to what was observed in the cat following

V1 cooling[32] - we predict that L5ET projections from extrastriate areas may provide additional driving inputs. Further work is needed to conclusively address this possibility and whether L5 inputs from multiple cortical areas might even provide combined driving input to some neurons. Species differences in the distributions of CT neurons retrogradely labeled from the pulvinar[4,5,28,35,36,69–73] also suggest that L5 driving and L6 modulatory pathways might be more distributed across cortical areas in rodents versus more hierarchically organized in primates. The functional consequences of this difference require further study through comparative anatomy and physiology.

Our results also show that subcortical excitatory inputs from the SC can intermingle with L5 driving inputs within the lateral pulvinar and even converge onto individual neurons. In fact, while relatively rare, we found cases of units whose firing rates, tuning and/or receptive fields were influenced by both L5ET and SC inactivation (Figure 2.7; see also Figure 2.S14). This would suggest that some neurons integrate information conveyed by cortical (L5) and subcortical sources, which has also been described in the cat LP-pulvinar[69] and in the rodent HO somatosensory thalamic nucleus, POm[74]. Given the role of the SC in processing object motion, eye movements and spatial attention[75], integration of various visual, motor, and other signals within the pulvinar could play a key role in sensory-guided behaviors. This idea is in line with evidence that the rodent pulvinar conveys contextual information (e.g., a mismatch between visual flow and running speed) to extrastriate areas[5] and even back to V1[4]. It is notable, however, that SC inactivation/lesion was shown to considerably impair visual responses in regions of the pulvinar homologous to the mouse lPulv[50] in rabbits[29], but not in macaques[33]. It is therefore possible that subcortical inputs might play a more prominent role in shaping pulvinar visual response properties in non-primates[29].

Altogether, our results demonstrate a functional dissociation between L6 and L5 corticothalamic pathways that has long been supposed but never directly proven. Many notable distinctions between FO and HO thalamic nuclei – such as their connectivity patterns with the cortex versus sensory peripheral organs[8], relative proportions of different synapse types[24–26], and transcriptional profiles[76] – could have led "driver" and "modulator"-type inputs to differently contribute to activity in the HO compared to FO

thalamus. Instead, we find that the effects of inactivating L5CT versus L6CT pathways from V1 on visual responses in the pulvinar of awake mice are consistent with their hypothesized "driving" versus "modulatory" functions. Given the similarities in CT synapse types[48] and the consistent effects of cortical lesion/inactivation on sensory activity in the HO thalamus across systems and species[27,28,31–34], we suggest that this functional distinction between L5CT and L6CT projections to HO thalamus is a common organizational principle of corticothalamic function. We also found that the superior colliculus can play important driving roles in the rodent pulvinar and can even converge with the L5 cortical driving pathway; the extent to which this, too, generalizes across species will be of considerable interest for future studies of pulvinar function. Our results thus illuminate how sensory information is routed to the HO thalamus through distinct cortical (and subcortical) channels, which has important implications for understanding how the HO thalamus supports sensation and behavior in the awake animal.

Methods

Animals

The following transgenic mouse lines were used in this study:

- Ntsr1-Cre GN220 (GENSAT[38]) - L6CT-inactivation and combined L5CT & L6CT inactivation experiments
- Npr3-IRES-Cre-neo[43] - L5ET-inactivation experiments
- PV-Cre and Dlx5-Flp/CCK-IRES-Cre - V1 inactivation by activating PV+/Dlx5+ inhibitory interneurons
- PV-Cre/Ai32 - V1 inactivation by activating constitutively ChR2-expressing PV interneurons
- Ntsr1-Cre/Ai14 - L6CT quantification

Cre-negative animals were also used for control physiology experiments and anatomy experiments not requiring Cre-dependent AAV expression (e.g., Figure 2.S2). Both female and male mice were used between 8-17 weeks of age (more commonly 9-14 weeks) at the time of AAV injection and <20 weeks at the time of in vivo recordings. All experimental procedures followed protocols approved by the Salk Institute Animal Care and Use Committee.

Experimental design and procedures

Surgeries

For injections, mice were anesthetized with a ketamine/xylazine cocktail (100mg/kg ketamine, 10mg/kg xylazine) via intraperitoneal injection and secured in a stereotax (David Kopf Instruments Model 940 series). A small craniotomy was made at the injection site, and a glass pipette (24-30µm tip diameter) was lowered to the desired depth and was left for 3-5 minutes before injecting. AAV or a cholera toxin subunit B-Alexa Fluor conjugate (see below) was pressure-injected with a syringe at an approximate rate of 20µl/minute and let rest for at least 5 minutes (10+ minutes for subcortical injections) before raising to prevent backflow. The following stereotactic coordinates were used for injection sites (all left hemisphere, in mm relative to bregma; A/P, M/L, D/V):

- V1: -3.2, -2.65, -0.64-0.3 (2 depths)
- lPulv: -1.6, -1.8, -2.45
- rmPulv: -1.05, -1.2, -2.55
- SC, medial site: -3.5, -0.45, -1.1-1.2; SC, lateral: -3.5, -0.8, -1.25-1.3
- Pons: -3.5, -0.85, -5.75-5.9

At the end of injections, the skin incision was closed with Vetbond (3M) and mice were given a subcutaneous injection of buprenex (0.5-1.0 mg/kg) and Ibuprofen in their water bottles.

At least four days and up to 1 week prior to recordings, mice underwent an acute surgery for headframe implantation. Under isoflurane anesthesia, skin was cut away and a circular headframe (7-mm inner diameter) was secured to the skull with dental cement (C&B-Metabond, Parkell). A dull pipette attached to a micromanipulator (MP-285, Sutter Instrument) was used to relocate bregma and mark positions with a waterproof pen for aiming craniotomies for thalamus recordings (coordinates relative to bregma: 1.50-2.75mm lateral, 1.8-1.9mm posterior for lPulv, 1.0-2.0mm lateral, 1.0mm posterior for rmPulv). The exposed skull was covered with a silicone elastomer (Kwik-Cast, World Precision Instruments) and mice were given a subcutaneous injection of buprenex (0.5-1.0 mg/kg), Ibuprofen in their water bottles, and at least one full day undisturbed in their cages.

Viruses

The following AAV vectors were used for optogenetics experiments in this study:

- AAV5-EF1a-DIO-eNpHR3.0-eYFP (120-200nl, 3-4e12 GC/ml, UNC) - for L6CT/L5ET halorhodopsin inactivation
- AAV1-hsyn1-SIO-stGtACR2-FusionRed (120-200nl, 0.9-1.8e12 GC/ml, Addgene) - for stGtACR2 inactivation
- AAV5-Ef1a-fDIO-stGtACR2-FusionRed (200-240nl, 1.77e12 GC/ml, Salk Vector Core) - for L5CT inactivation

- AAV5-hsyn-eNpHR3.0-eYFP-WPRE-pA (60-70nl, 5.5e12 GC/ml, UNC) - for SC inactivation
- AAV1-EF1a-fDIO-hChR2 (H134R)-EYFP (150nl, 7.78e11 GC/ml, Salk Vector Core) - V1 inactivation in Dlx5-Flp/CCK-IRES-Cre mice
- AAV1-EF1a-DIO-hChR2 (H134R)-eYFP.WPRE.hGH (Addgene20298P) (100nl, 8.4e12 GC/ml, UPenn Vector Core) - V1 inactivation in PV-Cre mice
- AAV5-EF1a-DIO-eNpHR3.0-mCherry-WPRE (90-100nl, 4.7e12 GC/ml, UNC) - halorhodopsin inactivation of lateral visual cortex

The Cre-dependent halorhodopsin AAV was injected into V1 of Ntsr1-Cre mice and was allowed up to 6 weeks for expression (as well as for non-specific halorhodopsin expression in the SC). However, slightly smaller (120-150nl) halorhodopsin injections were made in Npr3-IRES-Cre-neo mice and restricted to 3 weeks expression time because expression in other layers and an unhealthy-looking L5 appeared at longer timepoints and/or with larger injection volumes in this mouse line. Consequently, animals in which axons were visible in areas not targeted by L5ETs (e.g., TRN) were excluded.

Viruses for anterograde tracing were:

- AAV5-CAG-FLEX-GFP (120-160nl, 5.2GC/ml, Salk Vector Core)
- AAV5-EF1a-DIO-eYFP (120-180nl, 2-4e12 GC/ml, UNC)
- AAV8-CAG-mRuby2 (100nl, 2.4 GC/ml, Salk Vector Core)

For Flp-dependent stGtACR2 expression in L5CTs, we injected 20-40nl of AAVretro-EF1a-FLP (3.6e11, Salk Vector Core) into both lPulv and rmPulv injection sites. For retrograde tracing of L6CTs, we injected 40nl of cholera toxin subunit B (CTB) conjugated to Alexa Fluor 488 (0.5%) or 647 (0.25%; Life Technologies) into the pulvinar. In 2/3 of these experiments, we injected one of each of these CTBs into lPulv and rmPulv sites (remaining animal was only injected in lPulv). For retrograde tracing of L5CTs, we used a self-complimenting (sc)AAVRetro-hSyn-mCherry (1.51e12 GC/ml, Salk Vector Core) because we observed more widespread and brighter labeling of L5CTs than with CTB. 20nl were injected into both lPulv and rmPulv injection sites.

For diphtheria toxin experiments, we injected 120-170nl of a mixture of AAV8-mCherry-flex-dtA (3.7 GC/ml, UNC) and either of the DIO-eYFP/GFP anterograde viruses (above, at 1:1 ratio; volume split across two V1 injection sites in one Npr3-Cre animal), as well as a 1:2 dilution of the same anterograde virus at the same injection sites and volumes in the right hemisphere. Mice were recorded from 10-15 days later.

In vivo electrophysiology

Following 2-4 days of habituation to the running wheel at the recording rig (30+minute sessions), mice were anesthetized with isoflurane to make craniotomies above the desired recording sites. Mice were then head-fixed on their wheel, where they were free to run at their will and their movement was tracked with a rotary encoder. A black curtain was secured around the headframe holder to prevent the mice from seeing light from optogenetic stimulation. Individual recording sessions typically lasted 2-3 hours. In the case of multiple recording sessions from a single animal, mice were given at least 30 minutes and up to a day undisturbed in their cages with food and water between sessions.

For our recordings, we used 64- or 128-channel silicon microprobes[44,77] connected to an Intan RHD2164 128-channel amplifier board. Data was acquired at 20kHz with the OpenEphys data acquisition system[78]. For the majority of recordings, V1/SC and thalamus recordings were conducted simultaneously using two separate 128-channel amplifier boards (thus 192-256 channels recorded simultaneously through OpenEphys). For V1 and SC recordings, we used either 64D (64 channels on one shank, 1.05mm vertical extent of electrodes) or 128AN (two shanks each with 64D configuration, separated by 300µm) probe configurations. For thalamus recordings, we always used a 4-shank probe (128DN or 128D; 32 channels per shank over 775µm depth, 150µm or 330µm separation between shanks, respectively). All probes were gold-electroplated with an Intan RHD electroplating board to reach ~0.2MΩ electrode impedances.

Probes were lowered slowly into the brain with a digital and/or manual micromanipulator (MP-285, Sutter Instrument Co; 1760-61, David Kopf Instruments also used for simultaneous V1/SC recordings, 80° orientation) to approximate depths of 1.1mm (V1), 1.5mm (SC), or 2.5mm (pulvinar).

Agarose (~3.5%; A9793, Sigma-Aldrich) was then poured to fill the well of the headframe holder, thus covering the probe shank (s) and the tip of the optical fiber (s); this helped with grounding as well as recording stability. After lowering, the probes were left in place untouched for at least 30 minutes before data acquisition commenced. For all recordings, probes were coated with a 1-2.5% solution DiI or DiD (D282 or D7757, Thermo Fisher) in order to verify recording locations post-mortem. For thalamus recordings, probes were typically lowered once without DiI/DiD to check their location (based on presence or lack of highly temporally modulated visual responses, which indicated placement in dLGN) before being raised and relowered with DiI/DiD (for some experiments using 128D probes, they were not raised and relowered with DiI/DiD in the same position until after data acquisition was complete).

Visual stimulation

Visual stimuli were generated through custom MATLAB code using Psychtoolbox and presented on a 24" LED monitor (GL2450-B, BenQ). The monitor screen was positioned 12cm from the mouse's right eye. For drifting gratings experiments, full-field square-wave gratings were presented at four orientations in eight directions, 0.04 cycles/° spatial frequency, and 2Hz temporal frequency. A full trial consisted of a 0.5-second pre-stimulus period (grey screen), 2 seconds of drifting grating presentation, and 1.5-2 seconds post-stimulus period (grey screen). 20% of trials were "blank" trials, in which the screen remained grey for the full trial duration; these trials were used for assessing effects on spontaneous activity (see Analysis section below). Each unique drifting grating stimulus was presented at least 16 times under each light stimulation condition across the full experiment.

For receptive field mapping, a sparse noise stimulus protocol was used in which individual black or white 8° squares were displayed at random on a grey background anywhere within a chosen areal grid (10x12, 12x14 or 14x16). Each square was presented for 250ms. A "trial" consisted of both black and white squares being presented exactly once at all possible stimulus locations, and the same pattern of stimulus presentations was repeated in each light stimulation condition (see below). Timings of individual stimulus presentations were identified with a photodiode attached to the upper left corner of the monitor,

whose luminance changed at each new stimulus presentation (i.e., every 250ms). Across the full experiment, each stimulus (black or white square) was presented at each location in the grid 12-24 times under each light stimulation condition.

For V1 recordings, an additional 2-minute run of 2-second full-field screen flashes (2 seconds screen on, 2 seconds screen off, etc.) was presented at the beginning and end of the recording session. These were used for current source density analysis to identify cortical layers (see Unit Classification section below).

Optogenetic stimulation

Optogenetic stimulation was controlled via an Arduino Zero microcontroller board, which interfaced with MATLAB through a serial port connection. A 12-bit DAC and/or a digital output pin was connected to an LED driver (ThorLabs T-Cube LED driver or Plexon PlexBright LD-1 single channel LED driver) or a laser module (635nm collimated diode laser, Laserglow Technologies). LEDs were used for the majority of experiments, but the 635nm laser was used for five L6CT-halorhodopsin experiments. For other halorhodopsin stimulation experiments, we used a 617nm fiber-coupled LED module (ThorLabs), and for stGtACR2 and ChR2 experiments we used a 465nm (PlexBright, Plexon) or a 470nm (ThorLabs) fiber-coupled LED module. Alternatively, a 455nm LED (ThorLabs) was used for combined halorhodopsin and stGtACR2 CT inactivation experiments (Figure 2.5) to avoid the blue LED falling within halorhodopsin's excitation range. LED/laser light was outputted through a custom optical fiber patch cord (1mm diameter, 0.39 NA, ThorLabs; or 400µm diameter, 0.39NA, ThorLabs for dual-optogenetics experiments) and positioned as close as possible to the pial surface without hitting the recording probes. Light powers measured from the optical fiber tip (with PM100D with S121C power sensor, ThorLabs) were: 4-5.5mW from 1mm fiber or 0.75-1.0mW from 400µm fiber for halorhodopsin stimulation (617nm LED or 635nm laser); 1mW from 1mm fiber or 0.12-.16mW from 400µm fiber for L5-stGtACR2 stimulation (455nm or 465nm LEDs); 2.2mW from 1mm fiber or 0.25mW from 400µm fiber for L6CT-stGtACR2 stimulation (455nm or 465nm LEDs); 5-10mW from 1mm fiber for AAV-

targeted ChR2-stimulation of interneurons for V1 inactivation (470nm LED); and 0.8-1.1mW from 1mm fiber or 0.46mW from 400µm fiber for V1 inactivation in PV-Cre/Ai32 mice (465nm or 470nm LEDs).

In drifting grating experiments, light stimulation began 250ms after the trial start and 250ms prior to the visual/blank stimulus presentation and stayed on for 2 seconds. All drifting grating stimuli (including "blank" stimuli) were presented an equal number of times under every light stimulation condition (including no light). Trials in different light stimulation conditions were randomly interleaved throughout the experiment.

In receptive field mapping experiments, light alternated between ON and OFF in 2 second intervals for the full trial duration, and each unique pattern of sparse noise stimuli was presented with all possible patterns of light stimulation (e.g., 1st repeat: light ON, light OFF…; 2nd repeat: light OFF, light ON…). For dual-optogenetic experiments, there were four possible light stimulation patterns: 1) LED#1 ON and LED#2 OFF, LED#1 OFF and LED#2 ON…; 2) LED#1 OFF and LED#2 ON, LED#1 ON and LED#2 OFF…; 3) LEDs#1&2 ON, LEDs#1&2 OFF…; 4) LEDs#1&2 OFF, LEDs#1&2 ON….

Histology

At the end of recordings, animals were given an intraperitoneal injection of euthasol (15.6mg/ml) and perfused with phosphate-buffered saline (PBS) followed by 4% paraformaldehyde. Brains were dissected out, post-fixed in 2% PFA and 15% sucrose solution at 4°C for ~24 hours, moved to 30% sucrose at 4°C for another ~24 hours, and then frozen in sucrose and sliced on a freezing microtome. Brains were sliced coronally into 50µm sections, starting from the anterior edge of the hippocampus to the posterior end of cortex. All sections were counterstained with 10µM DAPI in PBS before being mounted and cover-slipped with Polyvinyl alcohol mounting medium containing DABCO. Additional immunohistochemistry for calretinin was performed on thalamic sections (except in cases with DiD and both red- and green-fluorescent axons in the thalamus; e.g., combined SC and L5/V1 inactivation experiments) by incubating at 4°C for 16-20 hours with rabbit anti-calretinin primary antibody (1:1000; Swant 7697) in 1% Donkey Serum/.1% Triton-X 100/PBS, followed by donkey anti-rabbit conjugated to

Alexa 647 (1:500; A-31573, Life Technologies) before DAPI counterstaining. Imaging was performed on an Olympus BX63 microscope (10x objective for most images, 20x for cortical z-stacks for cell counting) or a Zeiss LSM880 confocal microscope (20x).

Quantification and statistical analysis

Data Processing

We used Kilosort2[79] to semi-automatically spike-sort extracellularly recorded data. First, different recordings from the same recording session (drifting gratings and RF mapping experiments) were concatenated together into a single binary file. We then subtracted out the large voltage deflections caused by light onsets and offsets prior to high-pass filtering (>150Hz) in Kilosort2 because otherwise we found that spike detection within ~10ms of the light onset/offset times was compromised. Additional "spikes" were removed within 1.5ms of the light onset/offset times to ensure that no further optogenetic artifacts were included in the analyses.

Phy2[80] was used to validate and further curate as needed the clusters outputted by Kilosort2. In some experiments where optogenetic artifacts couldn't be completely removed during Kilosort2, they were typically easily removed in Phy2 because they appeared as outliers in its principal component features view. Units were considered "good" single-units whose waveforms clearly deviated from the noise, had a clear refractory period in their auto-correlogram and no evident refractory period in their cross-correlogram with other units. From there, "good" units were included in subsequent analyses which had fewer than 0.5% refractory period violations, visually evoked and/or spontaneous firing rates >=.25Hz, and "unit quality" (isolation distance[81]) greater than 16.

Unit classification

For thalamus recordings, the fluorescent traces left by the lipophilic dyes (DiI or DiD) on the probe shanks were identified in histology and used to assign all units recorded from each shank to a particular thalamic nucleus. This was aided by calretinin immunohistochemistry, which provided clear

boundaries between rmPulv/cmPulv (calretinin+ cell bodies), lPulv (calretinin-), and dLGN (calretinin+ axons). While calretinin does not distinguish between rmPulv and cmPulv, the distinction was clear because V1 axons were only in rmPulv, but not cmPulv[30]. Thus, for pulvinar recordings, we only included units in our analyses that were recorded on shanks that passed through fluorescent V1 axons (in the absence of V1 axons, e.g., L5ET-dtA experiments, we compared our calretinin staining and the shape of the dentate gyrus to the Allen Brain Institute's Reference Atlas and our own images with both calretinin staining and V1 axons). Because the boundaries of dLGN were perfectly clear with calretinin staining, any shanks in the dLGN, even if they did not pass through L6CT terminals, were included in our analyses. The dorsal/ventral boundaries of our thalamic recordings were determined by assessing visual responsivity (see below for criteria for being "visually responsive"); since the top channels of our recording probe were typically in the hippocampus and thus virtually silent, we considered the most dorsal channel with a visually responsive unit as the top of dLGN/pulvinar (hence, "depth" in LMI plots throughout this study are relative to the position of this first channel). Similarly, the ventral boundary of the thalamus was identified as the last channel with a visually responsive unit, and all units recorded from those and intervening channels were included in analyses.

Units were considered "visually responsive" if there was a significant difference in spike counts during either the initial (first 200ms) or sustained (250-1750ms) period following the onset of the drifting grating stimulus, compared between preferred visual stimulus trials (i.e., the direction with the biggest difference from baseline) and blank trials (using the Wilcoxon rank-sum test with $p=0.025$ significance threshold) in which the mouse was stationary. For non-optogenetic experiments (i.e., diphtheria toxin experiments), there were no "blank" trials and so instead the first 200ms or sustained 500ms (250-750ms) periods from visual stimulus onset were compared to the same durations at the start of the trial (pre-stimulus) with the paired Wilcoxon signed-rank test.

A similar approach was used to determine the significance of a unit's light modulation; spike counts during the sustained (250-1750ms from visual stimulus onset) period were compared between blank (stationary) trials with and without light stimulation. We used the Benjamini-Hochburg method for

false discovery rate correction to limit the estimated rate of false positives among our modulated cells to <10% (typical significance threshold ~p=0.025, no less than .01). These significantly modulated cells were then classified as "suppressed" or "enhanced" based on whether their spontaneous light modulation index was less than (suppressed) or greater than 0 (enhanced). In joint SC and L5ET/V1 inactivation experiments where we sought to separately assess the effects of four different light stimulation conditions (no light, SC-inactivation, L5/V1-inactivation, SC&L5-inactivation), instead of the rank-sum test we used the Kruskal-Wallis test with the Dunn–Šidák post-hoc test. We did this separately for both visual (preferred direction) and blank trials and designated units as SC-suppressed, L5/V1-suppressed, or suppressed by both if comparisons were significant for either their visual or spontaneous activity (since we noticed that unlike with L5/V1-inactivation, SC inactivation often impacted visual but not spontaneous activity[29]). As an additional catch for false positives, units had to be significantly ($p<0.025$) suppressed in their visual or spontaneous activity during the combined inactivation condition (L5/V1- and SC-inactivation) as well as in at least one of the conditions when only one population was inactivated to be classified as SC-suppressed, L5/V1-suppressed, or suppressed by both.

For V1, the short recordings of cortical activity in response to screen flashes (see Visual Stimulation above) were used for current source density (CSD) analysis to determine recorded units' laminar position. We used CSDPlotter[82] to compute the second spatial derivative of the low-pass-filtered (<1000Hz) local field potential during the transitions between screen-off and screen-on periods. We then assigned electrode channels to cortical layers based on typical spatiotemporal patterns of current sources and sinks immediately following a screen flash (see Figure 2.2c), and units whose largest voltage deflection was picked up from a particular channel were assigned to that channel's layer. Units were classified as "fast-spiking" if the time from the trough to the peak of their waveforms was less than .475ms (which typically marked a clear division in the bimodal distribution of trough-to-peak times); all others were considered "regular-spiking". Units were considered putatively opsin-expressing ("inactivated" units) if they were regular-spiking, in the expected layer (L5 or L6 in Npr3-Cre and Ntsr1-

Cre mice, respectively), their visually evoked activity was significantly light modulated (as described above), and LMI_{vis} <-.33 (i.e., >50% suppression of visually evoked activity).

Quantification and analysis – drifting gratings experiments

Average visually evoked and spontaneous firing rates (FR_{vis} and FR_{spont}) were calculated in the window 250-1750ms after stimulus onset across visual and blank trials, separately for trials in different light stimulation conditions. Only "stationary" (speed < 2cm/s) trials were used for these calculations because running has been shown to affect firing rates in V1[83] and the thalamus[84], and our mice did not run very often (typically <10% of trials). Light modulation indices (LMIs) were then calculated as the difference divided by the sum of average firing rates (FR_{vis} or FR_{spont}) in no-light versus light stimulation conditions. The visually evoked FR change (Figure 2.3j) was calculated as the absolute value of the difference between FR_{vis} and $FR_{spont,}$ separately for each light condition. F1 responses were calculated by computing the Fast Fourier Transform (FFT) of the baseline-subtracted (baseline from the same time window in blank trials for each light stimulation condition separately) average peristimulus time histogram (10ms bins) across preferred direction trials during the sustained response period (250-1750ms after visual stimulus onset). The F1 response was the component of the resulting spike-response amplitude spectrum at the temporal frequency of the visual stimulus (2Hz). Bursting rates were calculated as the ratio of the number of spikes occurring in bursts to the total number of spikes during the sustained stimulation period in visual and stationary trials, separately for each light condition. Burst spikes were defined as those preceded by an inter-spike interval (ISI) $\geq$ 100ms and followed by an ISI $\leq$ 4ms (first spikes in a burst), as well as all subsequent spikes which were preceded by an ISI $\leq$ 4ms.

Quantification and analysis – RF mapping experiments

For each unit, we generated a peristimulus time histogram matrix *M* of average baseline-subtracted firing rates for each unique stimulus type (white or black square at each possible stimulus position under each light stimulation condition; baseline = mean of first 20ms) at each 10ms time bin

following the start of the stimulus (250ms total stimulus presentation = 25bins). We then performed singular value decomposition (SVD) of this matrix *M*:

$$M_{i,j} = (USV')_{i,j} = S_{1,1}U_{1,i}V_{1,j} + S_{2,2}U_{2,i}V_{1,j} + \ldots$$

to extract spatial ($U_{1,i}$) and temporal ($V_{1,j}$) filter approximations of the spatiotemporal receptive field.

The following criteria were then used for identifying significant receptive fields:

1. The relative variance of the first singular value ($S_{1,1}$ ($\sum_i S_{i,i}^2$)$^{-1}$) was >10%, AND the peak of the temporal filter ($V_{1,j}$) exceeded the mean over the first three time bins (($\sum_{j=1}^{3} V_{1,j}$)/3) by at least 5 standard deviations.
2. The "spatial SNR" of $U_{1,i}$ (reshaped to $U_{1,x,y}$) - the ratio of the maximum variance at any x/y position to the mean variance at the furthest two x/y positions, across x and y dimensions separately - exceeded the 2.5% tails of a null distribution of spatial SNRs (from 1000 shuffles of entries in $U_{1,x,y}$) in either x or y dimensions. In other words, there was a non-random spatial organization of the estimated receptive field. OR, units also passed this step if a value of $U_{1,x,y}$ exceeded 5 standard deviations above the mean of $U_{1,x,y}$ (otherwise, units with very small RFs - most common in dLGN - did not pass the spatial SNR criterion).
3. At least one value of $U_{1,i}$ was significant relative to a null distribution (from SVD of 500 shuffled *M* matrices), with a significance threshold corrected for <20% FDR (Benjamini-Hochburg method).

For units who passed these criteria for at least 1/4 of their computed receptive field estimates (on and off subfields, light on and light off conditions), we then used the p-values generated in step 3 as a mask for the spatial filter map ($U_{1,x,y}$). This significant RF map was then bilinearly interpolated to 1° resolution, smoothed with a 2D Gaussian filter (σ=4), and binarized, from which the borders and area of the estimated RF could be determined.

For analyses of retinotopic alignment, we used the estimated receptive field off- and on-fields exclusively from no-light (i.e., control) conditions. RF distance was calculated as the magnitude of the

vector connecting the center of all RFs from a single V1 penetration (median x and y positions of all individual unit RF centers) to the center of each thalamic RF, separately for off- and on-subfields. Whichever RF distance (between off- and on-subfields) was shorter was that unit's final RF distance used for analysis in Figure 2.4.

For ease of interpretation, all RFs in this manuscript are illustrated as baseline-subtracted firing rates (pre-SVD) at the peak timepoint (i.e., *j* at which $V_{1,j}$ is maximal). When the peak timepoint differed between light stimulation conditions, the same peak timepoint (from the no-light condition) was used for all conditions.

Quantification – cell counting

For quantification of L6CT cells in Ntsr1-Cre/Ai14 mice, we acquired z-stack images at 20x magnification with a Zeiss LSM880 confocal microscope. The counted region was restricted to the area of V1 (as identified by a thicker L4 in the DAPI channel and the relative lack of retrograde labeling in upper L6 relative to more lateral and medial cortical areas, as consistently described in other studies[4,5,36]). Within this area, L6 was then split into partitions (as in a prior study[85]); cells in the upper 10-40% of L6 were counted as $L6_{upper}$, cells in the lower 60-110% were counted as $L6_{lower}$, and all cells throughout the full depth of L6 were included for "all L6" quantification. Only animals in which the CTB injection was confined to the pulvinar and did not spread into dLGN were included in this quantification (n=3). Two or three sections spaced 200-400µm apart were counted per animal using FIJI.

For quantification of L5ETs, we acquired z-stack images at 20x magnification with an Olympus BX63 microscope. For quantification in Npr3-Cre mice, the area of GFP expression (from AAV injection) and the mCherry+ pulvinar axons (dense in L4 of extrastriate areas but not V1) were used to set the counting boundaries in V1. Three sections spaced 50-150µm apart were counted in each of four animals. For quantification of L5ETs with different subcortical targets, cells retrogradely labeled from the SC with CTB-647 were the most spatially restricted and thus were the main determiners of counting boundaries in V1 (V1 boundaries identified by mCherry+ axons as before). Since the SC injection was

also the most difficult because of its close proximity to retrosplenial cortex, animals were only included for quantification if all three injections were well targeted and yielded retrograde labeling in V1 but not in the LD thalamic nucleus (a major input to retrosplenial cortex; n=3). Five sections, each separated by 150μm, were counted for each animal. FIJI software was used for all cell counting.

Statistical analysis

For paired comparisons, we used the Wilcoxon signed-rank test. For independent comparisons with two groups, we used the Wilcoxon rank-sum test, and for more than two groups we used the Kruskal-Wallis test with the Dunn–Šidák post-hoc test for multiple comparisons. Statistical significance was assessed at the 0.05 level unless otherwise specified.

Appendix

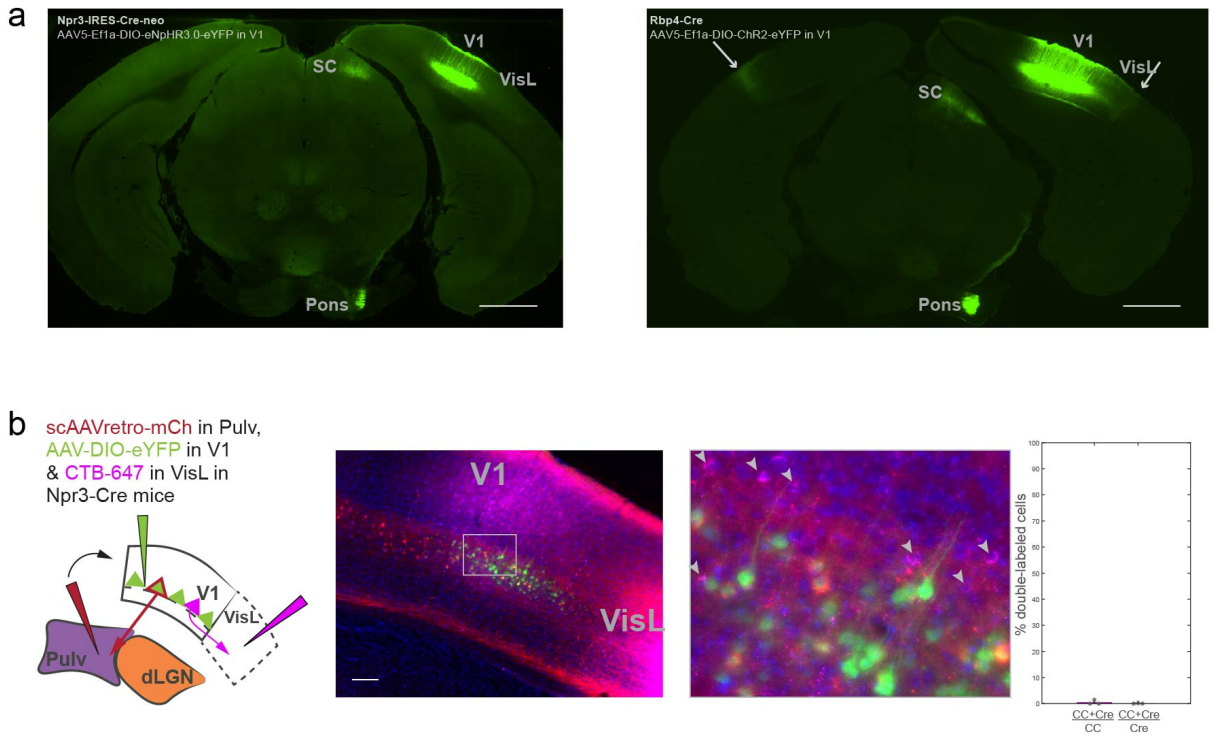

Figure 2.S1 The Npr3-IRES-Cre-neo knock-in mouse line is specific for extratelencephalic (ET), but not cortico-cortical (CC), cells in L5. a) Epifluorescence images of a Npr3-Cre mouse injected with AAV5-EF1a-DIO-eNpHR3.0-eYFP in V1 (left), and a Rbp4-Cre mouse injected with AAV5-Ef1a-ChR2-eYFP in V1 (right). In both cases, axons are visible in subcortical targets SC and pons, yet cortical axons (in contralateral cortex and in lateral visual cortex (VisL), indicated by arrows) are only visible in Rbp4-Cre mice, even at high exposures. 1mm scale bars. b) Corticothalamic and CC cells were retrogradely labeled from pulvinar and VisL, respectively, in Npr3-Cre mice injected with an AAV encoding Cre-dependent eYFP in V1 (three out of the four of the same experiments depicted in Figure 2.1f). Middle: epifluorescence images (at 20x, maximum intensity projection) of V1 and VisL. Arrowheads in zoomed in image (from boxed area) indicate retrogradely labeled CC cells which are neither mCh+ (CT) nor eYFP+ (Cre+). 100µm scale bar. Right: quantification of double-labeled (CTB+ and eYFP+) cells out of all CC (CTB+) and all Cre+ (eYFP+) cells. Only one doubled-labeled cell was found in any of the three animals, hence values are virtually zero (0.49% and .05%, means across n=3 animals).

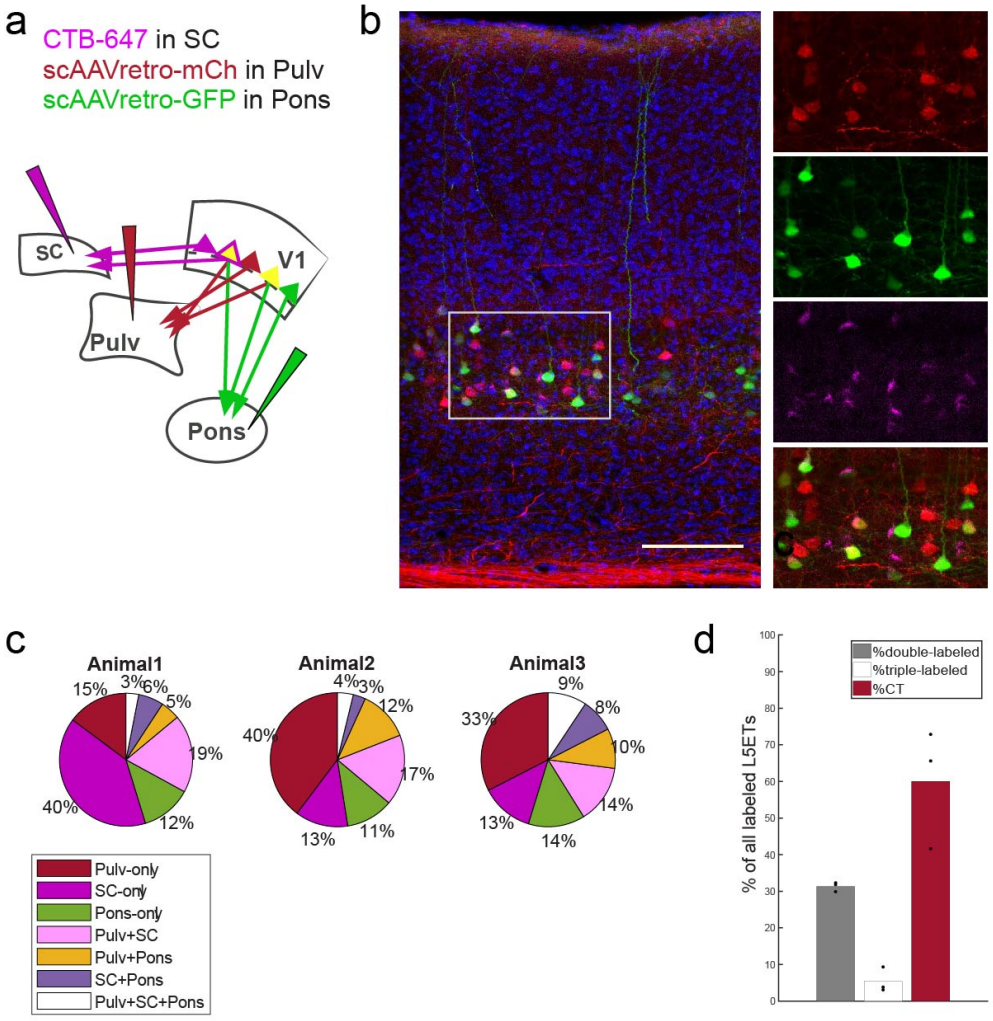

Figure 2.S2 Proportions of L5 extratelencephalic (L5ET) cells projecting to one or more subcortical targets. a) Three different retrograde tracers were injected into different subcortical targets of L5ETs (SC, Pulvinar and Pons). Right: confocal image of retrogradely labeled cells in V1, including higher-magnification single- and composite-channel images of boxed region. 100µm scale bar. b) Proportions of different retrogradely labeled cell types in each of three experimental animals. c) Proportions of double-labeled (2 subcortical projection targets), triple-labeled (all three projection targets), and pulvinar-projecting (CT) cells across all three mice. Proportions of CT cells are likely overestimates, as we observed more numerous and widespread retrogradely labeled cells from the pulvinar, likely because scAAVretro-mCh covered a larger proportion of the pulvinar than did scAAVretro-GFP in pons and CTB-647 in SC. Bars indicate means across n=3 animals.

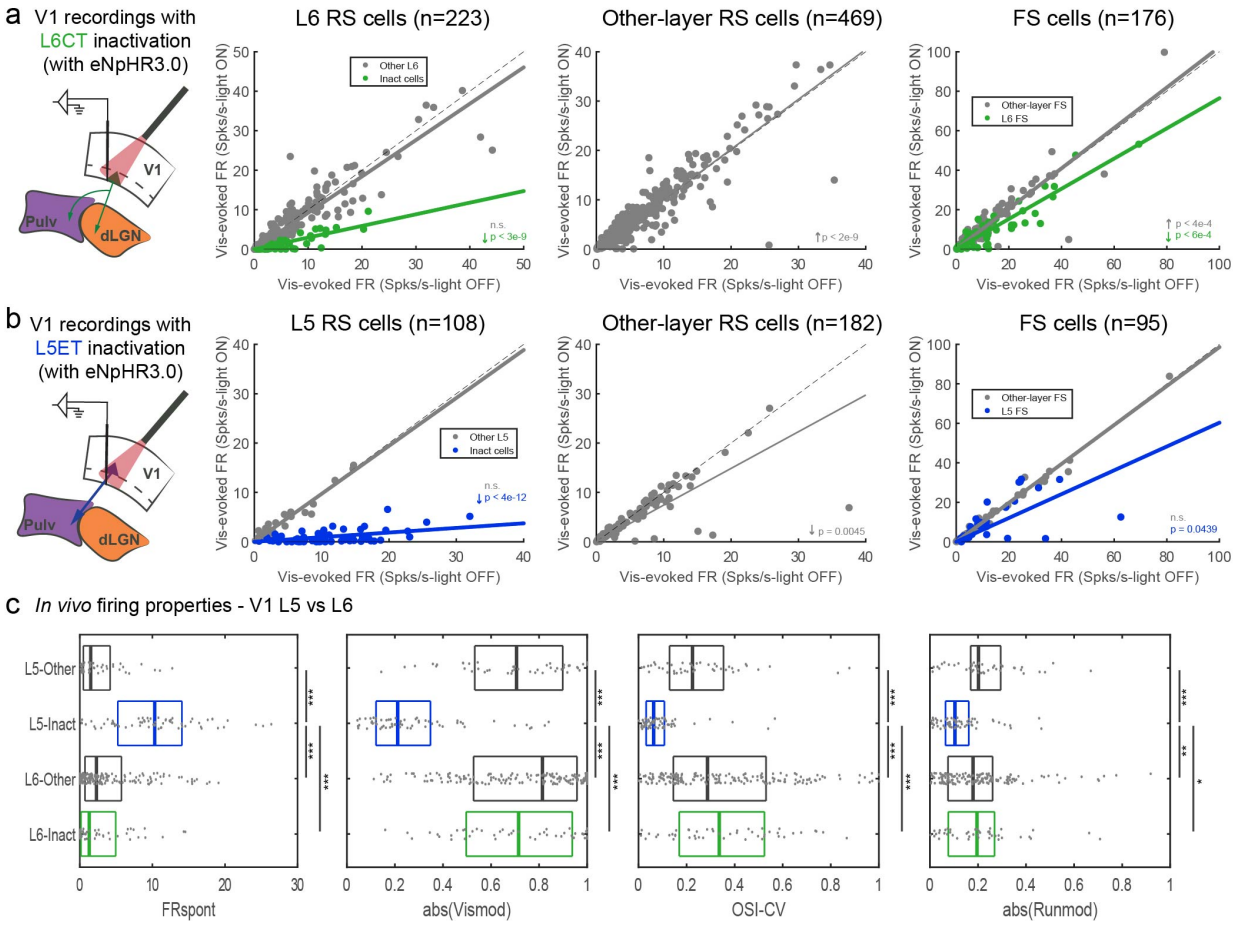

Figure 2.S3 L6CTs and L5ETs differ in how their inactivation influences other layers and in their firing and tuning properties. a) Visually evoked firing rates, with versus without L6CT inactivation for (left to right): regular-spiking cells within L6 ("inactivated" cells or "other"); all other RS cells (layers 2-5); and all RS cells (L6 vs. all other layers). Significance values are from Wilcoxon signed-rank tests, and arrows indicate the direction of significant modulation. b) Same as a) but for L5ET inactivation experiments (comparing L5 versus other layers). c) Left to right: boxplots of medians and quartiles of spontaneous firing rates (from blank trials); visual modulation index magnitudes (difference divided by sum of average firing rates from preferred visual and blank trials without LED stimulation); orientation selectivity indices (1- circular variance); and running modulation index magnitudes (difference divided by sum of average visually evoked firing rates from running versus stationary trials, only for experiments with >5% running trials). Other vs. Inact units in L5 versus L6 come from experiments in which L5ETs or L6CTs were inactivated, respectively. ***p<.001, **p<.01, *p<.05, Kruskal-Wallis non-parametric test with the Dunn–Šidák post-hoc test for multiple comparisons.

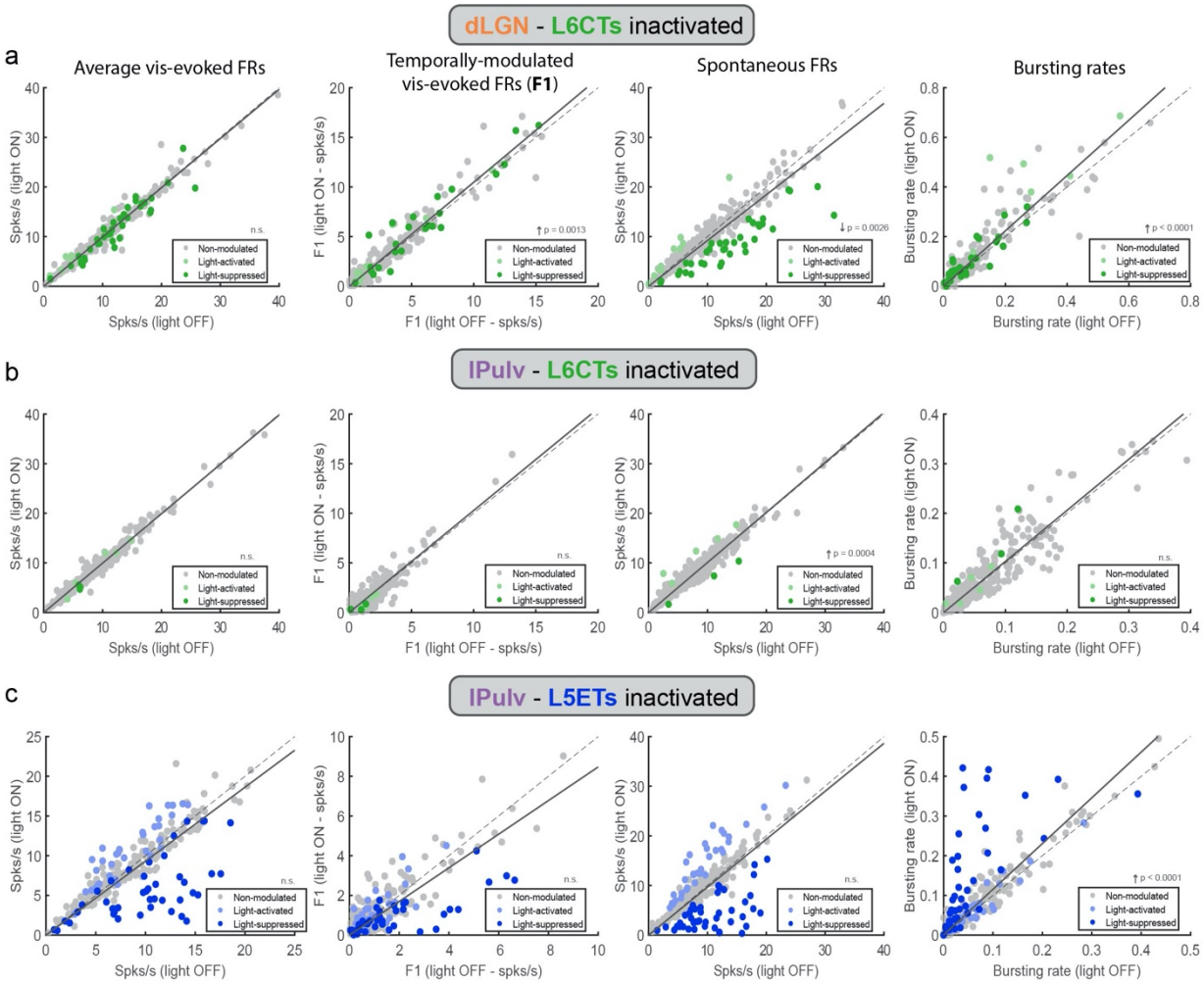

Figure 2.S4 Population-level effects of L6CT vs. L5ET inactivation on activity in the dLGN and lateral pulvinar. a) Effects of L6CT inactivation on dLGN units' (left to right): average visually evoked activity across all visual trials; temporally modulated response (i.e., F1) to the preferred visual stimulus; spontaneous firing rates (from blank trials); and bursting rates. Units are colored according to whether their spontaneous activity was suppressed, activated, or non-modulated by light stimulation (same classification as in Figure 2.3). P-values from Wilcoxon signed-rank tests (all units combined). b) Same as a) but for lPulv units recorded with L6CT inactivation. c) Same as a) but for lPulv units recorded with L5ET inactivation.

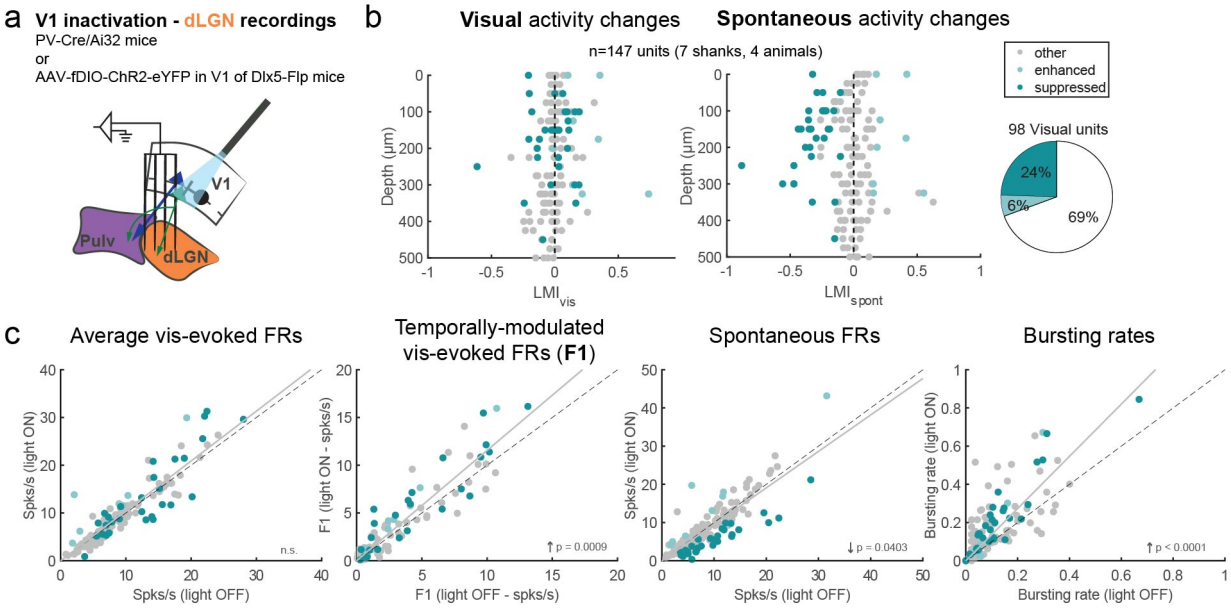

Figure 2.S5 Non-specific V1 inactivation also has distinct effects on visual versus spontaneous activity in the dLGN. a) Schematic of thalamus recordings during V1 inactivation (see Figure 2.S10 for V1 and pulvinar data). b) Light modulation indices across visual and blank trials (LMI_{vis} and LMI_{spont}) by depth for all dLGN units. Right: proportion of units whose spontaneous activity was significantly suppressed, enhanced or unmodulated (same criteria as for Figure 2.3). c) Effects of L6CT inactivation on (left to right): average visually evoked FRs across all visual trials; temporally modulated response (i.e., F1) to the preferred visual stimulus; spontaneous FRs (from blank trials); and bursting rates for all rmPulv units. P values are from Wilcoxon signed-rank tests, and arrows indicate direction of significant change.

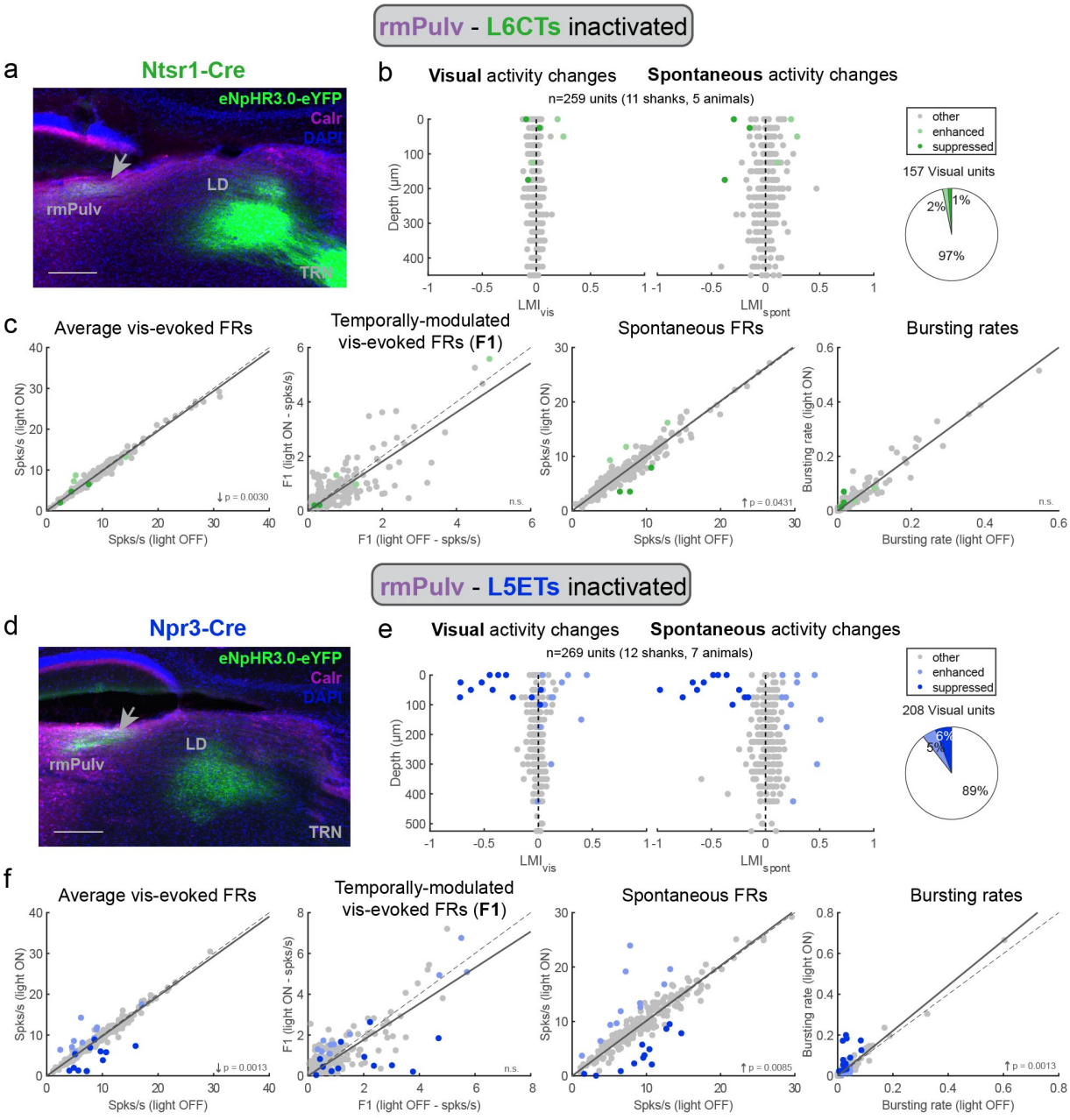

Figure 2.S6 Rostromedial pulvinar (rmPulv) also receives modulatory and driving input from V1 L6CTs vs L5ETs, respectively. a) L6CT axons in the rmPulv, as well as LD and TRN. rmPulv stains positive for calretinin (unlike lPulv). Scale bar = 200µm. b) Light modulation indices across visual and blank trials (LMI_{vis} and LMI_{spont}) by depth for all rmPulv units. Right: proportion of units whose spontaneous activity was significantly suppressed, enhanced or unmodulated (same criteria as for Figure 2.3). c) Effects of L6CT inactivation on (left to right): average visually evoked FRs across all visual trials; temporally modulated response (i.e., F1) to the preferred visual stimulus; spontaneous FRs (from blank trials); and bursting rates for all rmPulv units. d) L5ET axons in the rmPulv, as well as LD (but not TRN). e-f) same as b-c) but for L5ET inactivation experiments. P-values are from Wilcoxon signed-rank tests, arrows indicate direction of significant change.

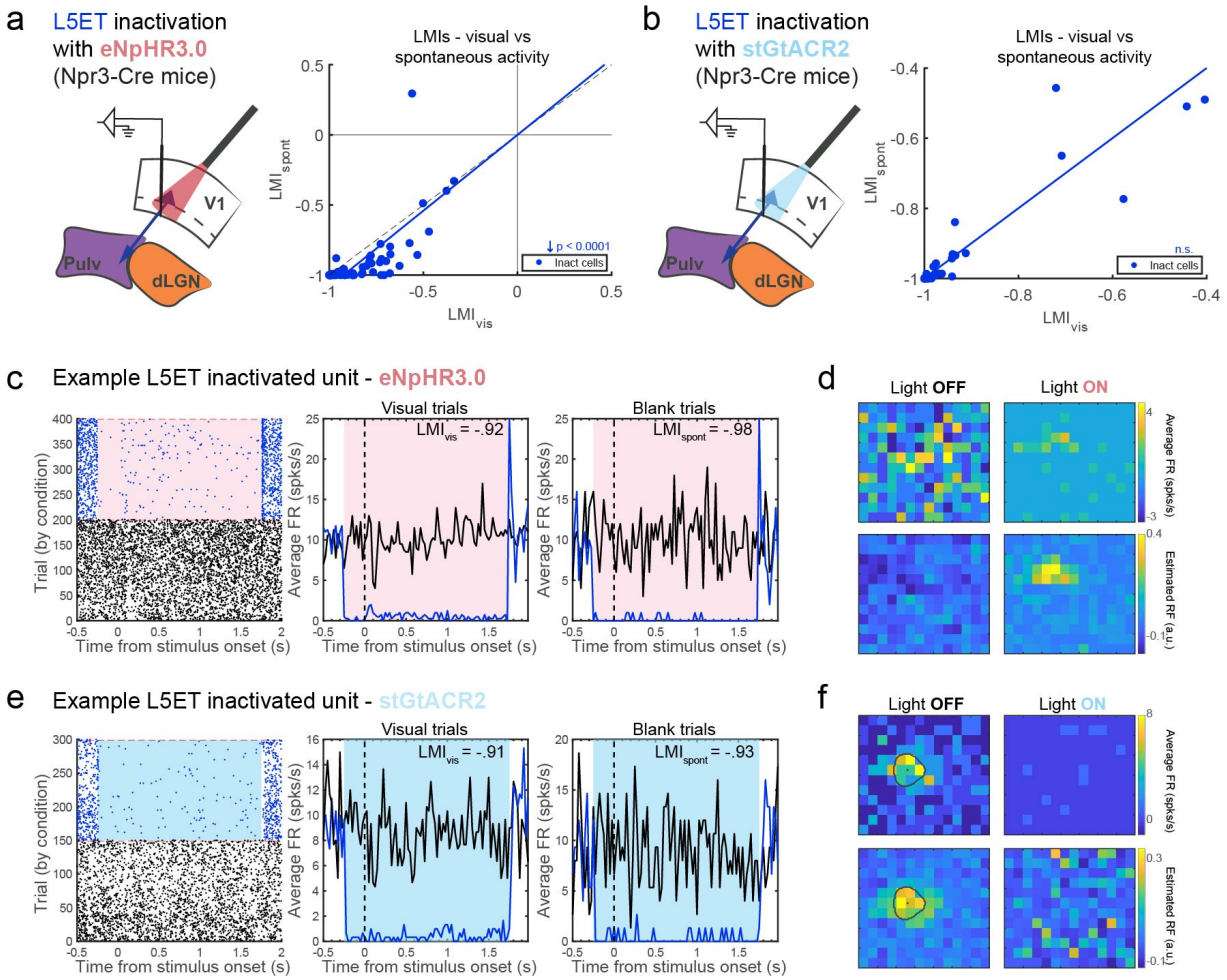

Figure 2.S7 Efficacy of halorhodopsin versus stGtACR2 in silencing spontaneous versus visual activity in L5ETs. a) Inactivation of halorhodopsin-expressing L5ET cells in V1 with red (617nm) LED light. Right: light modulation indices across visual versus blank trials (LMI_{vis} vs. LMI_{spont}) for putatively halorhodopsin-expressing L5ETs in V1. Individual units' LMIs were typically more negative (i.e., stronger inactivation) in blank than in visual trials ($p<0.0001$, Wilcoxon signed-rank test). b) Same as a) but for experiments with stGtACR2 expressed in V1 L5ETs, which was activated with blue light (455-470nm LED). There was no significant difference between visual and spontaneous LMIs. c) An example regular-spiking L5 cell that is putatively halorhodopsin-expressing given its high degree of inactivation. Left: raster plot. Middle: PSTH across visual trials. Right: PSTH across blank trials. Shading indicates the period of LED stimulation. d) Top row: the same example unit's average baseline-subtracted FRs at the peak delay time in response to sparse noise stimuli (luminance increases) presented at various locations, without (left) or with (right) LED stimulation for L5ET inactivation. Bottom: the estimated spatial receptive field from singular value decomposition of the matrix of PSTHs across all stimulus locations (see Methods for details). Despite visual and spontaneous LMIs <-0.90, this unit does not have a discernable RF under normal conditions, but with background activity levels suppressed by LED stimulation, the signal-to-noise ratio improves such that a clear RF emerges. e) An example putative stGtACR2-expressing L5ET unit. f) Same as d) but for the unit in e). In this case, the unit's response to stimuli presented in its RF is entirely abolished.

Figure 2.S8. Relating the retinotopic distance between pulvinar units and V1 inactivation to light modulation of drifting grating responses and the area of opsin expression, for halorhodopsin and stGtACR2 L5ET inactivation experiments. a) An example L5ET inactivation experiment (with halorhodopsin) in which both V1 and lPulv was recorded from (not simultaneously). Left: overlayed RFs (OFF fields) recorded from V1. a.i-iii: three example lPulv units' RFs with and without light for L5ET inactivation (middle), and average PSTHs in response to drifting gratings (right). RF maps depict baseline-subtracted firing rates at each position in the grid at the peak timepoints. Black outlines and dots indicate the boundaries and centers of their estimated RFs (see Methods for details). Grey dots demark the center of RFs recorded in V1 (accounting for the wider grid of stimulus positions that was used in the pulvinar than in the V1 recordings). "RFdist" is the distance (in degrees) from each unit's RF center to the center of all V1 RFs. Note that a.i and a.ii have similar RF locations and distances, yet only a.i is significantly suppressed by L5ET inactivation during drifting grating experiments. Meanwhile, a.iii has an even shorter RF distance to the inactivation/recording site in V1, yet was unaffected by L5ET inactivation. b) Opsin expression diameter in V1 versus the largest RF distance of a significantly suppressed pulvinar cell recorded in that animal, among halorhodopsin- and stGtACR- expressing animals. c) Relationship between light modulation (in drifting grating experiments) and RF distance in L5ET-stGtACR2 experiments in which sparse noise stimulation was used for both pulvinar and V1 recordings. Dots indicate LMI_{vis} (right y-axis) of enhanced, suppressed, and other cells (same as Figure 2.5: classified from blank trials). Bars indicate the proportion of units significantly suppressed or enhanced (left y-axis), binned by retinotopic distance to V1 inactivation site (10° bins). 'Other Vis' are all other units from the same experiments whose RFs could not be determined. White bars reflect means of 1000 shuffled distributions (shuffled separately for each experiment). Asterisks indicate where actual proportions fell beyond either tail (2.5%) of shuffled distributions. Fewer RFs were identified in these experiments than in halorhodopsin experiments (Figure 2.4), likely because we used twice the number of light conditions (including SC inactivation; Figure 2.7) and thus fewer repeated presentations. d) In L5ET-stGtACR2 experiments, the percent of all pairs of units from the same recording shank consisting of at least one suppressed unit in which the second unit was also suppressed or enhanced, binned by vertical distance between units in a pair. White bars reflect means of 1000 shuffled distributions (shuffled separately for each recording shank). Asterisks indicate where actual proportions fell beyond either tail (2.5%) of shuffled distributions.

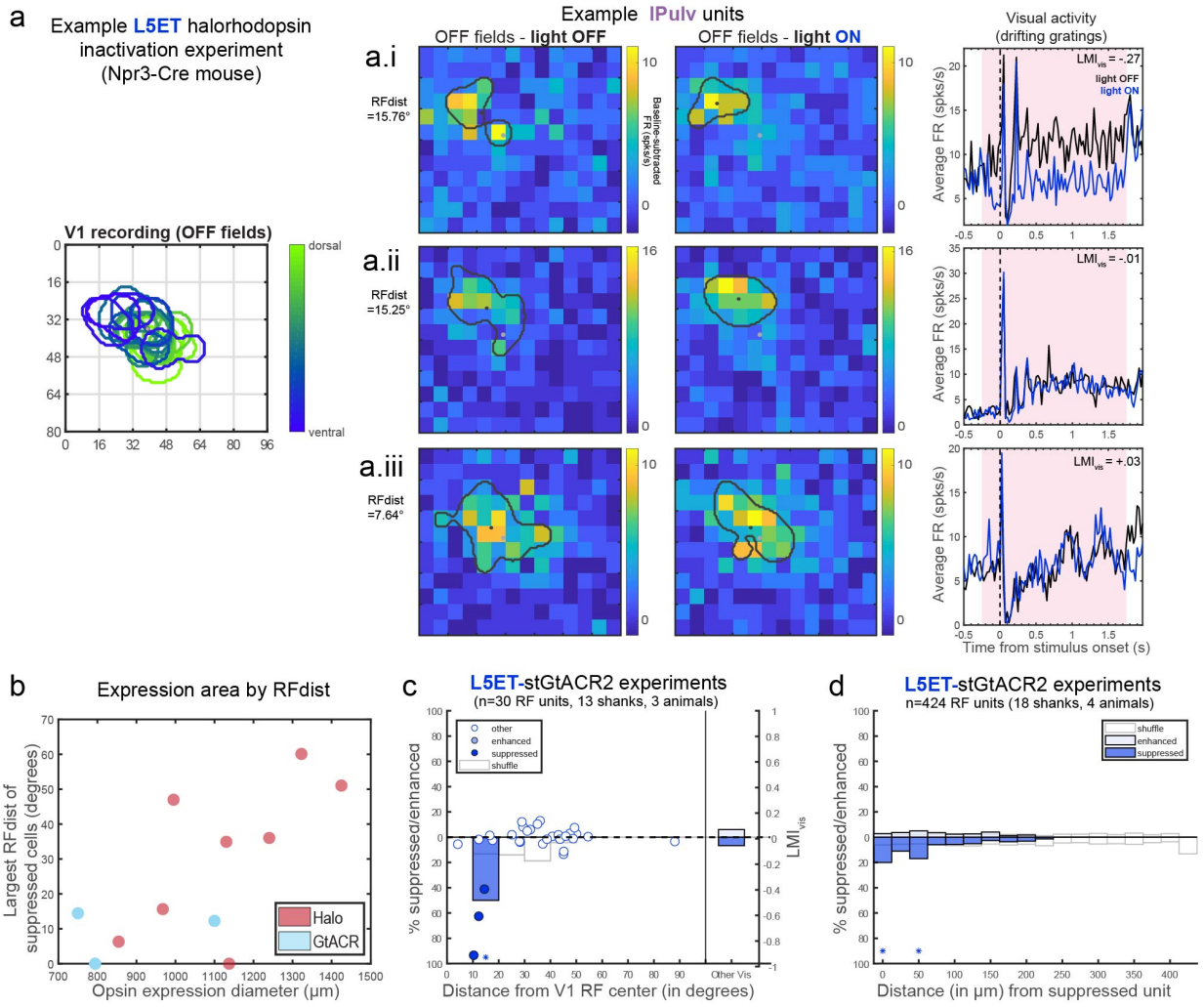
a
Example L5ET halorhodopsin inactivation experiment (Npr3-Cre mouse)
V1 recording (OFF fields)
dorsal
ventral
Example lPulv units
OFF fields - light OFF
OFF fields - light ON
Visual activity (drifting gratings)
a.i
RFdist =15.76°
a.ii
RFdist =15.25°
a.iii
RFdist =7.64°
Baseline-subtracted FR (spks/s)
LMIvis = -.27
light OFF
light ON
LMIvis = -.01
LMIvis = +.03
Average FR (spks/s)
Time from stimulus onset (s)
b
Expression area by RFdist
Largest RFdist of suppressed cells (degrees)
Opsin expression diameter (µm)
Halo
GtACR
c
L5ET-stGtACR2 experiments
(n=30 RF units, 13 shanks, 3 animals)
other
enhanced
suppressed
shuffle
% suppressed/enhanced
LMIvis
Other Vis
Distance from V1 RF center (in degrees)
d
L5ET-stGtACR2 experiments
n=424 RF units (18 shanks, 4 animals)
shuffle
enhanced
suppressed
% suppressed/enhanced
Distance (in µm) from suppressed unit

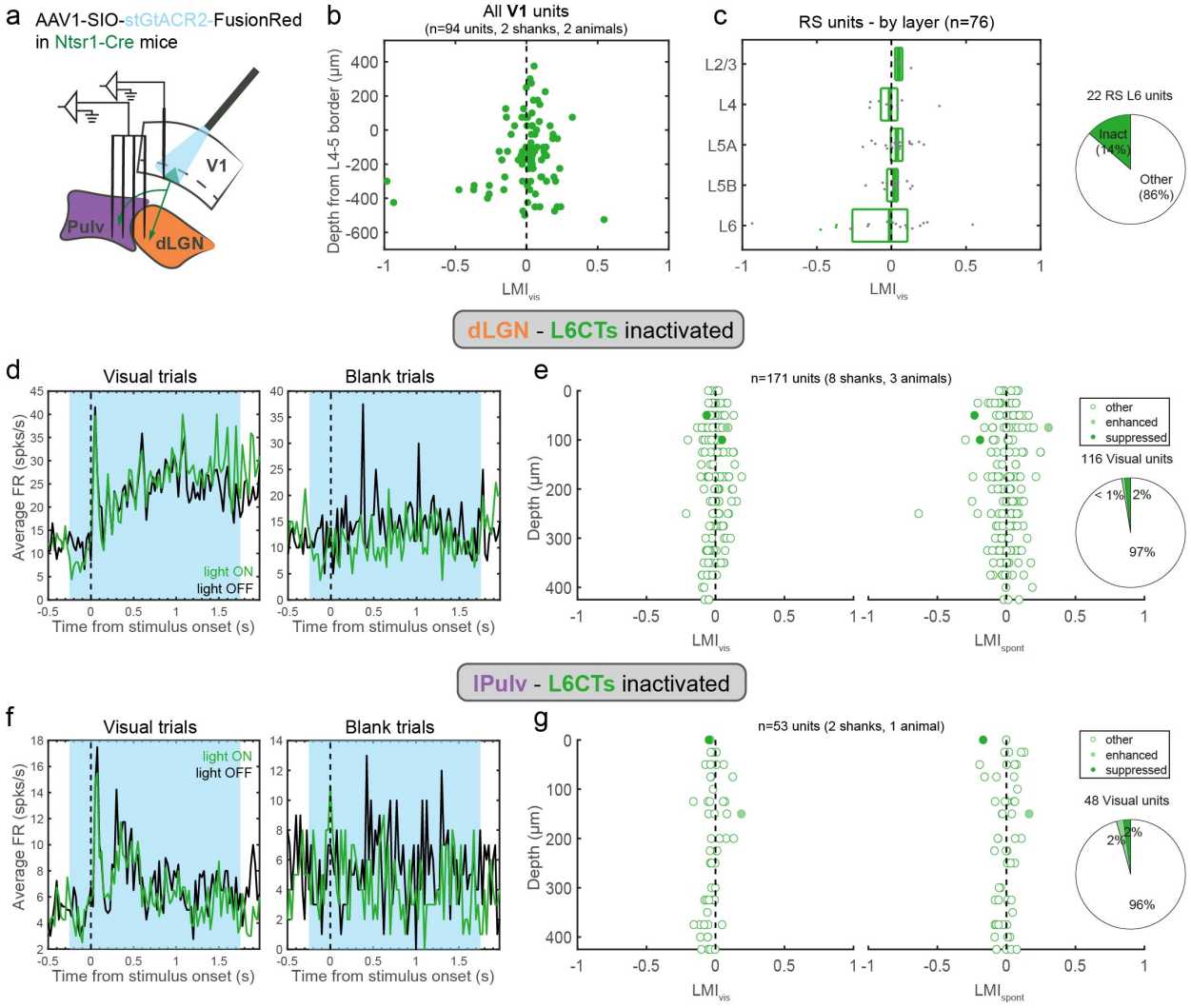

Figure 2.S9 Inactivating L6CTs with stGtACR2 still does not affect visual activity in the dLGN or pulvinar. a) Schematic of simultaneous V1 and thalamus recordings. b) Light modulation indices from visual trials (LMI_{vis}) of all recorded V1 units by their relative depth. c) LMI_{vis} of regular-spiking units, by layer. Putative inactivated units are colored dots. Right: proportion of all RS L6 units putatively inactivated. d) An example of a dLGN unit whose spontaneous, but not visually evoked, activity was suppressed by L6CT inactivation with stGtACR2. Average PSTHs from visual (left) and blank (right) trials. Blue shading indicates the period of LED stimulation for L6CT inactivation. e) Visual (left) and spontaneous (right) LMIs by depth for all recorded dLGN units, classified according to whether their spontaneous activity was significantly suppressed, enhanced, or non-modulated ("other"; same criteria as in Figures 2.3 and 2.5). Far right: proportion of all visually responsive units in each class. f-g) Same as d-e) but for units recorded in the lateral pulvinar.

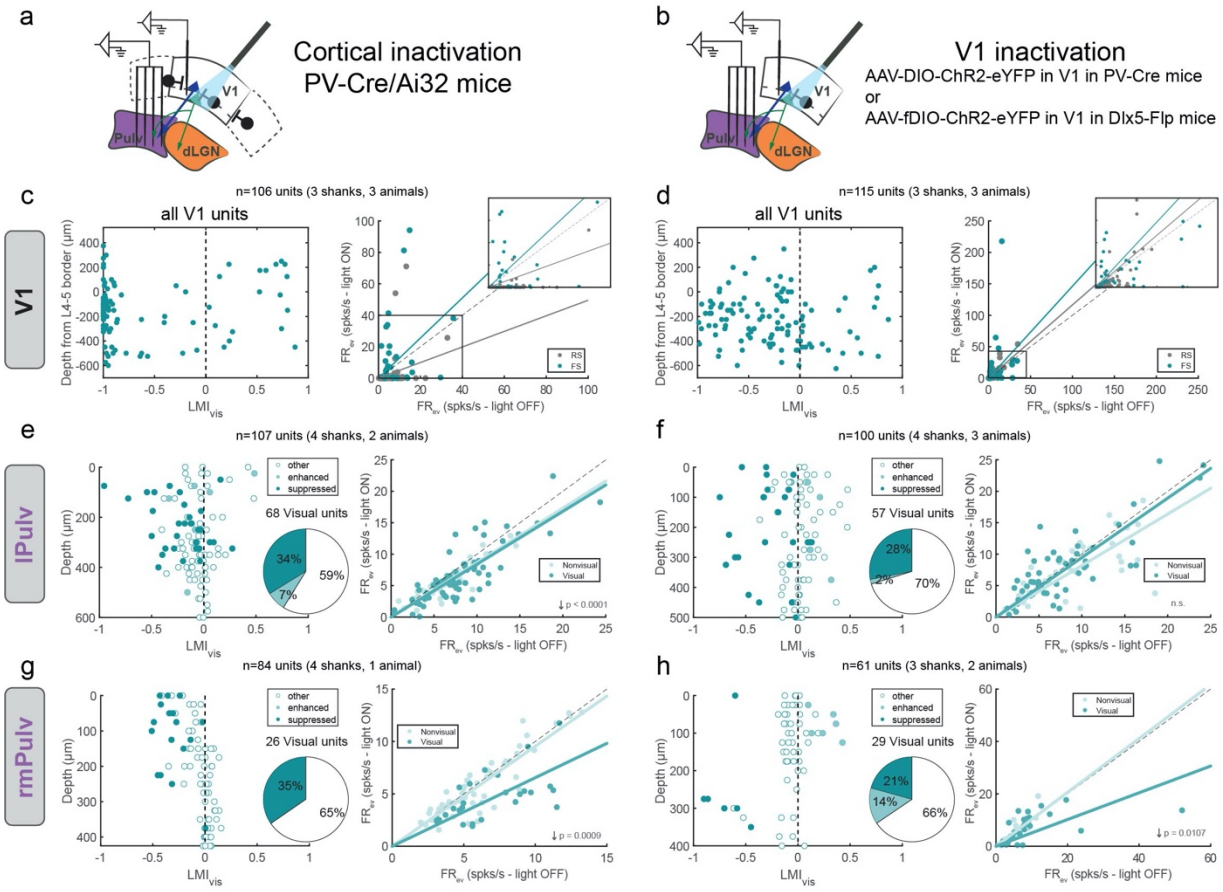

Figure 2.S10 Effects of V1 inactivation on pulvinar activity. a) Schematic of V1 inactivation experiments in PV-Cre/Ai32 mice. PV interneurons across the brain expressed ChR2, but blue LED stimulation was targeted just to V1. Cortical and thalamus recordings were conducted simultaneously. b) Schematic of V1 inactivation experiments in PV-Cre mice (with AAV-DIO-ChR2 injection in V1; n=2 animals) or Dlx5-Flp/CCK-Cre mice (with AAV-fDIO-ChR2 injection in V1; n=2 animals). c) V1 recordings in PV-Cre/Ai32 mice. Left: Light modulation indices of visually evoked activity (LMI_{vis}) of all V1 units by depth, relative to the end of L4. Right: Visually evoked firing rates (FR_{vis}) in light OFF versus light ON (V1 inactivated) conditions for putative fast-spiking (FS) and regular-spiking (RS) cells. Inset is a zoomed-in view of boxed area. d) Same as c) but for AAV-injected mice (V1 was not recorded from in one PV-Cre animal; hence n=3). e) lPulv recordings in PV-Cre/Ai32 mice. Left: LMI_{vis} values by depth for suppressed, enhanced and non-modulated ("other") units (classified on basis of their spontaneous activity, as in Figures 2.3 and 2.5). Inset: pie chart showing proportions of different unit types among all visually responsive units. Right: FR_{vis} in light OFF versus light ON (V1 inactivated) conditions for visual and non-visual cells. f) Same as e) but for lPulv units recorded in AAV-injected mice. g-h) Same as e-f) but for units recorded in rmPulv. P-values are from Wilcoxon signed-rank tests; arrows indicate the directions of significant modulations.

Figure 2.S11 Independent optogenetic control of halorhodopsin- and stGtACR2-expressing L6CT and L5CT cells with red and blue LEDs, respectively. a) Experimental schematic. Ntsr1-Cre (+) mice were injected with Cre-dependent halorhodopsin and Flp-dependent stGtACR2 (but AAVretro-Flp was NOT injected to pulvinar, so only halorhodopsin was expressed in L6CTs). Right: four different LED stimulation conditions (randomly interspersed). b) Example L6CT inactivated unit in V1. Left: raster plot, with trials organized by LED stimulation condition. Right: PSTH of average firing rates across visual trials. Grey shading indicates the period of LED stimulation. c) Visual LED modulation (LMI_{vis}) calculated from trials with both LEDs on (left), blue LED only (middle), and red LED only (right) trials. Colored units are those whose FRs were significantly suppressed by at least 50% in visual trials with both LEDs, and the dot outlined in pink is the example unit in b). d) Visually evoked firing rates of L6 inactivated cells in conditions with the blue LED alone compared to both LEDs together. Their FRs were largely unaffected by blue LED stimulation. e) Experimental schematic - same as a) except AAVretro-Flp was injected to the pulvinar, and injections were made in Ntsr1-Cre (-) mice, resulting in only L5CT expression of fDIO-stGtACR2. Right: four LED stimulation conditions. f) Example L5CT inactivated unit in V1. g) Same as c) but in a L5CT inactivation experiment, and colored dots are L5 inactivated units (outlined dot is the example unit in f)). h) Visually evoked firing rates of L5 inactivated cells in conditions with the red LED alone compared to both LEDs together. FRs were unaffected by red LED stimulation.

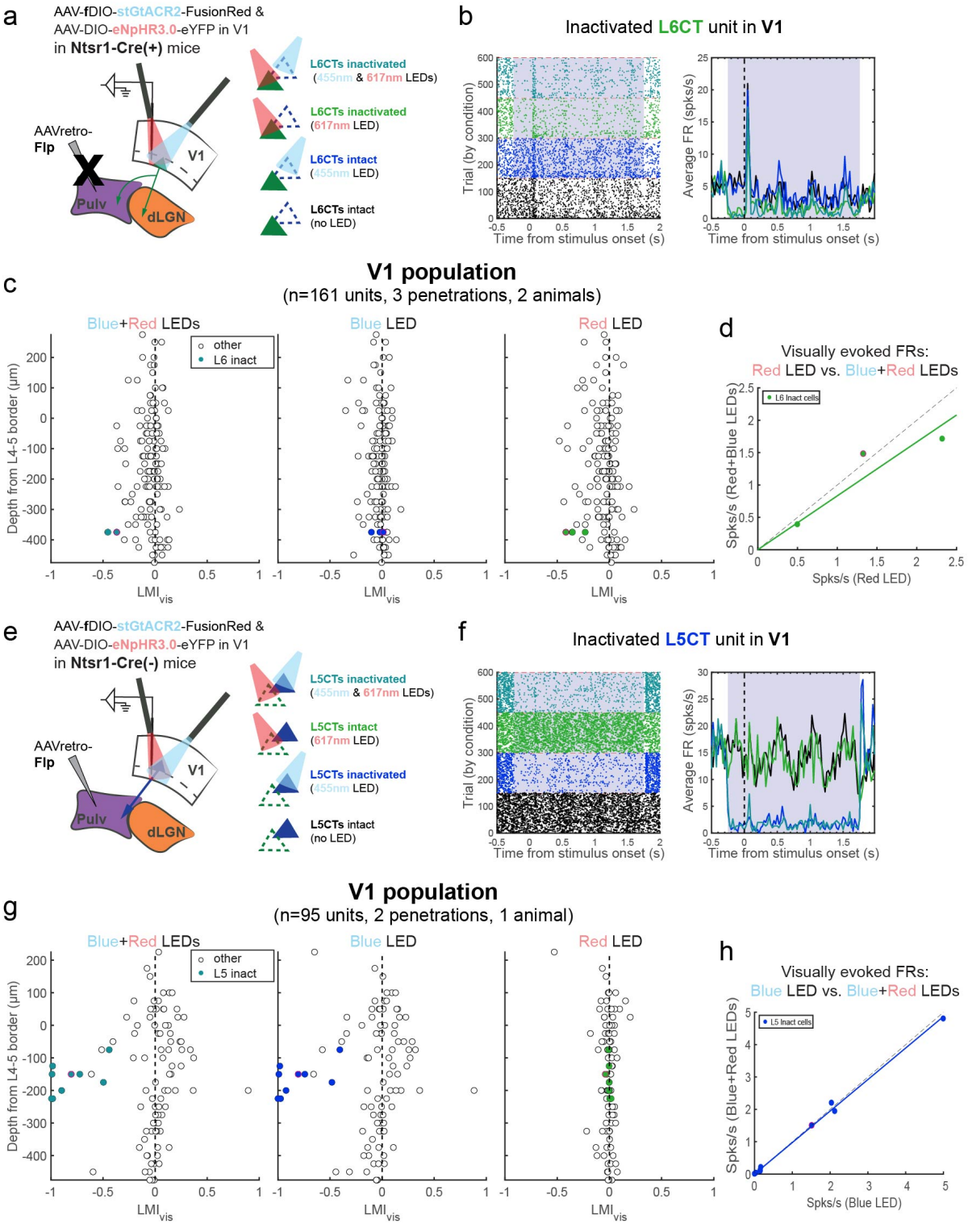
a
AAV-fDIO-stGtACR2-FusionRed &
AAV-DIO-eNpHR3.0-eYFP in V1
in Ntsr1-Cre(+) mice
AAVretro-
Flp
V1
Pulv
dLGN
L6CTs inactivated
(455nm & 617nm LEDs)
L6CTs inactivated
(617nm LED)
L6CTs intact
(455nm LED)
L6CTs intact
(no LED)
b
Inactivated L6CT unit in V1
Trial (by condition)
Time from stimulus onset (s)
Average FR (spks/s)
Time from stimulus onset (s)
c
V1 population
(n=161 units, 3 penetrations, 2 animals)
Blue+Red LEDs
Blue LED
Red LED
other
L6 inact
Depth from L4-5 border (μm)
LMIvis
d
Visually evoked FRs:
Red LED vs. Blue+Red LEDs
L6 Inact cells
Spks/s (Red+Blue LEDs)
Spks/s (Red LED)
e
AAV-fDIO-stGtACR2-FusionRed &
AAV-DIO-eNpHR3.0-eYFP in V1
in Ntsr1-Cre(-) mice
AAVretro-
Flp
V1
Pulv
dLGN
L5CTs inactivated
(455nm & 617nm LEDs)
L5CTs intact
(617nm LED)
L5CTs inactivated
(455nm LED)
L5CTs intact
(no LED)
f
Inactivated L5CT unit in V1
Trial (by condition)
Time from stimulus onset (s)
Average FR (spks/s)
Time from stimulus onset (s)
g
V1 population
(n=95 units, 2 penetrations, 1 animal)
Blue+Red LEDs
Blue LED
Red LED
other
L5 inact
Depth from L4-5 border (μm)
LMIvis
h
Visually evoked FRs:
Blue LED vs. Blue+Red LEDs
L5 Inact cells
Spks/s (Blue+Red LEDs)
Spks/s (Blue LED)

Figure 2.S12 Targeted ablation of V1 L5ETs or L6CTs does not impair visual activity in the visual thalamus. a) Experimental design of L6CT ablation. Left: in one hemisphere of Ntsr1-Cre mice, two AAVs - one encoding Cre-dependent GFP and the other encoding Cre-dependent diphtheria toxin (dtA) with non-Cre-dependent mCherry was injected into V1. This resulted in no L6CT GFP expression anywhere that the dtA virus spread, while the GFP virus spread further (likely due to the difference in AAV serotypes) and labeled L6CTs on the outskirts of the ablation zone. In V1 of the opposite hemisphere, the same Cre-dependent GFP virus was injected without the dtA virus (but with an equal volume of HBSS to attain the same dilution). Right: images of coronal sections containing V1 injection areas (top) and sections containing GFP+ axons in the visual thalamus (bottom). Notice that only in the dtA-injected hemisphere is there a considerable gap in GFP+ axons in the dLGN, indicating that L6CTs were successfully ablated. Scale bars = 1mm. b) Simultaneous V1 and thalamic recordings in L6CT-ablated mice. Visually evoked (middle) and spontaneous (right) firing rates of regular-spiking L6 V1 units in dtA experiments are depicted and compared to optogenetics experiments (L6 units from halorhodopsin and stGtACR2 experiments are combined). Boxplots depict medians and quartiles. There was a significant reduction in L6 visually evoked firing rates ($p=0.0132$), but not spontaneous firing rates ($p>0.3$) in dtA ablation experiments (Wilcoxon rank-sum tests). c) Overlayed RFs of simultaneous dLGN, lPulv, and V1 recordings from an example experiment. d-e) Example dLGN (d) and lPulv (e) units recorded in the same experiment as in c). These units exhibited robust visual responses to drifting gratings (left, raster plot; middle, PSTH of average FRs across all visual trials), even though they were retinotopically aligned with the recorded area of L6CT ablation (right; compare to V1 RFs in c). RF maps depict mean baseline-subtracted FRs for each ON stimulus position at the peak timepoint. f) L5ET ablation experimental design - same as a) but in Npr3-Cre mice. g) Same as b) but for L5 units in dtA versus optogenetic experiments. L5 spontaneous firing rates ($p=0.0005$), but not visually evoked firing rates ($p>0.1$), were significantly reduced in dtA experiments (Wilcoxon rank-sum tests), indicating successful L5ET ablation (because these cells have uniquely high spontaneous firing rates; see Figure 2.S3). h) Overlayed RFs from rmPulv, lPulv and V1, recorded simultaneously in the same example experiment. i-j) Same as d-e) but for example rmPulv (i) and lPulv (j) units recorded in the same L5ET dtA experiment as in h) whose RFs were aligned to the area of L5ET ablation yet maintained their visual responses. k) Left: Visually evoked firing rates of dLGN units recorded in L6CT dtA experiments compared to L6CT optogenetic inactivation experiments (halorhodopsin and stGtACR2 experiments combined). Dots are individual units. Right: percent of recorded dLGN units which were visually responsive in dtA versus optogenetic experiments. Circles/dots indicate individual animals. l) same as k) but for rmPulv recordings, comparing both L5ET and L6CT dtA and optogenetic inactivation experiments. m) Same as l) but for lPulv. ***$p<.001$, Kruskal-Wallis non-parametric tests with the Dunn–Šidák post-hoc test for multiple comparisons. No other comparisons were significant.

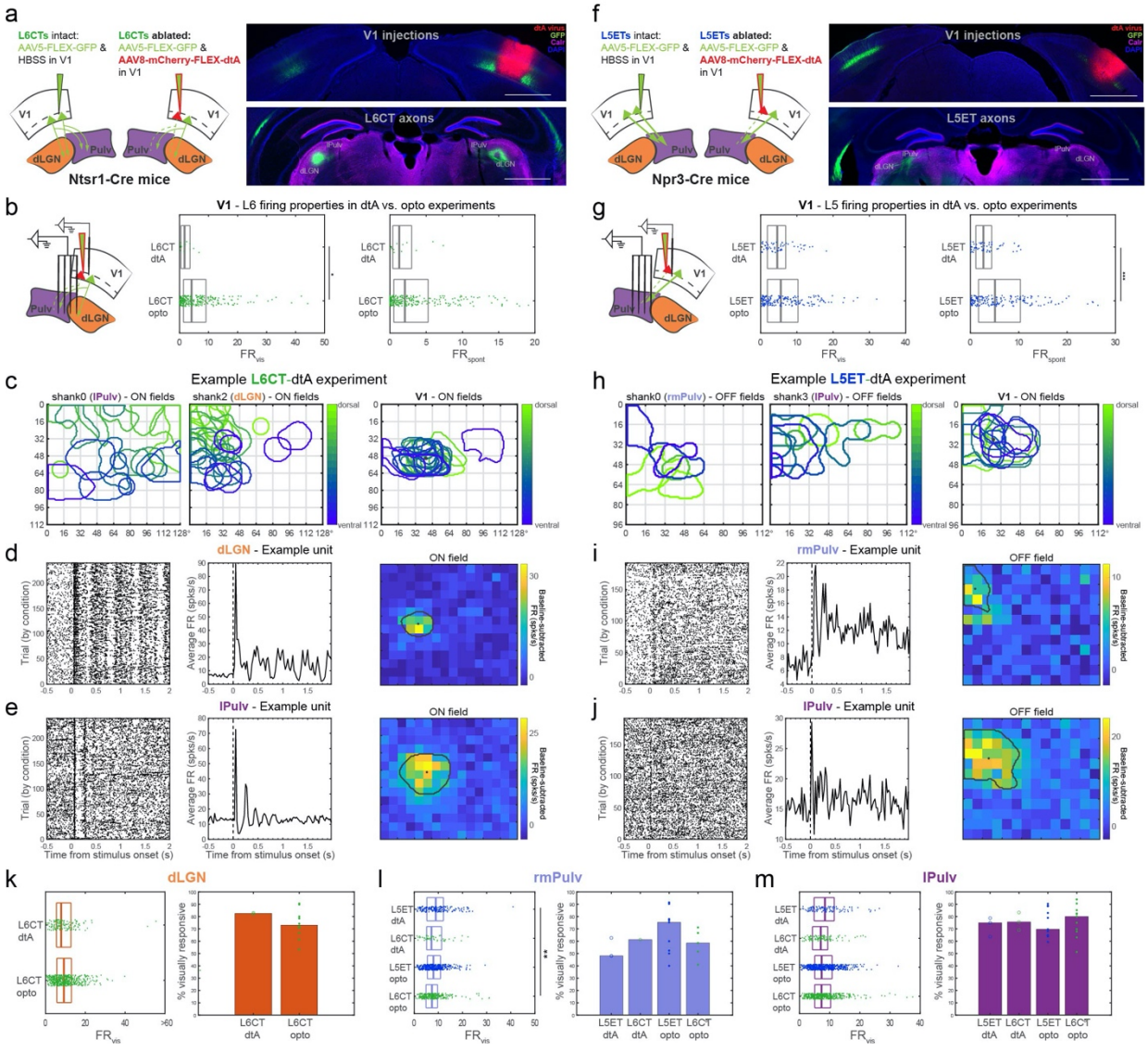
a
L6CTs intact:
AAV5-FLEX-GFP &
HBSS in V1
L6CTs ablated:
AAV5-FLEX-GFP &
AAV8-mCherry-FLEX-dtA
in V1
V1 injections
L6CT axons
Ntsr1-Cre mice
f
L5ETs intact:
AAV5-FLEX-GFP &
HBSS in V1
L5ETs ablated:
AAV5-FLEX-GFP &
AAV8-mCherry-FLEX-dtA
in V1
V1 injections
L5ET axons
Npr3-Cre mice
b
V1 - L6 firing properties in dtA vs. opto experiments
L6CT dtA
L6CT opto
g
V1 - L5 firing properties in dtA vs. opto experiments
L5ET dtA
L5ET opto
c
Example L6CT-dtA experiment
shank0 (lPulv) - ON fields
shank2 (dLGN) - ON fields
V1 - ON fields
h
Example L5ET-dtA experiment
shank0 (rmPulv) - OFF fields
shank3 (lPulv) - OFF fields
V1 - ON fields
d
dLGN - Example unit
ON field
i
rmPulv - Example unit
OFF field
e
lPulv - Example unit
ON field
j
lPulv - Example unit
OFF field
k
dLGN
l
rmPulv
m
lPulv

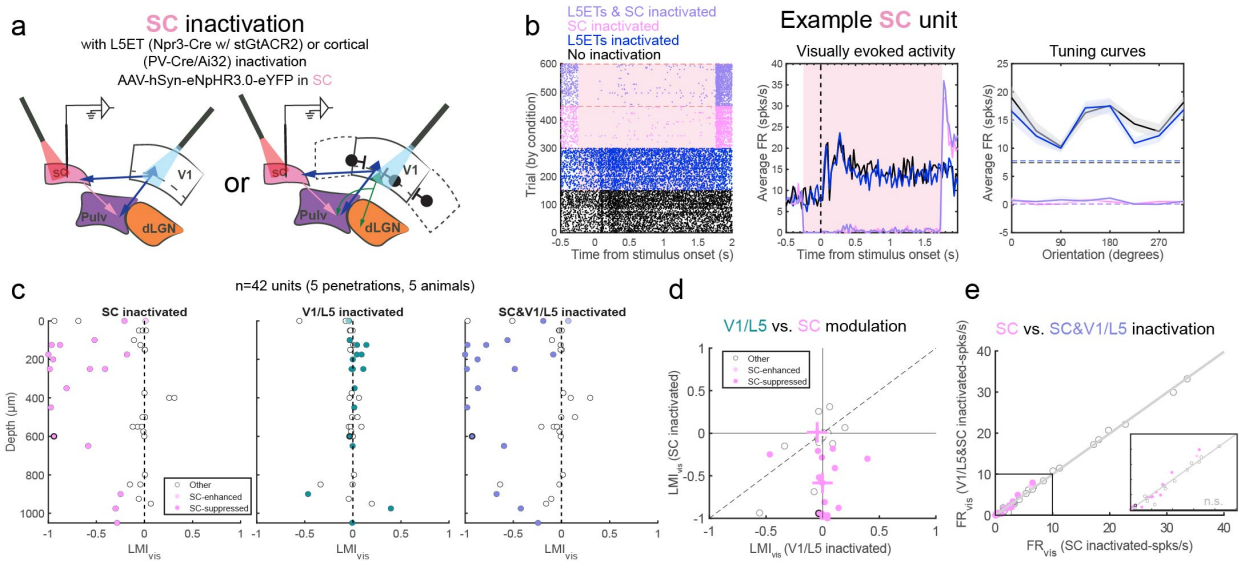

Figure 2.S13. Effective SC inactivation with non-specific halorhodopsin (with or without L5ET or cortical inactivation). a) Schematic of SC recordings with non-specific halorhodopsin expression for SC inactivation with a red LED. In addition, either L5ETs specifically (AAV-DIO-stGTACR2 injection in Npr3-Cre mice; n=3) or V1 non-specifically (in PV-Cre/Ai32 mice) were inactivated with a blue LED. b) An example unit recorded in the SC that was completely silenced by SC inactivation alone or together with L5ET inactivation, but not by L5ET inactivation alone. Left: raster plot of trials organized by LED stimulation condition. Middle: PSTH of average FRs across visual trials. Right: average FRs at each of eight drifting grating orientations under different LED stimulation conditions. Dotted lines indicate spontaneous FRs under different conditions. c) Light modulation indices of visually evoked activity (LMI_{vis}), calculated from trials with SC inactivation only (left), V1/L5 inactivation only (middle), or combined SC and V1/L5 inactivation (right), by recording depth. Colored dots indicate units whose spontaneous activity was significantly suppressed, enhanced, or unmodulated by SC inactivation alone. The outlined dot is the example unit from b). d) Units' LMI_{vis} in V1/L5 inactivation versus SC-only inactivation conditions. Units are colored as in c). Crosses indicate medians of each unit class. e) Visually evoked firing rates with SC inactivation alone compared to combined V1/L5 and SC inactivation. Inset: zoom of boxed region. Units are colored as in c-d). p's>0.8 for suppressed cells only or all cells combined; Wilcoxon signed-rank tests.

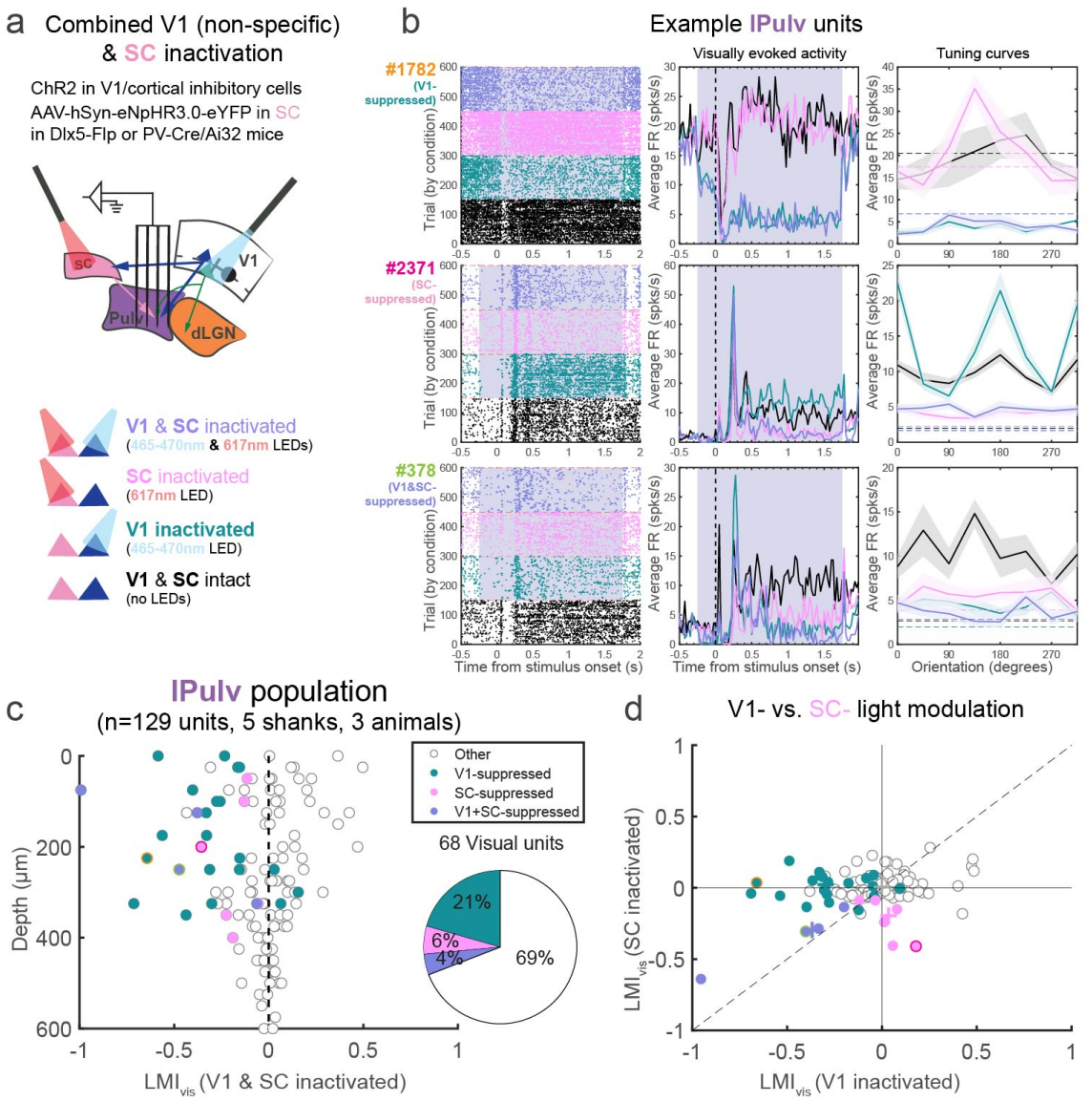

Figure 2.S14. Heterogeneous effects of V1 and SC inactivation in the lateral pulvinar. a) In vivo pulvinar recordings with dual-optogenetic inactivation of SC and V1 in Dlx5-Flp mice with AAV-fDIO-ChR2 in V1 (n=2) or in PV-Cre/Ai32 mice (n=1). Bottom: Different LED stimulation conditions. b) Three example lPulv units which were suppressed by V1 inactivation (top), SC inactivation (middle; but an increase in activity and tuning with V1 inactivated), or both (bottom). From left to right: raster plots of trials organized by LED stimulation conditions; PSTHs of average FRs across visual trials; and average FRs at each of eight drifting grating orientations under different LED stimulation conditions. Dotted lines in tuning curve plots indicate spontaneous FRs under different inactivation conditions. c) Light modulation of visually evoked activity (LMI_{vis}) from combined V1 & SC inactivation trials, by depth. Units are classified according to whether they were also significantly suppressed by SC inactivation, V1 inactivation, or both (see Methods for details). Color-outlined points correspond to example units in b). Right: proportion of different suppressed unit classes out of all visually responsive units. d) Units' light modulation of visually evoked activity (LMI_{vis}) in V1 inactivation versus by SC inactivation trials. Units are colored as in c). Units which fall in the lower left quadrant were inactivated by both V1 and SC inactivation. Crosses indicate medians of each unit class.

Acknowledgements

We thank Dr. Hongkui Zeng (Allen Institute) for informing us about and sharing the Npr3-IRES-Cre-neo line used in this study. This work was supported by NIH grants F31 EY028853 (M.A.K.), R01 MH063912 and R01 EY022577 (E.M.C.).

Chapter 2, in full, is currently being prepared for submission for publication and will include Alexis D. Franklin as a co-author and Professor Edward Callaway as the senior author. The dissertation author was the primary investigator and author of this material.

References

1. Halassa, M. M. & Sherman, S. M. Thalamocortical Circuit Motifs: A General Framework. *Neuron* **103**, 762–770 (2019).

2. Saalmann, Y. B., Pinsk, M. A., Wang, L., Li, X. & Kastner, S. The pulvinar regulates information transmission between cortical areas based on attention demands. *Science (New York, N.Y.)* **337**, 753–6 (2012).

3. Zhou, H., Schafer, R. & Desimone, R. Pulvinar-Cortex Interactions in Vision and Attention. *Neuron* **89**, 209–220 (2016).

4. Roth, M. M., Dahmen, J. C., Muir, D. R., Imhof, F., Martini, F. J. & Hofer, S. B. Thalamic nuclei convey diverse contextual information to layer 1 of visual cortex. *Nature neuroscience* **19**, 299–307 (2016).

5. Blot, A., Roth, M. M., Gasler, I. T., Javadzadeh, M., Imhof, F. & Hofer, S. B. Visual intracortical and transthalamic pathways carry distinct information to cortical areas. *Biorxiv* 2020.07.06.189902 (2020) doi:10.1101/2020.07.06.189902.

6. Sherman, S. M. Thalamus plays a central role in ongoing cortical functioning. *Nature Neuroscience* **16**, (2016).

7. Bickford, M. E. Thalamic Circuit Diversity: Modulation of the Driver/Modulator Framework. *Frontiers in neural circuits* **9**, 86 (2015).

8. Sherman, S. M. & Guillery, R. W. Functional organization of thalamocortical relays. *Journal of neurophysiology* **76**, 1367–95 (1996).

9. Sherman, S. M. & Guillery, R. W. On the actions that one nerve cell can have on another: Distinguishing "drivers" from "modulators." *Proceedings of the National Academy of Sciences* **95**, 7121–6 (1998).

10. Cleland, B. G., Dubin, M. W. & Levick, W. R. Sustained and transient neurones in the cat's retina and lateral geniculate nucleus. *The Journal of physiology* **217**, 473–96 (1971).

11. Usrey, W. M., Reppas, J. B. & Reid, R. C. Specificity and strength of retinogeniculate connections. *Journal of neurophysiology* **82**, 3527–40 (1999).

12. Briggs, F. & Usrey, W. M. Emerging views of corticothalamic function. *Current opinion in neurobiology* **18**, 403–7 (2008).

13. Reichova, I. & Sherman, S. M. Somatosensory corticothalamic projections: distinguishing drivers from modulators. *Journal of neurophysiology* **92**, 2185–97 (2004).

14. Li, J., Guido, W. & Bickford, M. E. Two distinct types of corticothalamic EPSPs and their contribution to short-term synaptic plasticity. *Journal of neurophysiology* **90**, 3429–40 (2003).

15. Li, J., Wang, S. & Bickford, M. E. Comparison of the ultrastructure of cortical and retinal terminals in the rat dorsal lateral geniculate and lateral posterior nuclei. *The Journal of comparative neurology* **460**, 394–409 (2003).

16. Bourassa, J. & Deschênes, M. Corticothalamic projections from the primary visual cortex in rats: a single fiber study using biocytin as an anterograde tracer. *Neuroscience* **66**, 253–63 (1995).

17. Rockland, K. S. Two types of corticopulvinar terminations: round (type 2) and elongate (type 1). *The Journal of comparative neurology* **368**, 57–87 (1996).

18. Mathers, L. H. The synaptic organization of the cortical projection to the pulvinar of the squirrel monkey. *Journal of Comparative Neurology* **146**, 43–59 (1972).

19. Sherman, S. M. & Guillery, R. W. The role of the thalamus in the flow of information to the cortex. *Philosophical Transactions Royal Soc Lond Ser B Biological Sci* **357**, 1695–1708 (2002).

20. Kirchgessner, M. A., Franklin, A. D. & Callaway, E. M. Context-dependent and dynamic functional influence of corticothalamic pathways to first- and higher-order visual thalamus. *Proc National Acad Sci* 202002080 (2020) doi:10.1073/pnas.2002080117.

21. Crandall, S. R., Cruikshank, S. J. & Connors, B. W. A corticothalamic switch: controlling the thalamus with dynamic synapses. *Neuron* **86**, 768–82 (2015).

22. Born, G., Erisken, S., Schneider, F. A., Klein, A., Mobarhan, M. H., Lao, C. L., Spacek, M. A., Einevoll, G. T. & Busse, L. Corticothalamic feedback sculpts visual spatial integration in mouse thalamus. *Biorxiv* 2020.05.19.104000 (2020) doi:10.1101/2020.05.19.104000.

23. Guo, W., Clause, A. R., Barth-Maron, A. & Polley, D. B. A Corticothalamic Circuit for Dynamic Switching between Feature Detection and Discrimination. *Neuron* **95**, 180-194.e5 (2017).

24. Wang, S., Eisenback, M. A. & Bickford, M. E. Relative distribution of synapses in the pulvinar nucleus of the cat: implications regarding the "driver/modulator" theory of thalamic function. *The Journal of comparative neurology* **454**, 482–94 (2002).

25. Horn, S. C. V. & Sherman, S. M. Fewer driver synapses in higher order than in first order thalamic relays. *Neuroscience* **146**, 463–70 (2007).

26. Horn, S. C. V., Erişir, A. & Sherman, S. M. Relative distribution of synapses in the A-laminae of the lateral geniculate nucleus of the cat. *The Journal of comparative neurology* **416**, 509–20 (2000).

27. Beltramo, R. & Scanziani, M. A collicular visual cortex: Neocortical space for an ancient midbrain visual structure. *Science* **363**, 64–69 (2019).

28. Bennett, C., Gale, S. D., Garrett, M. E., Newton, M. L., Callaway, E. M., Murphy, G. J. & Olsen, S. R. Higher-Order Thalamic Circuits Channel Parallel Streams of Visual Information in Mice. *Neuron* **102**, 477-492.e5 (2019).

29. Casanova, C. & Molotchnikoff, S. Influence of the superior colliculus on visual responses of cells in the rabbit's lateral posterior nucleus. *Experimental brain research* **80**, 387–96 (1990).

30. Zhou, N. A., Maire, P. S., Masterson, S. P. & Bickford, M. E. The mouse pulvinar nucleus: Organization of the tectorecipient zones. *Visual neuroscience* **34**, E011 (2017).

31. Mease, R. A., Sumser, A., Sakmann, B. & Groh, A. Cortical Dependence of Whisker Responses in Posterior Medial Thalamus In Vivo. *Cerebral Cortex* **26**, 3534–3543 (2016).

32. Casanova, C., Savard, T. & Darveau, S. Contribution of Area 17 to Cell Responses in the Striate-recipient Zone of the Cat's Lateral Posterior-Pulvinar Complex. *Eur J Neurosci* **9**, 1026–1036 (1997).

33. Bender, D. B. Visual activation of neurons in the primate pulvinar depends on cortex but not colliculus. *Brain Research* **279**, 258–261 (1983).

34. Diamond, M. E., Armstrong-James, M., Budway, M. J. & Ebner, F. F. Somatic sensory responses in the rostral sector of the posterior group (POm) and in the ventral posterior medial nucleus (VPM) of the rat thalamus: Dependence on the barrel field cortex. *J Comp Neurol* **319**, 66–84 (1992).

35. Scholl, L. R., Foik, A. T. & Lyon, D. C. Projections between visual cortex and pulvinar in the rat. *J Comp Neurol* (2020) doi:10.1002/cne.24937.

36. Souza, B. O. F. de, Frigon, É., Tremblay-Laliberté, R., Casanova, C. & Boire, D. Laminar distribution of cortical projection neurons to the pulvinar: A comparative study in cats and mice. *J Comp Neurol* (2020) doi:10.1002/cne.25072.

37. Tervo, D. G., Hwang, B.-Y. Y., Viswanathan, S., Gaj, T., Lavzin, M., Ritola, K. D., Lindo, S., Michael, S., Kuleshova, E., Ojala, D., Huang, C.-C. C., Gerfen, C. R., Schiller, J., Dudman, J. T., Hantman, A. W., Looger, L. L., Schaffer, D. V. & Karpova, A. Y. A Designer AAV Variant Permits Efficient Retrograde Access to Projection Neurons. *Neuron* **92**, 372–382 (2016).

38. Gong, S., Doughty, M., Harbaugh, C. R., Cummins, A., Hatten, M. E., Heintz, N. & Gerfen, C. R. Targeting Cre recombinase to specific neuron populations with bacterial artificial chromosome constructs. *The Journal of neuroscience : the official journal of the Society for Neuroscience* **27**, 9817–23 (2007).

39. Olsen, S. R., Bortone, D. S., Adesnik, H. & Scanziani, M. Gain control by layer six in cortical circuits of vision. *Nature* **483**, 47–52 (2012).

40. Bortone, D. S., Olsen, S. R. & Scanziani, M. Translaminar inhibitory cells recruited by layer 6 corticothalamic neurons suppress visual cortex. *Neuron* **82**, 474–85 (2014).

41. Tasic, B., Yao, Z., Graybuck, L. T., Smith, K. A., Nguyen, T. N., Bertagnolli, D., Goldy, J., Garren, E., Economo, M. N., Viswanathan, S., Penn, O., Bakken, T., Menon, V., Miller, J., Fong, O., Hirokawa, K. E., Lathia, K., Rimorin, C., Tieu, M., Larsen, R., Casper, T., Barkan, E., Kroll, M., Parry, S., Shapovalova, N. V., Hirschstein, D., Pendergraft, J., Sullivan, H. A., Kim, T. K., Szafer, A., Dee, N., Groblewski, P., Wickersham, I., Cetin, A., Harris, J. A., Levi, B. P., Sunkin, S. M., Madisen, L., Daigle, T. L., Looger, L., Bernard, A., Phillips, J., Lein, E., Hawrylycz, M., Svoboda, K., Jones, A. R., Koch, C. & Zeng, H. Shared and distinct transcriptomic cell types across neocortical areas. *Nature* **563**, 72–78 (2018).

42. Harris, J. A., Mihalas, S., Hirokawa, K. E., Whitesell, J. D., Choi, H., Bernard, A., Bohn, P., Caldejon, S., Casal, L., Cho, A., Feiner, A., Feng, D., Gaudreault, N., Gerfen, C. R., Graddis, N.,

Groblewski, P. A., Henry, A. M., Ho, A., Howard, R., Knox, J. E., Kuan, L., Kuang, X., Lecoq, J., Lesnar, P., Li, Y., Luviano, J., McConoughey, S., Mortrud, M. T., Naeemi, M., Ng, L., Oh, S. W., Ouellette, B., Shen, E., Sorensen, S. A., Wakeman, W., Wang, Q., Wang, Y., Williford, A., Phillips, J. W., Jones, A. R., Koch, C. & Zeng, H. Hierarchical organization of cortical and thalamic connectivity. *Nature* **575**, 195–202 (2019).

43. Daigle, T. L., Madisen, L., Hage, T. A., Valley, M. T., Knoblich, U., Larsen, R. S., Takeno, M. M., Huang, L., Gu, H., Larsen, R., Mills, M., Bosma-Moody, A., Siverts, L. A., Walker, M., Graybuck, L. T., Yao, Z., Fong, O., Nguyen, T. N., Garren, E., Lenz, G. H., Chavarha, M., Pendergraft, J., Harrington, J., Hirokawa, K. E., Harris, J. A., Nicovich, P. R., McGraw, M. J., Ollerenshaw, D. R., Smith, K. A., Baker, C. A., Ting, J. T., Sunkin, S. M., Lecoq, J., Lin, M. Z., Boyden, E. S., Murphy, G. J., Costa, N. M. da, Waters, J., Li, L., Tasic, B. & Zeng, H. A Suite of Transgenic Driver and Reporter Mouse Lines with Enhanced Brain-Cell-Type Targeting and Functionality. *Cell* **174**, 465-480.e22 (2018).

44. Du, J., Blanche, T. J., Harrison, R. R., Lester, H. A. & Masmanidis, S. C. Multiplexed, high density electrophysiology with nanofabricated neural probes. *PloS one* **6**, e26204 (2011).

45. Vélez-Fort, M., Rousseau, C. V., Niedworok, C. J., Wickersham, I. R., Rancz, E. A., Brown, A. P., Strom, M. & Margrie, T. W. The stimulus selectivity and connectivity of layer six principal cells reveals cortical microcircuits underlying visual processing. *Neuron* **83**, 1431–43 (2014).

46. Kato, N. Cortico-thalamo-cortical projection between visual cortices. *Brain Res* **509**, 150–152 (1990).

47. Theyel, B. B., Llano, D. A. & Sherman, S. M. The corticothalamocortical circuit drives higher-order cortex in the mouse. *Nature neuroscience* **13**, 84–8 (2010).

48. Rouiller, E. M. & Welker, E. A comparative analysis of the morphology of corticothalamic projections in mammals. *Brain Research Bulletin* **53**, 727–41 (2000).

49. Allen, A. E., Procyk, C. A., Howarth, M., Walmsley, L. & Brown, T. M. Visual input to the mouse lateral posterior and posterior thalamic nuclei: photoreceptive origins and retinotopic order. *The Journal of Physiology* **594**, 1911–29 (2016).

50. Baldwin, M. K. L. K., Balaram, P. & Kaas, J. H. The evolution and functions of nuclei of the visual pulvinar in primates. *The Journal of comparative neurology* **525**, 3207–3226 (2017).

51. Juavinett, A. L., Kim, E. J., Collins, H. C. & Callaway, E. M. A systematic topographical relationship between mouse lateral posterior thalamic neurons and their visual cortical projection targets. *The Journal of comparative neurology* **528**, 95–107 (2020).

52. Tohmi, M., Meguro, R., Tsukano, H., Hishida, R. & Shibuki, K. The extrageniculate visual pathway generates distinct response properties in the higher visual areas of mice. *Current biology : CB* **24**, 587–97 (2014).

53. Chalupa, L., Williams, R. & Hughes, M. Visual response properties in the tectorecipient zone of the cat's lateral posterior-pulvinar complex: a comparison with the superior colliculus. *Journal of Neuroscience* **3**, 2587–96 (1983).

54. Mahn, M., Gibor, L., Patil, P., Malina, K. C.-K., Oring, S., Printz, Y., Levy, R., Lampl, I. & Yizhar, O. High-efficiency optogenetic silencing with soma-targeted anion-conducting channelrhodopsins. *Nat Commun* **9**, 4125 (2018).

55. Wiegert, J. S., Mahn, M., Prigge, M., Printz, Y. & Yizhar, O. Silencing Neurons: Tools, Applications, and Experimental Constraints. *Neuron* **95**, 504–529 (2017).

56. Masterson, S. P., Li, J. & Bickford, M. E. Frequency-dependent release of substance P mediates heterosynaptic potentiation of glutamatergic synaptic responses in the rat visual thalamus. *Journal of neurophysiology* **104**, 1758–67 (2010).

57. Masterson, S. P., Li, J. & Bickford, M. E. Synaptic organization of the tectorecipient zone of the rat lateral posterior nucleus. *Journal of Comparative Neurology* **515**, 647–63 (2009).

58. Rovó, Z., Ulbert, I. & Acsády, L. Drivers of the Primate Thalamus. *The Journal of Neuroscience* **32**, 17894–908 (2012).

59. Briggs, F. Role of Feedback Connections in Central Visual Processing. *Annu Rev Vis Sc* **6**, 1–22 (2020).

60. Bienkowski, M. S., Benavidez, N. L., Wu, K., Gou, L., Becerra, M. & Dong, H. Extrastriate connectivity of the mouse dorsal lateral geniculate thalamic nucleus. *J Comp Neurol* **527**, 1419–1442 (2019).

61. Durand, S., Iyer, R., Mizuseki, K., Vries, S. de, Mihalas, S. & Reid, C. R. A Comparison of Visual Response Properties in the Lateral Geniculate Nucleus and Primary Visual Cortex of Awake and Anesthetized Mice. *Journal of Neuroscience* **36**, 12144–12156 (2016).

62. Ansorge, J., Humanes-Valera, D., Pauzin, F. P., Schwarz, M. K. & Krieger, P. Cortical layer 6 control of sensory responses in higher-order thalamus. *J Physiology* **598**, (2020).

63. Hoerder-Suabedissen, A., Hayashi, S., Upton, L., Nolan, Z., Casas-Torremocha, D., Grant, E., Viswanathan, S., Kanold, P. O., Clasca, F., Kim, Y. & Molnár, Z. Subset of Cortical Layer 6b Neurons Selectively Innervates Higher Order Thalamic Nuclei in Mice. *Cerebral cortex (New York, N.Y. : 1991)* **28**, 1882–1897 (2018).

64. Leopold, D. A. Primary Visual Cortex: Awareness and Blindsight*. *Neuroscience* **35**, 91–109 (2012).

65. Kim, E. J., Juavinett, A. L., Kyubwa, E. M., Jacobs, M. W. & Callaway, E. M. Three Types of Cortical Layer 5 Neurons That Differ in Brain-wide Connectivity and Function. *Neuron* **88**, 1253–1267 (2015).

66. Halassa, M. M. & Acsády, L. Thalamic Inhibition: Diverse Sources, Diverse Scales. *Trends in neurosciences* **39**, 680–693 (2016).

67. Bokor, H., Frère, S. G., Eyre, M. D., Slézia, A., Ulbert, I., Lüthi, A. & Acsády, L. Selective GABAergic control of higher-order thalamic relays. *Neuron* **45**, 929–40 (2005).

68. Barthó, P., Freund, T. F. & Acsády, L. Selective GABAergic innervation of thalamic nuclei from zona incerta. *The European journal of neuroscience* **16**, 999–1014 (2002).

69. Benedek, G., Norita, M. & Creutzfeldt, O. D. Electrophysiological and anatomical demonstration of an overlapping striate and tectal projection to the lateral posterior-pulvinar complex of the cat. *Exp Brain Res* **52**, 157–169 (1983).

70. Raczkowski, D. & Diamond, I. T. Projections from the superior colliculus and the neocortex to the pulvinar nucleus in Galago. *The Journal of comparative neurology* **200**, 231–54 (1981).

71. Lund, J. S., Lund, R. D., Hendrickson, A. E., Bunt, A. H. & Fuchs, A. F. The origin of efferent pathways from the primary visual cortex, area 17, of the macaque monkey as shown by retrograde transport of horseradish peroxidase. *Journal of Comparative Neurology* **164**, 287–303 (1975).

72. Conley, M. & Raczkowski, D. Sublaminar organization within layer VI of the striate cortex in Galago. *The Journal of comparative neurology* **302**, 425–36 (1990).

73. Moore, B., Li, K., Kaas, J. H., Liao, C., Boal, A. M., Mavity-Hudson, J. & Casagrande, V. Cortical projections to the two retinotopic maps of primate pulvinar are distinct. *Journal of Comparative Neurology* **527**, 577–588 (2019).

74. Groh, A., Bokor, H., Mease, R. A., Plattner, V. M., Hangya, B., Stroh, A., Deschenes, M. & Acsády, L. Convergence of Cortical and Sensory Driver Inputs on Single Thalamocortical Cells. *Cerebral Cortex* **24**, 3167–79 (2014).

75. Krauzlis, R. J., Lovejoy, L. P. & Zénon, A. Superior Colliculus and Visual Spatial Attention. *Neuroscience* **36**, 165–182 (2013).

76. Phillips, J. W., Schulmann, A., Hara, E., Winnubst, J., Liu, C., Valakh, V., Wang, L., Shields, B. C., Korff, W., Chandrashekar, J., Lemire, A. L., Mensh, B., Dudman, J. T., Nelson, S. B. & Hantman, A. W. A repeated molecular architecture across thalamic pathways. *Nature Neuroscience* **22**, 1925–1935 (2019).

77. Yang, L., Lee, K., Villagracia, J. & Masmanidis, S. C. Open source silicon microprobes for high throughput neural recording. *J Neural Eng* **17**, 016036 (2020).

78. Siegle, J. H., López, A. C., Patel, Y. A., Abramov, K., Ohayon, S. & Voigts, J. Open Ephys: an open-source, plugin-based platform for multichannel electrophysiology. *J Neural Eng* **14**, 045003 (2017).

79. Pachitariu, M., Steinmetz, N., Kadir, S., Carandini, M. & D., H. K. Kilosort: realtime spike-sorting for extracellular electrophysiology with hundreds of channels. *Biorxiv* 061481 (2016) doi:10.1101/061481.

80. Rossant, C., Kadir, S. N., Goodman, D. F., Schulman, J., Hunter, M. L., Saleem, A. B., Grosmark, A., Belluscio, M., Denfield, G. H., Ecker, A. S., Tolias, A. S., Solomon, S., Buzsáki, G., Carandini, M. & Harris, K. D. Spike sorting for large, dense electrode arrays. *Nature neuroscience* **19**, 634–41 (2016).

81. Schmitzer-Torbert, N., Jackson, J., Henze, D., Harris, K. & Redish, A. D. Quantitative measures of cluster quality for use in extracellular recordings. *Neuroscience* **131**, 1–11 (2005).

82. Pettersen, K. H., Devor, A., Ulbert, I., Dale, A. M. & Einevoll, G. T. Current-source density estimation based on inversion of electrostatic forward solution: Effects of finite extent of neuronal activity and conductivity discontinuities. *J Neurosci Meth* **154**, 116–133 (2006).

83. Niell, C. M. & Stryker, M. P. Modulation of visual responses by behavioral state in mouse visual cortex. *Neuron* **65**, 472–9 (2010).

84. Erisken, S., Vaiceliunaite, A., Jurjut, O., Fiorini, M., Katzner, S. & Busse, L. Effects of locomotion extend throughout the mouse early visual system. *Current biology : CB* **24**, 2899–907 (2014).

85. Frandolig, J., Matney, C., Lee, K., Kim, J., Chevée, M., Kim, S.-J., Bickert, A. & Brown, S. The Synaptic Organization of Layer 6 Circuits Reveals Inhibition as a Major Output of a Neocortical Sublamina. *Cell Reports* **28**, 3131-3143.e5 (2019).

General Discussion

This dissertation has explored the roles of different corticothalamic (CT) neuron populations of the primary visual cortex (V1) in shaping activity and visual response properties in the visual thalamus. In Chapter 1, we found that optogenetically stimulating L6CTs had very similar effects on single-unit activity recorded in the dLGN (FO visual thalamus) and pulvinar (HO) of awake mice. Yet, we also found that L6CT influence is highly dynamic and sensitive to the degree and manner of their stimulation in both nuclei. This highlights the flexible, diverse and fundamentally "modulatory" roles that L6CTs play in both FO and HO thalamus. In Chapter 2, we further explored the endogenous, putatively modulatory functions of these L6CTs, as well as of L5CT neurons that project to HO, but not FO, thalamus. By using inhibitory optogenetics with different transgenic mouse lines to selectively inactivate these different CT populations in V1, we found that the L5CT pathway specifically is important for visual responses recorded from individual neurons of the pulvinar in awake mice. L6CTs sometimes contributed to neurons' baseline activity levels but not visual response properties in either the dLGN or pulvinar. This provides the first evidence *in vivo* of distinct "driving" versus "modulatory" functions of L5CT versus L6CT projections to a HO thalamic nucleus, which have been proposed for decades but never conclusively shown. Altogether, these findings elucidate how V1 influences and communicates with the visual thalamus by way of functionally distinct CT channels and highlight important organizational principles of CT pathways that likely extend to other systems and species.

L6CT "modulatory" pathways to FO and HO thalamus

Our results presented in Chapter 1 demonstrate a fundamental, functional similarity between L6CT pathways to FO and HO thalamic nuclei, but also highlight the complex influences those projections can have in both areas. Specifically, continuous optogenetic activation of L6CTs dramatically suppressed both spontaneous and visually evoked activity in the dLGN and the pulvinar, yet temporally controlled stimulation at 10Hz resulted in powerfully facilitated spiking in both areas. These results demonstrate the dynamic, frequency-dependent nature of L6CT pathways, which is very similar to what

has been described in the somatosensory system in vitro[1]. Our results also suggest that the thalamic reticular nucleus (TRN) plays a central role in that flexibility, mediating a dynamic inhibitory route from cortical L6 to the dLGN and pulvinar that runs in parallel to direct L6CT excitation. These monosynaptic excitatory and disynaptic inhibitory pathways thus appear to be in careful balance with one another, and a variety of factors – the manner and degree by which L6CTs are activated, short-term plasticity characteristics of different synapses, intrinsic properties of thalamic neurons, and likely more – can lead their balance to shift in favor of excitation or inhibition under different circumstances.

While Chapter 1 explored L6CT function with optogenetic activation, the optogenetic *in*activation experiments featured in Chapter 2 may seem to paint a somewhat different picture of how L6CTs normally influence thalamic activity. Even though the specific effects of L6CT activation differed considerably depending on whether we used controlled (10Hz) or uncontrolled (continuous) stimulation, their effects on thalamic activity were quite strong in both cases. In fact, 10Hz L6CT stimulation elicited robust and facilitating spiking responses, almost as though L6CT projections were "driving" thalamic activity (Figure 1.2). Yet, in Chapter 2, L6CT inactivation had neither strong suppressive nor facilitatory effects on visual activity in the dLGN or pulvinar; instead, effects were largely limited to suppressed baseline activity in a subset of thalamic (mainly dLGN) neurons (Figure 2.3).

While these results may seem contradictory on their face, they are in fact quite complimentary and together support the notion that L6CT projections form a fundamentally modulatory CT pathway. Optogenetic stimulation, though artificial, is useful for assessing what effects a particular neuronal population *can* have. It does not, however, show what that population *actually* does under normal circumstances. For that, optogenetic inactivation is needed to assess the necessity of a neuronal population for a particular function. Our optogenetic L6CT stimulation experiments thus demonstrate the capabilities of these projections; they can bi-directionally excite or suppress their thalamic targets through direct excitation (since they are glutamatergic) or indirect inhibition (through the GABAergic TRN). However, Chapter 2 demonstrates that neither those excitatory nor inhibitory influences are *necessary* for visual activity in either the dLGN or the pulvinar and are therefore fundamentally modulatory.

Since L6CTs can have dynamic, context-dependent effects but are apparently not required for conveying visual information to the thalamus, what functions do they serve? This is the essential next question in the study of L6CT influence, and one that is already the focus of much ongoing research. To date, L6CT feedback to FO thalamus has been implicated in a variety of modulatory functions, such as spatiotemporal precision of visual activity[2,3], controlling the "burst" versus "tonic" firing mode of thalamic neurons[4,5], sensory adaption[6], surround suppression[7], shifting between distinct modes of sensory detection or discrimination depending on behavioral demands[8], and more. Many of these proposed functions critically involve both monosynaptic excitation and disynaptic inhibition through TRN. For example, a recent study implicating L6CTs in dLGN surround suppression found that whereas L6CT excitation of dLGN neurons was retinotopically precise – consistent with our own observations with L6CT inactivation (Figure 2.4) – TRN neurons had larger receptive fields and were not surround-suppressed[7]. Since L6CT stimulation suppressed rather than facilitated dLGN neurons that were retinotopically mismatched, spatially precise excitation combined with spatially broad recruitment of inhibition from TRN is a likely circuit mechanism for surround suppression in the dLGN[7]. This may help explain why continuous optogenetic L6CT stimulation primarily suppressed both dLGN and pulvinar activity in Chapter 1; since many L6CTs with different receptive fields were likely activated by our optogenetics approach, surround suppression may have masked whatever excitatory effects we might have seen with more restricted L6CT stimulation (and in fact, we did observe some spatially clustered facilitatory effects in the dLGN in particular, Figure 1.1 – likely corresponding to those thalamic neurons which were directly excited by our stimulated L6CTs).

While L6CT inactivation did not significantly affect visually evoked activity in our study, we did observe a pronounced, suppressive effect on spontaneous activity in retinotopically aligned dLGN neurons. Even though this is consistent with the notion that L6CTs exert topographically precise excitation, a role for L6CTs in baseline activity levels has not often been described. This may be due to the fact that the vast majority of prior studies on L6CT feedback were conducted under anesthesia, which considerably depletes spontaneous thalamic activity[9,10]. While our observed effects on baseline activity

are somewhat surprising, especially given L6CTs notoriously low spontaneous firing rates (Figure 2.S3), one of L6CTs' distinguishing characteristics is the prevalence of their synapses and high degree of convergence in the thalamus[11–13]. These features could lead to a cumulative effect on baseline activity levels. This might also explain why effects on spontaneous activity were more pronounced in the dLGN than in the pulvinar, as the latter receives a smaller proportion of its total L6CT input from V1 specifically (and a larger proportion from other cortical areas)[14]. As further validation, effects of L6CT inactivation on spontaneous dLGN activity were also reported in another recent study with awake mice[7], and we made similar observations in multiple independent sets of experiments (L6CT-halorhodopsin, Figure 2.3; V1-inactivation, Figure 2.S5; L6CT-stGtACR2, Figure 2.S10). Especially in light of recent reports that anesthesia reduces activity levels in deep-layer cortical neurons[15], an interesting question for future study is how V1 L6CTs themselves are impacted by anesthesia and whether they might directly contribute to some of the brain state-dependent differences in spontaneous activity that have been observed in the thalamus.

Along similar lines, whether L6CTs might provide other non-visual signals to thalamic processing is another fascinating area of ongoing investigation. For instance, L6CTs have been shown to exhibit increased activity in states of arousal[16]. Given our findings of their facilitating influence on thalamic spiking when stimulated at 10Hz – which is a physiologically plausible activity level in the presence of their preferred visual stimulus (Figure 2.S3) and/or during arousal[16] – it is feasible that the L6CT pathway could enhance the gain of thalamic responses to incoming sensory inputs (i.e., through the driving pathways) during heightened brain states. Although arousal (at least as measured by running) does not fully account for the modulatory effects of L6CT inactivation on dLGN activity (e.g., bursting, response reliability, etc.), the effects of each are remarkably similar and thus may engage similar mechanisms[5]. Additionally, the possibility has been raised that the L6CT pathway is poised to convey behaviorally relevant motor signals to the thalamus. L6CTs in the auditory cortex were found to increase activity levels in advance of task-relevant orofacial movements (but not running) and receive direct inputs from subcortical motor centers[17]. The extent to which these signals are actually transferred to and used by

the thalamus, and whether L6CTs in other cortical areas show task-related movement activity patterns as well, remains to be determined.

Finally, there is considerable speculation in the field about a potential role for L6CTs in attention[18]. It is an enticing possibility, considering that attention-related activity changes have been observed in the dLGN[19,20], and the TRN, which is directly engaged by L6CTs, appears to play an especially important role in attention[20–23]. The pulvinar is also heavily implicated[24,25] and has been described as an essential orchestrator of cortical activity patterns and synchronization during attention[26–29]. Still, a privileged role for L6CTs in attention has yet to be directly and conclusively addressed, likely due to the technical challenges in selectively measuring and/or manipulating the activity of L6CTs in an awake animal performing an attention task. Yet these challenges may be addressable as attention-related tasks are developed in mice[30,31] – in which selective manipulations of L6CTs are already tractable, as demonstrated by use of the Ntsr1-Cre mouse line throughout this dissertation – and/or as approaches for cell type-specific accessibility are improved in non-human primates.

L5CT "driving" pathways to HO thalamus

In contrast to the negligible effects of L6CT inactivation on visual responses in either the dLGN or pulvinar, inactivating L5 extratelencephalic neurons (L5ETs), which include L5CT projections, had pronounced suppressive effects on visual as well as spontaneous activity recorded in the pulvinar. This is broadly consistent with longstanding hypotheses that the L5CT projections to the pulvinar constitute a functionally "driving" pathway, analogous to retinal ganglion cell inputs to the dLGN[32,33]. In fact, when we were able to silence L5ET activity (Figure 2.5), we observed instances of retinotopically aligned pulvinar neurons whose tuning and receptive field properties were essentially abolished, thus firmly demonstrating the "driving" influence of these projections. Again, this differed markedly from the effects of L6CT silencing, even on individual pulvinar neurons that were suppressed by L5CT silencing (Figure 2.6).

On the other hand, effects of L5ET inactivation were, in some ways, less drastic than might have been expected from silencing a "driving" pathway. Only about 10-16% of visually responsive pulvinar neurons were significantly suppressed by L5ET inactivation, and many of those that were suppressed did not completely lose their tuning or receptive field properties. There are a number of possible explanations for this. First, it could be that we were only inactivating a restricted region of L5ETs within V1, and so pulvinar units receiving driving input from L5CTs in V1 that were not inactivated were unaffected. We found some evidence for this, as when we restricted our analyses to pulvinar neurons retinotopically aligned to the area of L5ET inactivation, a much higher proportion – about 50% - were significantly suppressed (Figure 2.4). Still, about half were not, and so this cannot fully explain the relative infrequency of suppression that we observed. Another possibility is that our L5ET inactivation was incomplete, in that activity of L5ETs themselves was dampened down but not completely silenced. However, we addressed this by using a more potent inhibitory opsin (stGtACR2; Figure 2.5) and even by virally ablating L5ETs (Figure 2.S12) and still observed persistent visual responses in the pulvinar. While we found that some neurons of the lateral pulvinar (some of which were also impacted by L5ET inactivation, and some of which were not) were suppressed by inactivation of the superior colliculus (SC; Figure 2.7), still, the visual responses of a large proportion of pulvinar neurons were unaffected. This leads us to expect that other pulvinar neurons likely receive their driving inputs from L5 neurons outside of V1, in the extrastriate cortex. This notion is supported by anatomical demonstrations of numerous L5 inputs to the rodent pulvinar arising from outside of V1[14,34–36], other observations of incomplete suppression of pulvinar visual responsivity from V1 inactivation by cooling[37], and by reports of suppressed calcium responses in pulvinar thalamocortical boutons due to inactivation of an extrastriate visual area[36]. While the functional influence of L6CTs in extrastriate areas also needs to be assessed, based on our observations of distinct effects of L5ET versus L6CT populations in the same area (V1), we would anticipate a similar "driver" versus "modulator" functional dissociation in other cortical areas as well. Moreover, since extrastriate L6CT projections to the pulvinar closely resemble V1 L6CT projections to dLGN in that they emanate from the full depth of L6 (as opposed to mainly lower L6 for

pulvinar-projecting L6CTs in V1; Figure 2.1b), we would expect their inactivation in the pulvinar to have similar effects of V1 L6CT inactivation in the dLGN: potentially more substantial effects on spontaneous activity, but little if any direct influence on visual activity.

What is the significance of the L5CT pathway specifically bearing the burden of "driving" visual responses in the pulvinar? Interestingly, L5ETs' thalamic projections are often collaterals of projections to their deeper subcortical targets, like the pons and/or SC[38]. While the precise estimates of the different proportions of L5ETs that project to individual or combinations of subcortical targets has varied[38–42] (see also Figure 2.S2), the presence of L5CT projections collateralizing in the HO thalamus from descending projections to motor centers like the SC and pons has raised some speculation about what roles these neurons might play in movement planning[13,38]. The L5CT collaterals have even been proposed to provide "efference copies" of motor plans being sent to subcortical motor centers, thus allowing the sensory consequences of planned movements to be computed through trans-thalamic circuits[13]. This idea still needs to be directly addressed, perhaps through similar inactivation experiments as in Chapter 2 but in the context of sensory-guided motor behaviors. Another intriguing feature of L5ETs is that they have tall, branched apical dendrites in cortical layer 1, which is the target of considerable corticocortical as well as thalamocortical feedback[43]. These neurons appear to be particularly impacted by anesthesia through "decoupling" of their somas from their apical dendrites, such that the same stimulation delivered to their apical tufts causes a back-propagating calcium spike that triggers spiking at the soma in awake, but not anesthetized states[10]. Thus, given their "driving" role in conveying sensory signals to HO thalamus, one might speculate upon a potential role for CT projections from these L5ET neurons in conscious perception.

Chapter 2 also provides evidence that L5CT projections are not the only drivers of pulvinar activity and can even converge with inputs from the SC to shape visual activity and response properties. The presence of convergent driver inputs is significant because it highlights a role for the pulvinar in integrating inputs from various sources, rather than purely "relaying" sensory information to higher order cortical areas in a feedforward manner. While a recent rabies tracing study showed that the majority of L5

inputs to HO cortex-projecting pulvinar neurons came from V1 – suggestive of a feedforward pathway - there were also considerable inputs from the SC, as well as from a variety of other visual and non-visual cortical areas[36]. In many ways, the contribution of the SC is particularly intriguing because its synapses in the pulvinar exhibit a combination of "driver"- and "modulator"-type synaptic features; they target proximal dendrites and exclusively activate ionotropic glutamate receptors like drivers, but they exhibit considerable convergence that is reminiscent of modulators[44]. They also are moderate-size terminals with moderately strong synapses that are neither depressing nor facilitating[44–46]. Within the SC itself, neurons tend to be highly motion-sensitive and direction-selective and have small receptive fields[47–49]. Multiple lines of evidence suggest that some of the larger receptive fields observed in the pulvinar could be formed by many convergent SC inputs[47–49]. This is somewhat different to a classic "driving" pathway, like in the primate dLGN where most neurons' receptive fields seem to be shaped by only one or a few RGC inputs[50]. However, it is reminiscent of "combination modes" of RGC input to the rodent dLGN, whereby multiple different RGC cell types with different or shared visual features converge onto single dLGN neurons[51,52]. Anatomical and physiological evidence also points to some convergence of collicular and RGC driver inputs onto individual neurons in the mouse dLGN "shell" region[53]. Thus, convergent driving inputs are not uncommon, especially in rodents. Given the importance of the SC in motion processing, eye movements and visual attention[54,55], it could confer additional signals relevant to behavioral context or planned movements to the pulvinar that are integrated with bottom-up sensory signals. Whether multiple drivers of different cortical origins (e.g., L5 inputs from V1 and extrastriatre areas) might also converge onto individual neurons, and whether they might collectively shape sensory response properties and/or link different behaviorally relevant signals, is also an interesting question requiring further investigation.

Towards a common framework of corticothalamic communication

While this dissertation has focused on the visual system in its exploration of corticothalamic pathways, the findings presented here are likely to extend to other sensory systems, and potentially even

non-sensory systems as well. The type 1 "modulator" and type 2 "driver" synapse classes are similarly observed across different visual, auditory and somatosensory FO and HO thalamic nuclei[11,12,56–58], suggesting that different input types may share functional properties. Existing evidence generally supports this intuition. For instance, the dynamic and context-dependent characteristics of L6CT projections that were described in the visual thalamus *in vivo* in Chapter 1 are highly consistent with *in vitro* studies conducted in the somatosensory system[1]. Work in the auditory system has also found time-varying effects of L6CT stimulation on thalamic activity *in vivo*, which can bias sound perception in favor of either detection or discrimination[8]. Other aspects of L6CT modulation, such as their effects on firing mode[5,6] and the topographic organization of their influence[7,59–61], have at least been described in both visual and somatosensory systems. Still, some interesting differences may emerge. For instance, L6CT activation overwhelmingly suppresses intracortical activity (by way of intralaminar fast-spiking interneurons) in the primary visual and somatosensory cortices[62,63], yet has the opposite effect in the primary auditory cortex[8]; whether these local differences might accompany long-range differences in corticothalamic influence as well is not clear. Meanwhile, similar physiological properties of "driver"- and "modulator"-type synapses have also been described in L5CT and L6CT projections from non-sensory areas, such as the prefrontal cortex, to other HO nuclei[64]. Especially since cortico-thalamo-cortical loops between frontal and motor cortical areas and their associated HO thalamic nuclei have been shown to play crucial roles in sustaining persistent activity patterns that are important for behavior[65–67], it will be interesting to parse apart the distinct "driving" versus "modulatory" functions that L5CT versus L6CT projections play in supporting those loops outside of the classic sensory systems.

There is also ample reason to expect that our findings in mice are applicable to other species, including primates. On one hand, there are considerable species differences in the extent to which L5CTs and L6CTs are distributed across cortical areas. For instance, in primates and carnivores, L6CT and L5CT projections to the pulvinar seem to come almost exclusively from extrastriate cortex and V1, respectively[14,68–71], whereas both CT populations are considerably more distributed across visual cortical areas in mice[14,34,36]. It is therefore possible that these different CT projections may be more hierarchically

arranged into “feedback” and “feedforward” pathways in primates compared to rodents. But even while specific cortical origins may vary, the anatomical and physiological properties of “type 1” and “type 2” glutamatergic synapses and the presence of L5 and L6 CT projections to HO thalamic nuclei have been observed in every mammalian species that has been studied[57]. Moreover, non-layer-specific manipulations of V1 activity in species in which CT projections from V1 come predominantly from L5 have also demonstrated considerable consequences for visual responses in the pulvinar[37,72], much like our own V1 L5-specific manipulations in mice (Chapter 2). This would strongly support the notion that CT projection pathways, while their exact configurations may differ, are similarly divided into L5 “driving” and L6 “modulatory” pathways across species.

Towards an understanding of function through the window of functional corticothalamic connectivity

This dissertation has focused on functionally disentangling cortical projections to the visual thalamus, and especially the pulvinar. The pulvinar is the largest thalamic subdivision in primates, accounting for a quarter of the thalamus’ total volume[73]. Yet, the overarching function(s) of the pulvinar has been difficult to pin down. While it has been broadly implicated in visual spatial attention, the limited number of human thalamic lesion studies where damage included the pulvinar have led to more subtle deficits, such as poorer stimulus discrimination in the face of distractors, rather than gross attentional impairments[28,74,75]. Still, the primate pulvinar displays robust activity changes due to attention[24,25] and appears to play a role in synchronizing activity among cortical areas[26,27,29]. Temporary pulvinar inactivation was even shown to disrupt cortical synchronization and diminish visual responses in those cortical areas while also impairing performance on a change detection attention task[27]. However, the functional implications of the pulvinar’s ability to coordinate cortical synchrony need not be limited to attention. In fact, computational models have demonstrated that, at least in theory, the same circuit architecture that could support cortical synchrony could also sustain persistent activity in tasks where a sensory stimulus must be maintained in working memory, resolve conflicts between bottom-up sensory

signals and top-down expectations, and compute decision confidence during sensory decision-making[76]. With a firmer grasp of the detailed circuit mechanisms underlying corticothalamic communication – such as distinct L5 and L6 "driving" and "modulatory" CT channels – these kinds of models can be elaborated and constrained to more closely reflect the true biological circuitry. Collectively, this may bring us closer to a broader conceptualization of pulvinar function that would ideally be applicable to other HO thalamic nuclei as well. This could be particularly useful for the study of psychiatric disorders. In schizophrenia, for instance, hypo-functional connectivity between the cortex and HO thalamus (at least, but likely not only, between the prefrontal cortex and the mediodorsal thalamic nucleus, MD) appears to be a key feature that underlies a wide range of symptoms, and thus may prove a promising target for clinical intervention[77].

The findings presented in this dissertation also raise important considerations and further questions with regards to existing theories of pulvinar function. Some theories have proposed an essential role for the HO thalamus in supporting feedforward propagation of sensory information through the cortical hierarchy[33,57,78–80]. Other theories emphasize a role for the HO thalamus in attention and cognition by coordinating cortical synchrony and functional connectivity[28]. Many of these latter ideas do not presume the pulvinar to be involved in direct sensory signal transmission to the cortex[28]; in this sense, a "driving" pathway from the cortex to the pulvinar need only confer temporally precise excitability, rather than tuning and receptive field properties. However, we found some evidence for the latter, not only for the L5CT pathway but also for the SC-pulvinar pathway. While we did not assess the extent to which the pulvinar, in turn, "drives" (or modulates) visual response properties or other signatures of activity downstream in the cortex, a handful of studies in primates have demonstrated that pulvinar inactivation substantially depletes visual responses in extrastriate cortex (specifically V4)[27], and even in V1[81]. A recent study in rodents also found that the tuning properties of pulvinar inputs to an extrastriate cortical area closely reflect those of the target area, and more so than the inputs from V1 (although the pulvinar was not inactivated and thus its necessity was not directly assessed)[36]. These findings would imply some degree of "driving" influence by pulvinar-cortical projections on cortical sensory processing. Pulvinar-

cortical axons, both to V1 and extrastriate cortex, have also been shown to carry contextual signals, such as the discrepancy between optic flow and running speed[35,36]. These findings raise a number of exciting questions, such as how those contextual signals make it to - or are computed within - the pulvinar (e.g., might convergent cortical and SC inputs play a role?) and what influence those signals have on cortical processing. Overall, the full extent to which the pulvinar in engaged in transmitting behaviorally relevant information (visual and/or non-visual) to the cortex versus affecting how information *within* the cortex is transmitted is not yet clear and requires further investigation. However, these potential HO thalamic functions need not be mutually exclusive. Perhaps the functionally distinct driving and modulatory CT pathways described in this study could support dual roles for the pulvinar in "driving" some aspects of cortical responses *and* "modulating" direct cortico-cortical communication, but complementary *in vivo* studies of thalamocortical pathways will be needed to more fully address this possibility.

To return to Ramón y Cajal's question about the possible roles of "centrifugal fibers", this dissertation highlights the diversity of those roles. Chapter 1 demonstrated that within L6CT pathways from V1 to either the dLGN or pulvinar, L6CT influence varies depending on timing, activation intensity, and a number of other factors. This circuit's high degree of flexibility may be optimized for the various contingencies that can arise during sensory-guided behaviors. In Chapter 2, we showed that two, seemingly parallel CT pathways – both excitatory in nature, originating in V1 and terminating in the pulvinar – can have very different influences on thalamic activity and response properties. Just as illuminating these principles of functional connectivity in corticothalamic circuitry has considerable implications for understanding the diverse functions of the thalamus and corticothalamic interactions, further detailed studies of functional diversity within and between circuits will prove essential to the pursuit of a mechanistic understanding of the brain.

References

1. Crandall, S. R., Cruikshank, S. J. & Connors, B. W. A corticothalamic switch: controlling the thalamus with dynamic synapses. *Neuron* **86**, 768–82 (2015).

2. Hasse, J. M. & Briggs, F. Corticogeniculate feedback sharpens the temporal precision and spatial resolution of visual signals in the ferret. *Proceedings of the National Academy of Sciences of the United States of America* **114**, E6222–E6230 (2017).

3. Andolina, I. M., Jones, H. E., Wang, W. & Sillito, A. M. Corticothalamic feedback enhances stimulus response precision in the visual system. *Proceedings of the National Academy of Sciences of the United States of America* **104**, 1685–90 (2007).

4. Wang, W., Jones, H. E., Andolina, I. M., Salt, T. E. & Sillito, A. M. Functional alignment of feedback effects from visual cortex to thalamus. *Nature neuroscience* **9**, 1330–6 (2006).

5. Spacek, M. A., Born, G., Crombie, D., Bauer, Y., Liu, X., Katzner, S. & Busse, L. Robust effects of corticothalamic feedback during naturalistic visual stimulation. *Biorxiv* 776237 (2020) doi:10.1101/776237.

6. Mease, R. A., Krieger, P. & Groh, A. Cortical control of adaptation and sensory relay mode in the thalamus. *Proceedings of the National Academy of Sciences of the United States of America* **111**, 6798–803 (2014).

7. Born, G., Erisken, S., Schneider, F. A., Klein, A., Mobarhan, M. H., Lao, C. L., Spacek, M. A., Einevoll, G. T. & Busse, L. Corticothalamic feedback sculpts visual spatial integration in mouse thalamus. *Biorxiv* 2020.05.19.104000 (2020) doi:10.1101/2020.05.19.104000.

8. Guo, W., Clause, A. R., Barth-Maron, A. & Polley, D. B. A Corticothalamic Circuit for Dynamic Switching between Feature Detection and Discrimination. *Neuron* **95**, 180-194.e5 (2017).

9. Durand, S., Iyer, R., Mizuseki, K., Vries, S. de, Mihalas, S. & Reid, C. R. A Comparison of Visual Response Properties in the Lateral Geniculate Nucleus and Primary Visual Cortex of Awake and Anesthetized Mice. *Journal of Neuroscience* **36**, 12144–12156 (2016).

10. Suzuki, M. & Larkum, M. E. General Anesthesia Decouples Cortical Pyramidal Neurons. *Cell* **180**, 666-676.e13 (2020).

11. Reichova, I. & Sherman, S. M. Somatosensory corticothalamic projections: distinguishing drivers from modulators. *Journal of neurophysiology* **92**, 2185–97 (2004).

12. Li, J., Guido, W. & Bickford, M. E. Two distinct types of corticothalamic EPSPs and their contribution to short-term synaptic plasticity. *Journal of neurophysiology* **90**, 3429–40 (2003).

13. Sherman, S. M. Thalamus plays a central role in ongoing cortical functioning. *Nature Neuroscience* **16**, (2016).

14. Souza, B. O. F. de, Frigon, É., Tremblay-Laliberté, R., Casanova, C. & Boire, D. Laminar distribution of cortical projection neurons to the pulvinar: A comparative study in cats and mice. *J Comp Neurol* (2020) doi:10.1002/cne.25072.

15. Redinbaugh, M. J., Phillips, J. M., Kambi, N. A., Mohanta, S., Andryk, S., Dooley, G. L., Afrasiabi, M., Raz, A. & Saalmann, Y. B. Thalamus Modulates Consciousness via Layer-Specific Control of Cortex. *Neuron* (2020) doi:10.1016/j.neuron.2020.01.005.

16. Stoelzel, C. R., Bereshpolova, Y., Alonso, J.-M. & Swadlow, H. A. Axonal conduction delays, brain state, and corticogeniculate communication. *J Neurosci Official J Soc Neurosci* **37**, 6342–6358 (2017).

17. Clayton, K. K., Williamson, R. S., Hancock, K. E., Tasaka, G., Mizrahi, A., Hackett, T. A. & Polley, D. B. Auditory Corticothalamic Neurons Are Recruited by Motor Preparatory Inputs. *Curr Biol* (2020) doi:10.1016/j.cub.2020.10.027.

18. Briggs, F. Role of Feedback Connections in Central Visual Processing. *Annu Rev Vis Sc* **6**, 1–22 (2020).

19. O'Connor, D. H., Fukui, M. M., Pinsk, M. A. & Kastner, S. Attention modulates responses in the human lateral geniculate nucleus. *Nat Neurosci* **5**, 1203–1209 (2002).

20. McAlonan, K., Cavanaugh, J. & Wurtz, R. H. Guarding the gateway to cortex with attention in visual thalamus. *Nature* **456**, 391–394 (2008).

21. Wimmer, R. D., Schmitt, L. I., Davidson, T. J., Nakajima, M., Deisseroth, K. & Halassa, M. M. Thalamic control of sensory selection in divided attention. *Nature* **526**, 705–9 (2015).

22. Halassa, M. M., Chen, Z., Wimmer, R. D., Brunetti, P. M., Zhao, S., Zikopoulos, B., Wang, F., Brown, E. N. & Wilson, M. A. State-dependent architecture of thalamic reticular subnetworks. *Cell* **158**, 808–21 (2014).

23. McAlonan, K., Cavanaugh, J. & Wurtz, R. H. Attentional Modulation of Thalamic Reticular Neurons. *J Neurosci* **26**, 4444–4450 (2006).

24. Petersen, S. E., Robinson, D. L. & Morris, J. D. Contributions of the pulvinar to visual spatial attention. *Neuropsychologia* **25**, 97–105 (1987).

25. Petersen, S. E., Robinson, D. L. & Keys, W. Pulvinar nuclei of the behaving rhesus monkey: visual responses and their modulation. *J Neurophysiol* **54**, 867–886 (1985).

26. Saalmann, Y. B., Ly, R., Pinsk, M. A. & Kastner, S. Pulvinar influences parietal delay activity and information transmission between dorsal and ventral visual cortex in macaques. *bioRxiv* 405381 (2018) doi:10.1101/405381.

27. Zhou, H., Schafer, R. & Desimone, R. Pulvinar-Cortex Interactions in Vision and Attention. *Neuron* **89**, 209–220 (2016).

28. Halassa, M. M. & Kastner, S. Thalamic functions in distributed cognitive control. *Nature neuroscience* **20**, 1669–1679 (2017).

29. Saalmann, Y. B., Pinsk, M. A., Wang, L., Li, X. & Kastner, S. The pulvinar regulates information transmission between cortical areas based on attention demands. *Science (New York, N.Y.)* **337**, 753–6 (2012).

30. McBride, E. G., Lee, S.-Y. J. & Callaway, E. M. Local and Global Influences of Visual Spatial Selection and Locomotion in Mouse Primary Visual Cortex. *Current Biology* **29**, 1592-1605.e5 (2019).

31. Wang, L. & Krauzlis, R. J. Visual Selective Attention in Mice. *Current biology : CB* **28**, 676-685.e4 (2018).

32. Sherman, S. M. & Guillery, R. W. On the actions that one nerve cell can have on another: Distinguishing "drivers" from "modulators." *Proceedings of the National Academy of Sciences* **95**, 7121–6 (1998).

33. Sherman, S. M. & Guillery, R. W. Functional organization of thalamocortical relays. *Journal of neurophysiology* **76**, 1367–95 (1996).

34. Scholl, L. R., Foik, A. T. & Lyon, D. C. Projections between visual cortex and pulvinar in the rat. *J Comp Neurol* (2020) doi:10.1002/cne.24937.

35. Roth, M. M., Dahmen, J. C., Muir, D. R., Imhof, F., Martini, F. J. & Hofer, S. B. Thalamic nuclei convey diverse contextual information to layer 1 of visual cortex. *Nature neuroscience* **19**, 299–307 (2016).

36. Blot, A., Roth, M. M., Gasler, I. T., Javadzadeh, M., Imhof, F. & Hofer, S. B. Visual intracortical and transthalamic pathways carry distinct information to cortical areas. *Biorxiv* 2020.07.06.189902 (2020) doi:10.1101/2020.07.06.189902.

37. Casanova, C., Savard, T. & Darveau, S. Contribution of Area 17 to Cell Responses in the Striate-recipient Zone of the Cat's Lateral Posterior-Pulvinar Complex. *Eur J Neurosci* **9**, 1026–1036 (1997).

38. Deschênes, M., Bourassa, J. & Pinault, D. Corticothalamic projections from layer V cells in rat are collaterals of long-range corticofugal axons. *Brain research* **664**, 215–9 (1994).

39. Bourassa, J. & Deschênes, M. Corticothalamic projections from the primary visual cortex in rats: a single fiber study using biocytin as an anterograde tracer. *Neuroscience* **66**, 253–63 (1995).

40. Rojas-Piloni, G., Guest, J. M., Egger, R., Johnson, A. S., Sakmann, B. & Oberlaender, M. Relationships between structure, in vivo function and long-range axonal target of cortical pyramidal tract neurons. *Nature communications* **8**, 870 (2017).

41. Swadlow, H. A. & Weyand, T. G. Efferent systems of the rabbit visual cortex: Laminar distribution of the cells of origin, axonal conduction velocities, and identification of axonal branches. *J Comp Neurol* **203**, 799–822 (1981).

42. Klein, B. G., Mooney, R. D., Fish, S. E. & Rhoades, R. W. The structural and functional characteristics of striate cortical neurons that innervate the superior colliculus and lateral posterior nucleus in hamster. *Neuroscience* **17**, 57–78 (1986).

43. Larkum, M. A cellular mechanism for cortical associations: an organizing principle for the cerebral cortex. *Trends in neurosciences* **36**, 141–51 (2013).

44. Bickford, M. E. Thalamic Circuit Diversity: Modulation of the Driver/Modulator Framework. *Frontiers in neural circuits* **9**, 86 (2015).

45. Masterson, S. P., Li, J. & Bickford, M. E. Synaptic organization of the tectorecipient zone of the rat lateral posterior nucleus. *Journal of Comparative Neurology* **515**, 647–63 (2009).

46. Masterson, S. P., Li, J. & Bickford, M. E. Frequency-dependent release of substance P mediates heterosynaptic potentiation of glutamatergic synaptic responses in the rat visual thalamus. *Journal of neurophysiology* **104**, 1758–67 (2010).

47. Casanova, C. & Molotchnikoff, S. Influence of the superior colliculus on visual responses of cells in the rabbit's lateral posterior nucleus. *Experimental brain research* **80**, 387–96 (1990).

48. Chalupa, L., Williams, R. & Hughes, M. Visual response properties in the tectorecipient zone of the cat's lateral posterior-pulvinar complex: a comparison with the superior colliculus. *Journal of Neuroscience* **3**, 2587–96 (1983).

49. Bennett, C., Gale, S. D., Garrett, M. E., Newton, M. L., Callaway, E. M., Murphy, G. J. & Olsen, S. R. Higher-Order Thalamic Circuits Channel Parallel Streams of Visual Information in Mice. *Neuron* **102**, 477-492.e5 (2019).

50. Cleland, B. G., Dubin, M. W. & Levick, W. R. Sustained and transient neurones in the cat's retina and lateral geniculate nucleus. *The Journal of physiology* **217**, 473–96 (1971).

51. Liang, L., Fratzl, A., Goldey, G., Ramesh, R. N., Sugden, A. U., Morgan, J. L., Chen, C. & Andermann, M. L. A Fine-Scale Functional Logic to Convergence from Retina to Thalamus. *Cell* **173**, 1343-1355.e24 (2018).

52. Rompani, S. B., Müllner, F. E., Wanner, A., Zhang, C., Roth, C. N., Yonehara, K. & Roska, B. Different Modes of Visual Integration in the Lateral Geniculate Nucleus Revealed by Single-Cell-Initiated Transsynaptic Tracing. *Neuron* **93**, 767-776.e6 (2017).

53. Bickford, M. E., Zhou, N., Krahe, T. E., Govindaiah, G. & Guido, W. Retinal and Tectal "Driver-Like" Inputs Converge in the Shell of the Mouse Dorsal Lateral Geniculate Nucleus. *The Journal of neuroscience : the official journal of the Society for Neuroscience* **35**, 10523–34 (2015).

54. Gandhi, N. J. & Katnani, H. A. Motor Functions of the Superior Colliculus. *Annu Rev Neurosci* **34**, 205–231 (2011).

55. Krauzlis, R. J., Lovejoy, L. P. & Zénon, A. Superior Colliculus and Visual Spatial Attention. *Neuroscience* **36**, 165–182 (2013).

56. Horn, S. C. V. & Sherman, S. M. Fewer driver synapses in higher order than in first order thalamic relays. *Neuroscience* **146**, 463–70 (2007).

57. Rouiller, E. M. & Welker, E. A comparative analysis of the morphology of corticothalamic projections in mammals. *Brain Research Bulletin* **53**, 727–41 (2000).

58. Landisman, C. E. & Connors, B. W. VPM and PoM Nuclei of the Rat Somatosensory Thalamus: Intrinsic Neuronal Properties and Corticothalamic Feedback. *Cerebral Cortex* **17**, 2853–2865 (2007).

59. Li, L. & Ebner, F. F. Cortical modulation of spatial and angular tuning maps in the rat thalamus. *The Journal of neuroscience : the official journal of the Society for Neuroscience* **27**, 167–79 (2007).

60. Andolina, I. M., Jones, H. E. & Sillito, A. M. Effects of cortical feedback on the spatial properties of relay cells in the lateral geniculate nucleus. *Journal of neurophysiology* **109**, 889–99 (2013).

61. Tsumoto, T., Creutzfeldt, O. D. & Legéndy, C. R. Functional organization of the corticofugal system from visual cortex to lateral geniculate nucleus in the cat (with an appendix on geniculo-cortical mono-synaptic connections). *Experimental brain research* **32**, 345–64 (1978).

62. Pauzin, F. P. P. & Krieger, P. A Corticothalamic Circuit for Refining Tactile Encoding. *Cell reports* **23**, 1314–1325 (2018).

63. Olsen, S. R., Bortone, D. S., Adesnik, H. & Scanziani, M. Gain control by layer six in cortical circuits of vision. *Nature* **483**, 47–52 (2012).

64. Collins, D. P., Anastasiades, P. G., Marlin, J. J. & Carter, A. G. Reciprocal Circuits Linking the Prefrontal Cortex with Dorsal and Ventral Thalamic Nuclei. *Neuron* **98**, 366-379.e4 (2018).

65. Guo, Z. V., Inagaki, H. K., Daie, K., Druckmann, S., Gerfen, C. R. & Svoboda, K. Maintenance of persistent activity in a frontal thalamocortical loop. *Nature* **545**, (2017).

66. Schmitt, L. I., Wimmer, R. D., Nakajima, M., Happ, M., Mofakham, S. & Halassa, M. M. Thalamic amplification of cortical connectivity sustains attentional control. *Nature* **545**, (2017).

67. Bolkan, S. S., Stujenske, J. M., Parnaudeau, S., Spellman, T. J., Rauffenbart, C., Abbas, A. I., Harris, A. Z., Gordon, J. A. & Kellendonk, C. Thalamic projections sustain prefrontal activity during working memory maintenance. *Nature neuroscience* **20**, 987–996 (2017).

68. Moore, B., Li, K., Kaas, J. H., Liao, C., Boal, A. M., Mavity-Hudson, J. & Casagrande, V. Cortical projections to the two retinotopic maps of primate pulvinar are distinct. *Journal of Comparative Neurology* **527**, 577–588 (2019).

69. Raczkowski, D. & Diamond, I. T. Projections from the superior colliculus and the neocortex to the pulvinar nucleus in Galago. *The Journal of comparative neurology* **200**, 231–54 (1981).

70. Lund, J. S., Lund, R. D., Hendrickson, A. E., Bunt, A. H. & Fuchs, A. F. The origin of efferent pathways from the primary visual cortex, area 17, of the macaque monkey as shown by retrograde transport of horseradish peroxidase. *Journal of Comparative Neurology* **164**, 287–303 (1975).

71. Conley, M. & Raczkowski, D. Sublaminar organization within layer VI of the striate cortex in Galago. *The Journal of comparative neurology* **302**, 425–36 (1990).

72. Bender, D. B. Visual activation of neurons in the primate pulvinar depends on cortex but not colliculus. *Brain Research* **279**, 258–261 (1983).

73. Grieve, K. L., Acuña, C. & Cudeiro, J. The primate pulvinar nuclei: vision and action. *Trends in neurosciences* **23**, 35–9 (2000).

74. Snow, J. C., Allen, H. A., Rafal, R. D. & Humphreys, G. W. Impaired attentional selection following lesions to human pulvinar: evidence for homology between human and monkey. *Proceedings of the National Academy of Sciences of the United States of America* **106**, 4054–9 (2009).

75. Danziger, S., Ward, R., Owen, V. & Rafal, R. Contributions of the human pulvinar to linking vision and action. *Cognitive Affect Behav Neurosci* **4**, 89–99 (2004).

76. Jaramillo, J., Mejias, J. F. & Wang, X.-J. Engagement of Pulvino-cortical Feedforward and Feedback Pathways in Cognitive Computations. *Neuron* **101**, 321-336.e9 (2019).

77. Parnaudeau, S., Bolkan, S. S. & Kellendonk, C. The Mediodorsal Thalamus: An Essential Partner of the Prefrontal Cortex for Cognition. *Biological Psychiatry* **83**, 648–656 (2017).

78. Theyel, B. B., Llano, D. A. & Sherman, S. M. The corticothalamocortical circuit drives higher-order cortex in the mouse. *Nature neuroscience* **13**, 84–8 (2010).

79. Kato, N. Cortico-thalamo-cortical projection between visual cortices. *Brain Res* **509**, 150–152 (1990).

80. Sherman, S. M. & Guillery, R. W. The role of the thalamus in the flow of information to the cortex. *Philosophical Transactions Royal Soc Lond Ser B Biological Sci* **357**, 1695–1708 (2002).

81. Purushothaman, G., Marion, R., Li, K. & Casagrande, V. A. Gating and control of primary visual cortex by pulvinar. *Nature Neuroscience* **15**, 905–12 (2012).